

NAVAL POSTGRADUATE SCHOOL
Monterey, California

2

AD-A277 914



DTIC
ELECTE
APR 11 1994
S F D

DISSERTATION

The Analysis of Wake-Induced Unsteady Aerodynamics as
Related to Higher Harmonic Control

by

Ahmed Ali Mohammed Hassan Abourahma
December 1993

Dissertation Supervisor:

E. Roberts Wood

Approved for public release; distribution is unlimited.

94-10800



16578

9 4 4 8 0 2 9

REPORT DOCUMENTATION PAGE

1a. REPORT SECURITY CLASSIFICATION UNCLASSIFIED		1b. RESTRICTIVE MARKINGS	
2a. SECURITY CLASSIFICATION AUTHORITY		3. DISTRIBUTION/AVAILABILITY OF REPORT Approved for public release; distribution is unlimited	
2b. DECLASSIFICATION/DOWNGRADING SCHEDULE			
4. PERFORMING ORGANIZATION REPORT NUMBER(S)		5. MONITORING ORGANIZATION REPORT NUMBER(S)	
6a. NAME OF PERFORMING ORGANIZATION Naval Postgraduate School	6b. OFFICE SYMBOL (if applicable) AA	7a. NAME OF MONITORING ORGANIZATION Naval Postgraduate School	
6c. ADDRESS (City, State, and ZIP Code) Monterey, California 93943-5000		7b. ADDRESS (City, State, and ZIP Code) Monterey, California 93943-5000	
8a. NAME OF FUNDING/SPONSORING ORGANIZATION	8b. OFFICE SYMBOL (if applicable)	9. PROCUREMENT INSTRUMENT IDENTIFICATION NUMBER	
8c. ADDRESS (City, State, and ZIP Code)		10. SOURCE OF FUNDING NUMBERS	
		PROGRAM ELEMENT NO.	PROJECT NO.
		TASK NO.	WORK UNIT ACCESSION NO.
11. TITLE (Include Security Classification) The Analysis of Wake-Induced Unsteady Aerodynamics as Related to Higher Harmonic Control			
12. PERSONAL AUTHOR(S) LTC Ahmed Ali Mohammed Hassan AbouRahma			
13a. TYPE OF REPORT Ph.D. Dissertation	13b. TIME COVERED From To	14. DATE OF REPORT (Year, Month, Day) December 1993	15. PAGE COUNT 165
16. SUPPLEMENTARY NOTATION The views expressed in this dissertation are those of the author and do not reflect the official policy or position of the Department of Defense or the U.S. Government.			
17. COSATI CODES		18. SUBJECT TERMS (Continue on reverse if necessary and identify by block number)	
FIELD	GROUP	WAKE-INDUCED, UNSTEADY AERODYNAMICS, PROPULSIVE FORCE, AEROELASTICITY, HELICOPTER	
	SUB-GROUP		
19. ABSTRACT (Continue on reverse if necessary and identify by block number) Performance data from the NASA-Army OH-6A higher harmonic control (HHC) flight test program showed significant reductions in main rotor shaft torque and engine power in hover and forward flight [1]. The unsteady aerodynamics with the higher harmonic control system application, including wake effects, were considered to study whether such power reductions are feasible. An airfoil oscillating in pure plunge can achieve propulsive force ("Katzmayr effect"), as in the case of birds' wings flapping in flight. Here it will be shown that this effect can be enhanced in the presence of layers of shed vorticity with the proper phasing. In addition, while it is known that an airfoil oscillating in pitch, will typically produce drag at most values of reduced frequency, it is found that the presence of another layer of shed vorticity of the proper phase, can reduce the drag on the pitching airfoil and depending upon wake spacing, reduced frequency, and phase. Under some conditions the added layer or layers of shed vorticity will even result in propulsive force acting on the pitching airfoil similar to the "Katzmayr" effect for the plunging case. It was found, for the OH-6A helicopter, that the measured reductions in main rotor shaft torque and engine power are feasible when evaluated with respect to the "Katzmayr effect" and the additional drag reduction or propulsive force obtained due to pitch and plunge oscillations with the effect of adjacent wake layers of shed vorticity.			
20. DISTRIBUTION/AVAILABILITY OF ABSTRACT <input checked="" type="checkbox"/> UNCLASSIFIED/UNLIMITED <input type="checkbox"/> SAME AS RPT. <input type="checkbox"/> DTIC USERS		21. ABSTRACT SECURITY CLASSIFICATION UNCLASSIFIED	
22a. NAME OF RESPONSIBLE INDIVIDUAL E. R. Wood		22b. TELEPHONE (Include Area Code) (408) 656-2897	22c. OFFICE SYMBOL Code AA/Wo.

Approved for public release; distribution is unlimited

The Analysis of Wake-Induced Unsteady Aerodynamics as Related to Higher Harmonic Control

by

Ahmed Ali Mohammed Hassan Abourahma
LTC, Egyptian Air Force
B.S., Military Technical College, Cairo, Egypt 1978
M.S.C.E., Faculty of Engineering, Zagazig University, 1988

Submitted in partial fulfillment of the
requirements for the degree of

DOCTOR OF PHILOSOPHY IN AERONAUTICS AND ASTRONAUTICS

from the

NAVAL POSTGRADUATE SCHOOL

December 1993

Author:

Ahmed A.
Ahmed Ali Mohammed Hassan Abourahma.

Approved By:

J. V. Sanders
J. V. Sanders
Associate Professor of Physics

G. V. Hobson
G. V. Hobson
Associate Professor
Aeronautics and Astronautics

D. A. Danielson
D. Danielson
Professor of Mathematics

M. F. Platzer
M. F. Platzer
Professor of
Aeronautics and Astronautics

E. R. Wood
E. R. Wood
Professor of Aeronautics and Astronautics

Approved by:

D. J. Collins
D. Collins, Chairman, Department of Aeronautics and Astronautics

Approved by:

Richard S. Elster
Richard S. Elster, Dean of Instruction

ABSTRACT

Performance data from the NASA-Army OH-6A higher harmonic control (HHC) flight test program showed significant reductions in main rotor shaft torque and engine power in hover and forward flight [1]. The unsteady aerodynamics with the higher harmonic control system application, including wake effects, were considered to study whether such power reductions are feasible.

An airfoil oscillating in pure plunge can achieve propulsive force ("Katzmayr effect"), as in the case of birds' wings flapping in flight. Here it will be shown that this effect can be enhanced in the presence of layers of shed vorticity with the proper phasing. In addition, while it is known that an airfoil oscillating in pitch, will typically produce drag at most values of reduced frequency, it is found that the presence of another layer of shed vorticity of the proper phase, can reduce the drag on the pitching airfoil depending upon wake spacing, reduced frequency, and phase. Under some conditions the added layer or layers of shed vorticity will even result in propulsive force acting on the pitching airfoil similar to the "Katzmayr" effect for the plunging case.

It was found, for the OH-6A helicopter, that the measured reductions in main rotor shaft torque and engine power are feasible when evaluated with respect to the "Katzmayr effect" and the additional drag reduction or propulsive force obtained due to pitch and plunge oscillations with the effect of adjacent wake layers of shed vorticity.

TABLE OF CONTENTS

I. INTRODUCTION

A. GENERAL	1
B. ROTARY WING UNSTEADY AERODYNAMICS	2
C. ADDITION OF WAKE EFFECT	5
D. HIGHER HARMONIC CONTROL (HHC)	6
E. OH-6A TEST PROGRAM DATA	7
F. SCOPE	12

II. BACKGROUND.....	15
---------------------	----

III. DRAG REDUCTION DUE TO WING FLAPPING

(KATZMAYR EFFECT)

A. INTRODUCTION	31
-----------------------	----

Accession For		1
NTIS	CRA&I	√
DTIC	USC	12
U.S. Army	TRC	13
Justification		
By		
Distribution/		
Availability Codes		
Dist	Avail and/or Special	
A-1		

B. THE PHYSICS OF FLAPPING AIRFOILS IN	
LOW-SPEED FLIGHT	32
C. PANEL CODE FOR STEADY INCOMPRESSIBLE	
INVISCID FLOW	34
D. UNSTEADY PANEL CODE	42
E. THEODORSEN'S ANALYSIS	46
F. GARRICK'S PROPULSIVE FORCE ANALYSIS	47
G. COMPARISON OF RESULTS	48
H. ESTIMATED POWER REDUCTION DUE TO HHC	
FOR OH-6A HELICOPTER	52
IV. ANALYSIS OF WAKE INTERFERENCE EFFECTS	
A. INTRODUCTION	60
B. UNSTEADY TWO-FOIL PANEL CODE	61
C. LOEWY'S ANALYSIS	63
D. EVALUATION OF TWO-FOIL PANEL CODE	68

E. ANALYSIS OF OSCILLATORY BLADE	
INTERFERENCE EFFECTS	74
V. PROPULSIVE EFFICIENCY AND FLUTTER ANALYSIS	
A. INTRODUCTION	106
B. PROPULSIVE EFFICIENCY	107
C. SINGLE-DEGREE-OF-FREEDOM AIRFOIL FLUTTER	115
VI. RESULTS AND CONCLUSIONS	
A. DISCUSSION OF RESULTS	120
B. CONCLUSIONS	132
C. RECOMMENDATIONS	134
 List of References	 135
 Initial Distribution List	 142

LIST OF TABLES

	Page
Table (3.1) The OH-6A helicopter rotor parameters	53
Table (3.2) C_d vs k for NACA 0015 plunging with $h_{\bar{a}} = 1$ "	55
Table (3.3) C_{dav} versus reduced frequency k_p at $h_{\bar{a}} = 1$ "	59
Table (4.1) Correction factor for a biplane	72
Table (6.1) Aerodynamic coefficients vs non-dimensional time (from time step 113 to 159) for the case of wake phasing, $m = 75$ degrees, wake spacing $h = 2$, reduced frequency $k = 0.0617$ and plunging amplitude $h_{\bar{a}} = 0.14$).	129

LIST OF ILLUSTRATIONS

- Figure (1.1) L / Lo phase diagram (Imaginary vs Real).
- Figure (1.2) Power reduction results from higher harmonic control
open loop test program (NASA/Army/Hughes - Sept. 1982)
- Figure (1.3) Comparison of 4/rev vertical vibration at the pilot seat versus
airspeed with HHC "on" and "off".
- Figure (1.4) Comparison of 4/rev. lateral vibration at the pilot seat versus
airspeed with HHC "on" and "off".
- Figure (2.1) Loewy's schematic elements of unsteady rotor flow field
- Figure (2.2) Schematic representation of unsteady rotor flow field.
- Figure (2.3) Two-dimensional models of unsteady rotor flow.
- Figure (3.1) Propulsive force on plunging airfoil
- Figure (3.2) Panel Method Geometry
- Figure (3.3) Relationship between geometrical quantities
- Figure (3.4) Panel method representation for unsteady flow
- Figure (3.5) Comparison of panel code results with Garrick ($k = 0.1$)
- Figure (3.6) Comparison of panel code results with Garrick ($k = 1$)
- Figure (3.7) Comparison of panel code results with Garrick ($k = 2$)
- Figure (3.8) Blade deflection vs radial station at 2P

- Figure (3.10) Blade deflection vs radial station at 4P.
- Figure (3.11) Blade deflection vs radial station at 5P.
- Figure (3.12) C_{dav} vs k_p (plunging amplitude").
- Figure (4.1) Aerodynamic unsteady model for a multi-bladed rotor.
- Figure (4.2 a) C_l/C_{l_0} vs h/c (Pane Code).
- Figure (4.2 b) C_l/C_{l_0} vs h/c (From Ref. [44]).
- Figure (4.3 a) Local velocity distribution, V_c/V vs X/C (Panel Code)
- Figure (4.3 b) Local velocity distribution, V_o/V vs X/C (after Wegley [46]).
- Figure (4.4) Correction factor, B vs the chord-gap ratio h/c .
- Figure (4.5 a) Pressure distribution vs X/C (Panel Code).
- Figure (4.5 b) Pressure distribution vs X/C (Panel Code).
- Figure (4.6) Wake pattern (airfoil # 2 plunging at high reduced frequency and close to airfoil # 1).
- Figure (4.7) Wake interference between two plunging airfoils in closer proximity.

- Figure (4.8) C_l vs T^* ($m=0$, $h=200$).
- Figure (4.9) C_d vs T^* ($m=0$, $h=200$).
- Figure (4.10) Wake pattern ($m=0$, $h=2$).
- Figure (4.11) C_l vs T^* ($m=0$, $h=2$).
- Figure (4.12) C_d vs T^* ($m=0$, $h=2$).
- Figure (4.13) Wake pattern ($m=0.20833$, $h=2$).
- Figure (4.14) C_l vs T^* ($m=0.20833$, $h=2$).
- Figure (4.15) C_d vs T^* ($m=0.20833$, $h=2$).
- Figure (4.16) Wake pattern ($m=0.25$, $h=2$).
- Figure (4.17) C_l vs T^* ($m=0.25$, $h=2$).
- Figure (4.18) C_d vs T^* ($m=0.25$, $h=2$).
- Figure (4.19) Wake pattern ($m=0.5$, $h=2$).
- Figure (4.20) C_l vs T^* ($m=0.5$, $h=2$).
- Figure (4.21) C_d vs T^* ($m=0.5$, $h=2$).
- Figure (4.22) Average propulsive force coefficient versus wake phasing.
- Figure (4.23) Wake pattern (pitch, $m=0$, $h=2$).
- Figure (4.24) C_l vs T^* (pitch, $m=0$, $h=2$).
- Figure (4.25) C_d vs T^* (pitch, $m=0$, $h=2$).
- Figure (4.26) C_l vs T^* (pitch, $m=0.20833$, $h=2$).
- Figure (4.27) C_d vs T^* (pitch, $m=0.20833$, $h=2$).
- Figure (4.28) C_l vs T^* (pitch, $m=0.25$, $h=2$).
- Figure (4.29) C_d vs T^* (pitch, $m=0.25$, $h=2$).
- Figure (4.30) Wake pattern (pitch, $m=0.5$, $h=2$).
- Figure (4.31) C_l vs T^* (pitch, $m=0.5$, $h=2$).

- Figure (4.32) C_d vs T^* (pitch, $m = 0.5$, $h = 2$).
- Figure (4.33) Average drag vs wake phasing in case of pitch.
- Figure (4.34) Average drag vs reduced frequency k .
- Figure (5.1) Propulsive efficiency η versus $1/k$ for a plunging airfoil.
- Figure (5.2) Propulsive efficiency η versus $1/k$ for an airfoil pitching about the leading edge.
- Figure (5.3) Propulsive efficiency η versus $1/k$ for an airfoil pitching about the quarter-chord point and mid-chord point.
- Figure (5.4) Propulsive efficiency η versus $1/k$ for an airfoil pitching about the three-quarter-chord point.
- Figure (5.5) An airfoil restrained to rotate about its leading edge in two-dimensional flow.
- Figure (5.6) Variation with reduced frequency k of the real and imaginary parts of the non-dimensional aerodynamic moment m_y due to pitching of an airfoil about its leading edge in an incompressible flow.
- Figure (5.7) Comparison of C_m (Imag.) vs. k_p (NACA0007 oscillating in pitch about the leading edge for $\alpha_0 = 1^\circ$ and $N=200$ panels).
- Figure (5.8) Imag. (m_y) vs k (for an airfoil pitching at $ea = -0.5, 0.0, 0.5$, and 1.0)
- Figure (6.1) Drag coefficient vs angle of attack.

NOMENCLATURE

α	angle of attack
a_0	pitching amplitude
ρ	air density
Ω	rotor angular speed
ω	frequency of oscillation
ω_h	natural frequency of oscillation in plunge
ω_α	natural frequency of oscillation in pitch
a	coordinate of axis of rotation
b	airfoil half-chord
c	airfoil chord
C_L	airfoil lift coefficient
C_{L1}	reference airfoil lift coefficient
C_{L2}	second airfoil lift coefficient
C_d	airfoil drag coefficient

$C_{d_{av}}$	average drag coefficient
C_{d1}	reference airfoil drag coefficient
C_{d2}	second airfoil drag coefficient
C_m	moment coefficient
C_{pxh}	propulsive force coefficient due to plunge
$C_{p\alpha}$	propulsive force coefficient due to pitch
D	average drag force
h	non-dimensional wake spacing
h_o	non-dimensional plunging amplitude
k	reduced frequency (based on airfoil half-chord)
kp	reduced frequency (used by panel code and based on airfoil chord)
L	lift force
L_α, L_h	aerodynamic coefficients used for Theodorsen analysis
M	moment
M_h, M_α	aerodynamic coefficients used for Theodorsen analysis

m	ratio of frequency of oscillation to rotor speed
N	number of blades
P_{xh}	propulsive force due to plunge
P	power
R	rotor radius
r	local radius
S	blade area
t^*	non-dimensional time
U, v	free stream velocity
x_0	coordinate of axis of rotation

Acknowledgments

This research was conducted at the Department of Aeronautics and Astronautics, Naval Postgraduate School, Monterey, California, under supervision of Prof. E. R. Wood, Chairman of my doctoral committee, Prof. M. F. Platzer, Prof. G. V. Hobson, Prof. D. Danielson (Department of Mathematics), and Prof. J. V. Sanders (Department of Physics).

I would like to express my sincere appreciation to Prof. E. Roberts Wood who provided me with this great opportunity to work in this area and for his continuous support, ideas, guidance, knowledge and encouragement. Special thanks and deep gratitude are also due to Prof. Max F. Platzer for his continuous support, guidance, knowledge and valuable hours of council. Also I would like to express my gratitude and appreciation to Prof. Garth Hobson for his help and support, guidance, encouragement, and improving my knowledge in classes and in conducting this research.

Deep appreciation goes to Prof. Donald Danielson for his sincere guidance and the great pleasure to discuss and understand the physics behind the mathematical problems during the hours of his special and useful Applied math. class. Special thanks to Prof. James Sanders and Prof. Allan Coppens for their great help, guidance and valuable knowledge they provided me in the Department of Physics.

Special appreciation is due my mother, my brother and my sister. Without moral support of my wife, Neven, my lovely daughter, Yasmin, and my nice son Aboda, this work could not have been carried out. To them I dedicate this thesis.

Summary

Open loop performance data from the NASA-Army OH-6A higher harmonic control (HHC) flight test program. Wood et al. [1], show significant reductions in main rotor shaft torque and engine power in the airspeed regime from hover to 100 knots. Depending upon HHC controller phase and helicopter airspeed, reductions in power were recorded as large as 20%, with reductions of the order of 10% being typical.

Higher harmonic control is an active helicopter vibration control concept which alters the aerodynamic loads on the rotor blades such that the blade response is reduced. This in turn reduces the vibratory forces and moments acting at the hub, which cause airframe vibration. Basically, HHC is an electronic, computer-controlled active vibration suppression system which senses and cancels vibrations in a helicopter by N /revolution feathering or pitch motion of the rotor blades, N being the number of blades¹. Very substantial vibration reduction was achieved under a NASA-Army sponsored program using a modified OH-6A helicopter. Higher harmonic blade pitch control was implemented by superimposing 4/rev. (32 Hz) swashplate motion upon basic cyclic and collective control inputs.

¹ E. Roberts Wood, R. W. Powers, J. H. Cline, and C. E. Hammond. "On Developing and Flight Testing a Higher Harmonic Control System." Journal of A.I.E.S. January, 1985.

During the program, in addition to reducing vibration levels, the HHC system showed the potential for decreased helicopter power requirements. Recent study of the OH-6A flight test data indicates that the mechanism by which the power reduction was achieved is related to the unsteady aerodynamics associated with HHC. This is supported by the fact that higher harmonic control by the very nature of the method by which it is implemented through oscillating an airfoil in pitch with resulting plunge motion, requires definition of unsteady aerodynamics to adequately model its physics¹.

The fundamental closed form solutions of Theodorsen [3], and Loewy [4] provide the basis for theoretical work in this area. The closed form theory shows rapid changes in the lift deficiency function with changes in reduced frequency, wake spacing and frequency ratio. In the past, emphasis in the study of unsteady aerodynamics has tended to focus on flutter instability and the effect of unsteady aerodynamics on generating lift and torsional loads.

In this research, we are interested in performance, and emphasis will be on the effect of unsteady aerodynamics on the drag of the airfoil. When the drag force is reversed, acting to propel the airfoil forward, it is generally referred to as either negative drag or propulsive force. The classic reference on this subject is that by Garrick [5].

¹ E. R. Wood, Max F. Platzer, Ahmed Abourahma, Mark A. Couch " On the Unsteady Aerodynamics of Higher Harmonic Control." Paper No. C 17, Nineteenth European Rotorcraft Forum, Cernobbio (Como), Italy, September 1993.

While Garrick's [5] work shows that an airfoil oscillating in pitch will typically produce drag in the lower reduced frequency range, k , it is found that the presence of another layer of shed vorticity of the proper phase can reduce the drag on pitching airfoils and depending upon wake spacing, reduced frequency, and phase, may even enhance the propulsive force acting on the airfoil similar to the "Katzmayr" effect for plunging airfoils.

The specific mechanisms that have been used in this research to discuss the phenomenon of OH-6A helicopter rotor power reduction, are: (1) the unsteady aerodynamics associated with a plunging airfoil and how that produces a propulsive force or decrease in rotor power; (2) the influence of a layer of wake vorticity on this propulsive force, which represents the influence of the unsteady aerodynamics of one rotor blade on adjacent rotor blades, (3) the unsteady aerodynamics associated with an airfoil oscillating in pure pitch and how this produces in general a drag force on the airfoil unless accompanied by layers of shed wake vorticity; and (4) the influence of the phasing of a layer of shed vorticity on this drag force, and how, depending upon specific phasing, the effect on the airfoil will be either drag or propulsive force.

The analysis of the above effects was based upon: (1) the classical flat plate unsteady aerodynamic theory for an incompressible fluid of Theodorsen [3], its extension to include chordwise forces (drag) by Garrick [5], the rotor wake analysis of Loewy [4], (2) the panel method developed by Platzer et al. [6], that can be applied for unsteady incompressible flow past airfoils or airfoil combinations of arbitrary geometry and amplitudes of different kinds of motions.

In the first approach, Theodorsen's well known lift deficiency function $C(k)$ has been modified by Loewy for the case of a hovering rotor. Airfoil drag or propulsive force was determined by the methods of Garrick [2]. In the second approach, the panel code allowed a systematic study of the lift and drag produced by oscillating airfoils and airfoil combinations in an incompressible inviscid flow.

The panel code results were checked against different references. The results showed good agreement with these references. For the parameters of the OH-6A rotor in hover, the main conclusion was that the reductions in drag and propulsive forces generated on an airfoil, oscillating in pitch or plunge, due to wake phasing, are sufficient to explain the reductions in power recorded on the OH-6A during the NASA-Army flight test program [1].

I. INTRODUCTION

A. GENERAL

The determination of the unsteady aerodynamics associated with a helicopter rotor has presented a challenge to the helicopter analyst since the conception of the helicopter. The effect of blade oscillations on resulting airloads has prompted new interest in oscillatory blade aerodynamics in connection with possible performance gains. Rotary wing unsteady aerodynamics is considerably more complex than fixed wing aerodynamics.

The simplest case is that of hover, but even here the problem is complicated by the influence of the shed helicopter wake from the rotor. In forward flight, the problem is further complicated by the fact that the velocity of a local blade element ranges at the blade tip from transonic on the advancing side to low subsonic on the retreating side, and at the blade root from low subsonic on the advancing side to reversed flow on the retreating side.

For this reason there is a great need for advances in the present theory in order to explain modern helicopter problems, yet, the number of advances in rotorcraft unsteady aerodynamic theory are very limited, so we need to review current unsteady aerodynamic theory for rotorcraft and to advance the theory in one of the areas where improvement is badly needed.

The goal of this thesis is to explain the measured power reductions in the OH-6A higher harmonic control (HHC) flight test program conducted by E. R. Wood et al [1]. This research will consider the unsteady aerodynamics with HHC system application, including wake effects, in order to determine whether such power reductions are feasible.

B. ROTARY WING UNSTEADY AERODYNAMICS

In this section, some elements of unsteady airfoil aerodynamics will be discussed. Consider an airfoil undergoing sinusoidal pitch and plunge motion. As the airfoil performs an oscillation, vortices are shed into the medium with a circulation strength equal in magnitude to the increase in circulation about the airfoil, but opposite in direction. These disturbances are stored in the fluid because the shed vorticity convects downstream at the local flow field velocity.

The counter-rotating vortices induce a sinusoidal flow field which further changes the

i. The result of this complex flow field is a time difference or delay between the airfoil's motion and the induced aerodynamic forces. This delay is known as the phase lag, ψ [34]. To simplify calculations for this type of motion, it is common to describe the airfoil position and the associated aerodynamic forces by complex variables. For pure plunge oscillations the vertical motion of the airfoil is described by the real part of the following equation:

$$h(t) = h_0 e^{i \omega t} \dots\dots\dots(1.1)$$

where h_0 is a complex number, and ω is the frequency of oscillation. Similarly, the lift is described by :

$$L = L_0 r e^{i \omega t} \dots\dots\dots(1.2)$$

where L_0 is the quasi-steady lift given by the expression :

$$L_0 = .5 \rho U^2 S C_{l\alpha} (\dot{h} / U) \dots\dots\dots(1.3)$$

This is termed quasi-steady because the angle of attack is represented by h/U . The values of r_0 and ψ represent the magnitude and the phase respectively, of the true instantaneous lift relative to the quasi-steady lift. The variables r_0 and ψ in general depend on the reduced frequency k , the Mach number M , and the Reynolds number. For inviscid, incompressible fluid the values of r_0 and ψ will be only a function of k [34]. A complete solution for the oscillating flat-plate airfoil in an incompressible inviscid flow has been obtained by Kussner and Theodorsen and reproduced from Reference [35] in Figure (1.1).

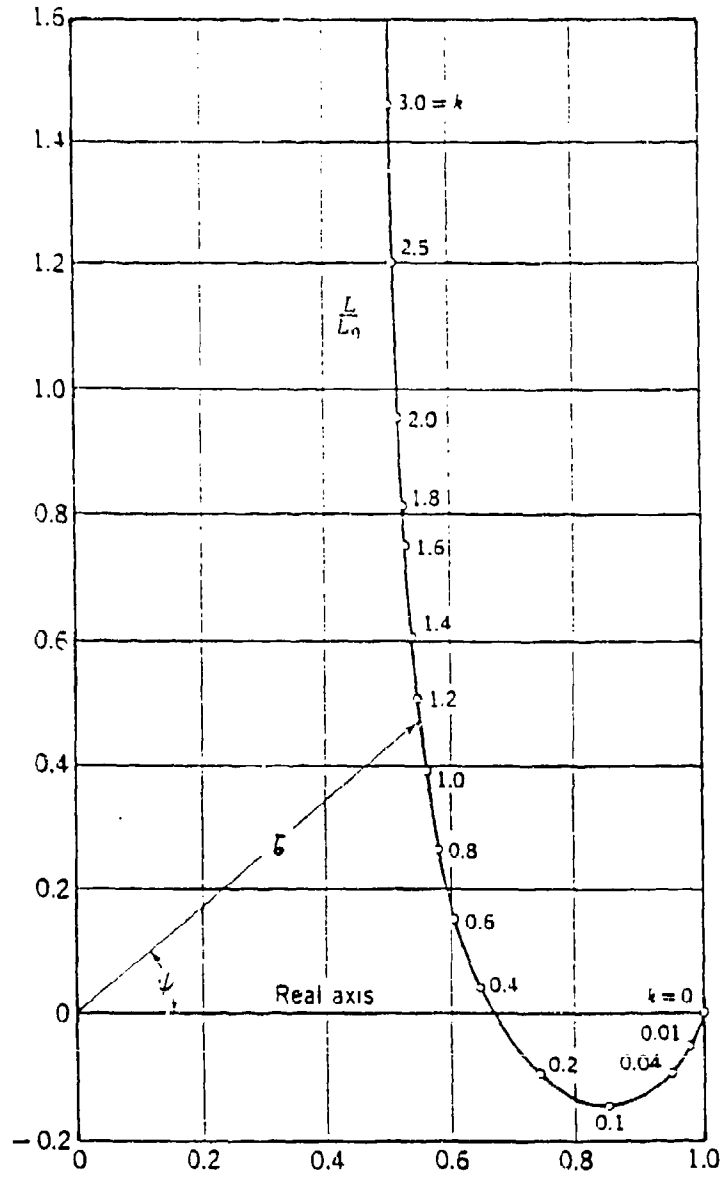


Figure (1.1) L/L_0 Phase Diagram (Imaginary vs Real).

C. ADDITION OF WAKE EFFECT

For the helicopter in hover, the rotation of the wing introduces a number of features that require special attention, notably the returning vortex wake, the time varying free stream, and radial flow, and a fundamentally transcendental geometry that requires either approximate or numerical solutions. The lift on a wing is due to its bound circulation. Conservation of vorticity in the flow requires that there be trailed and shed vorticity in the wake behind the wing.

The spanwise variation of bound circulation results in trailed vorticity parallel to the free stream direction. Time variation of the bound circulation leads to shed vorticity parallel to the wing span. The wake is composed of sheets of vorticity convected downstream from the trailing edge by the free stream velocity. The wake of a rotor in hover or in vertical flight consists of helical vortex sheets below the disk, one from each blade. Unsteady motion of the rotor blade will produce a shed vorticity in the wake spirals. With low disk loading (at low collective pitch settings), the wake remains near the rotor disk and therefore passes close to the following blades. Thus the wake vorticity is not convected downstream of the airfoil as with a fixed wing, and the shed vorticity sheets below the rotor disk must be accounted for to correctly estimate the unsteady loads.

For high inflow (high collective pitch settings) or in high-speed forward flight, the wake will be convected away from the blades. The returning shed wake influence is primarily a concern of hover and vertical flight, and forward flight at airspeeds less than 100 knots. Assuming high aspect ratio of the blade, lifting line theory requires a knowledge of the loads on the blade section, and the returning shed wake of the rotor must be incorporated into the two-dimensional unsteady airfoil theory.

The wake far from the blade section will have little influence, so the emphasis is on modeling the wake near the blade, which for low inflow consists of vortex sheets that are nearly planar surfaces parallel to the disk plane. Based on these considerations, a two-dimensional model for the unsteady aerodynamics of the rotor can be constructed. Loewy in 1957, developed a two-dimensional model for the unsteady aerodynamics of the blade in a hovering rotor, including the effect of the helical shed wake.

D. HIGHER HARMONIC CONTROL (HHC)

The primary source of helicopter vibration is the higher harmonic blade loads generated by the aerodynamic environment at the rotor disk. For an N-bladed rotor, the oscillatory $(N-1)P$, NP , and $(N+1)P$ blade loads are transmitted as exciting hub forces and moments to the airframe at a dominant frequency of N per rev (NP). A significant reduction in vibration level has been achieved by industry in the last twenty five years. The desired goal was to achieve 0.02 g and this goal cannot be met without a quantum advance in vibration control technology. The vibration levels first specified by the U. S Army for the AAH/UTTAS procurement in the early 1970s were later revised upward in the mid 1970s to better reflect realistic design goals consistent with the state-of-the-art in helicopter vibration control [1].

A higher harmonic control system drives the blades in pitch at the $(N-1)P$, NP , and $(N+1)P$ harmonics of rotor rotational speed, generating new unsteady airloads, which in combination with the new oscillatory inertial loads, cancel the harmonics of blade loads that cause airframe vibration. Therefore the vibrations are suppressed at the source. Although there are several ways to implement HHC on a rotor system, the approach generally followed to date has been by blade root feathering using swashplate oscillations.

By means of electro-hydraulic servo-actuators, the swashplate is excited in the collective, longitudinal cyclic, and lateral cyclic modes at NP resulting in blade pitch oscillations at three distinct frequencies of $(N-1)P$, NP, and $(N+1)P$ in the rotating frame. In the system considered, developed for the four-bladed OH-6A helicopter, higher harmonic blade feathering for vibration reduction is achieved by superimposing 4/rev swashplate motion upon basic collective and cyclic flight control inputs.

Perturbing the stationary swashplate at 4/rev both vertically and in pitch and roll results in third, fourth, and fifth harmonic blade feathering in the rotating system. Fourth harmonic blade feathering is achieved by oscillating the swashplate vertically about its collective position, while third and fifth harmonic blade feathering in the rotating system results from 4/rev tilting of the stationary swashplate in pitch and roll about its cyclic tilt position [2]. Results of experimental efforts by Hammond [52] showed that successful suppression of vibration can be achieved by oscillating the blades at relatively small angles.

E. OH-6A (NASA/ARMY/HUGHES) TEST PROGRAM DATA

The goal of this research has been a systematic study of the OH-6A helicopter HHC flight test program, in order to understand and explain the significant reduction in main rotor shaft torque and engine power that was measured in flight. Shown in Figure (1.2) are the power reduction results from the HHC Open Loop Flight Test Program (NASA/ Army/ Hughes - Sept. 1982).

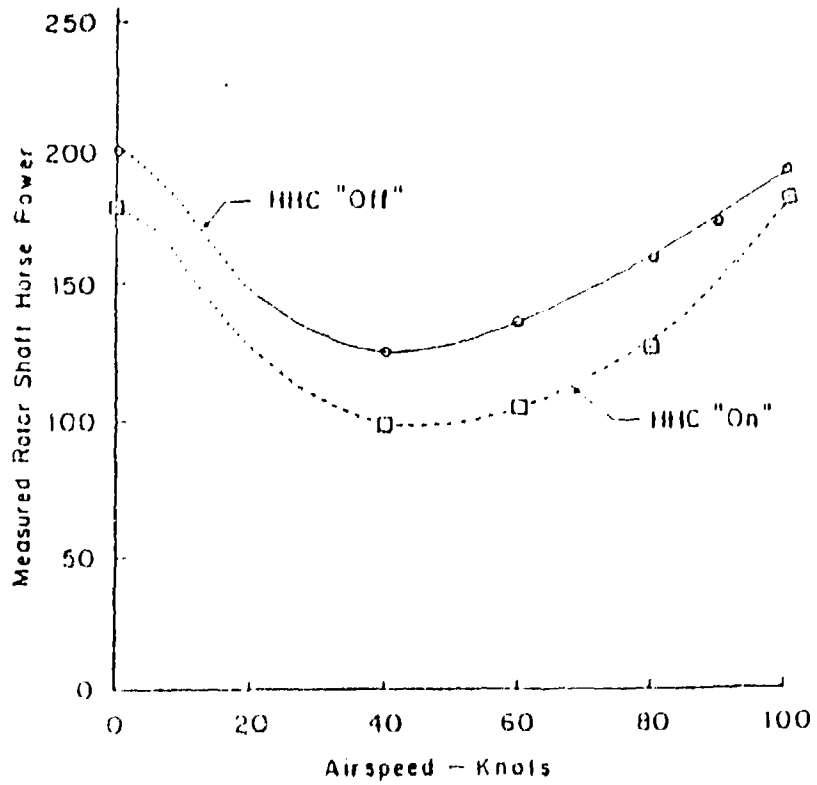


**Figure (1.2): Power Reduction Results from Higher Harmonic Control (HHC)
Open Loop Test Program (NASA/Army/Hughes - Sept. 1982)**

Figures (1.3) and (1.4) (From Ref. [1]) show the very substantial vibration reduction achieved under a NASA-Army sponsored program using a modified OH-6A helicopter. Higher harmonic blade pitch control was achieved by superimposing 4/rev. (32 Hz) swashplate motion upon basic cyclic and collective control inputs. The aircraft was flown from zero airspeed to 100 knots with the HHC system operated both open loop (manually) and closed loop (computer controlled).

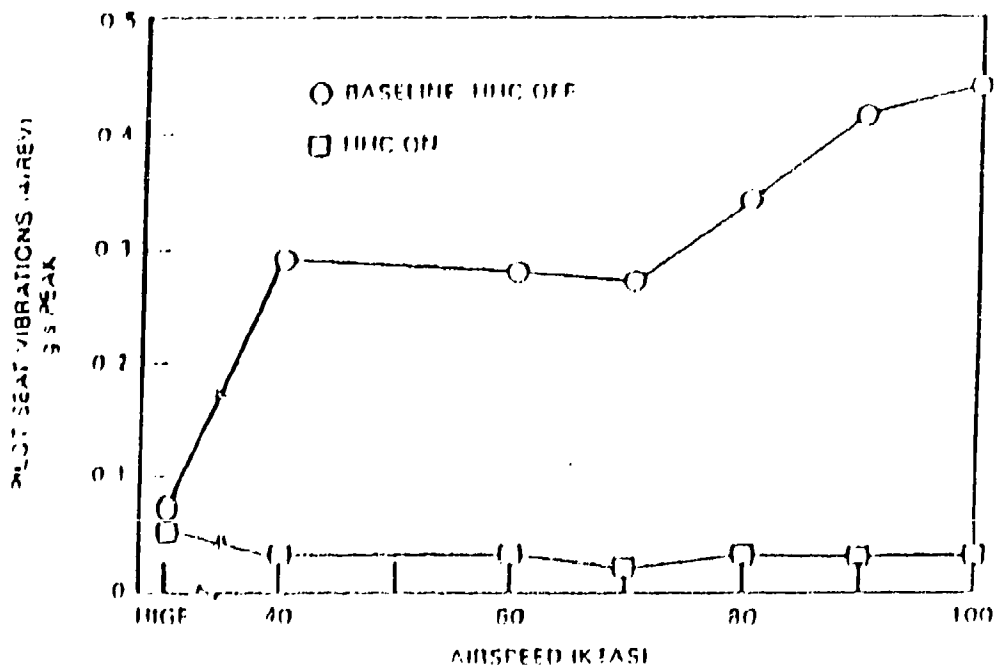


Figure (1.3): Comparison of 4/rev Vertical Vibration at the Pilot Seat Versus Airspeed with HHC "on" and "off".

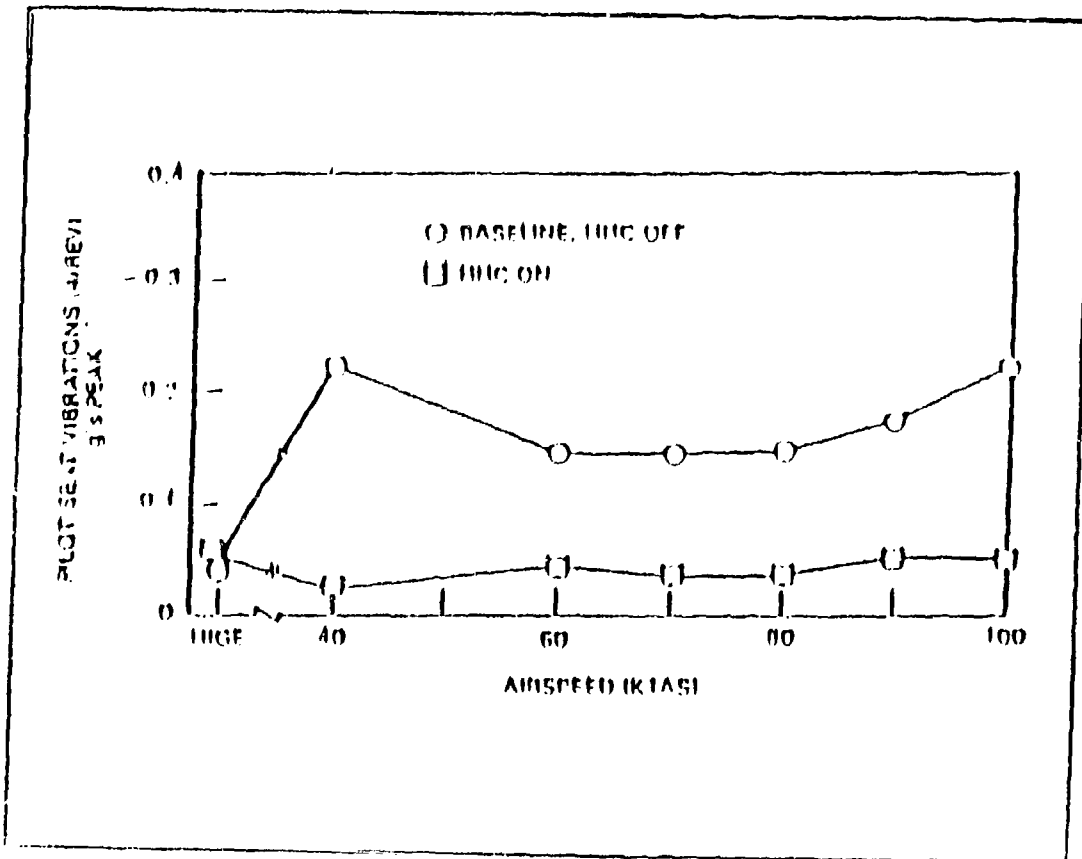


Figure (1.4): Comparison of 4/rev. Lateral Vibration at the Pilot Seat Versus Airspeed with HHC "on" and "off".

The significance of power reduction means that: (1) the helicopter payload can be increased, (2) the maneuverability can be markedly increased, (3) marginal operating conditions, such as at sea in high sea states can be better met, and (4) the helicopter operating costs can be substantially reduced. Increased interest in HHC and its potential benefits for the helicopter now require that we try to use the proper tool to understand this phenomenon. It would appear that we presently have the computational tools, namely the panel method for unsteady inviscid, incompressible flow past airfoils or airfoil combinations of arbitrary geometry, developed by Platzer et al [6], and the single wake closed form analysis developed from Loewy's theory by Wood and Couch [40].

F. SCOPE

Chapter II contains a quick review of the most important research starting with the work of Knoller [10] in 1909 and Betz [11] in 1912. They explained the bird's ability to generate forward thrust by means of wing flapping. In 1922, R. Katzmayr, experimentally verified the work of Knoller and Betz. Birnbaum, von Karman, Theodorsen, and Garrick in the years 1924 through 1936, were the pioneers of flapping wing aerodynamics.

The fundamental closed form solutions by Theodorsen [3], Loewy [4], Garrick [5], provide our basis for theoretical work in this field. While Loewy's work on wake-induced flutter helps to explain the phenomenon, it also points up difficulties to be overcome. That is the closed form theory shows rapid changes in the lift deficiency function with changes in reduced frequency, k ; wake spacing, h ; and frequency ratio, m .

Garrick further developed the work of Theodorsen by deriving the horizontal force formulas for airfoils or airfoil-aileron combinations oscillating in any of the three degrees of freedom: vertical flapping, torsional oscillation about a fixed axis, and angular oscillation of the aileron about a hinge. Also presented in Chapter II, Loewy's two-dimensional model for the unsteady aerodynamics of the blade of a hovering rotor, is presented to provide the base for discussing the obtained results. Also presented in Chapter II, is a quick survey of the most relevant references who developed and used panel methods to study unsteady aerodynamics of oscillating airfoils in an incompressible, inviscid flow.

In the third chapter, the propulsive force is estimated according to the OH-6A helicopter parameters obtained from reference [36]. In this analysis, the blade is divided into sections. Assuming hovering conditions, the reduced frequency at each section was evaluated. Using the unsteady panel code the time history of the airfoil drag (or propulsive force) coefficient was recorded. For the assumed plunging motion with plunging amplitude as obtained from reference [1], for a given mode of vibration, the average propulsive force for each section was calculated.

The total average propulsive force was obtained by adding together the contribution from each blade section. The obtained results showed that the resulting propulsive force from a single airfoil oscillating in plunge is not enough to explain the significant power reduction on the OH-6A helicopter. This led us to study the aerodynamic interference between two blades, which is the main subject of the fourth chapter.

In Chapter IV, the two-airfoil unsteady panel code developed by Pang [25], is used to study the wake interference between two airfoils. This code has been formulated to solve for the potential flow for two airfoils executing unsteady motion in an inviscid incompressible flow medium. It is an extension of the code, developed by Teng [24], for single airfoils. The technique uses the well known panel method for steady flow and extends it to unsteady flow by accounting for the continuous shedding of vortices into the trailing wake.

Numerous case-runs are presented to illustrate the aerodynamic interference between two oscillating airfoils. Results obtained for plunging and pitching airfoils show a significant production of propulsive force at certain wake phase angles. In Chapter V the question of propulsive efficiency due to plunging or pitching and the possibility of single-degree-of-freedom pitching flutter are discussed. Chapter VI discusses the findings of this research and presents the main conclusions.

II. BACKGROUND

The effect of plunge and pitch oscillations on the resultant drag of an airfoil has been the object of aeroelastic research back almost to the time of the Wright brothers (1903). In 1909 and 1912, respectively, Knoller [10], and Betz [11] were the first ones to explain the birds' ability to generate a forward thrust by means of wing flapping¹. Another one of the earliest investigators of this era was R. Katzmayer [7], who in 1922 conducted two series of experiments to explore the effects of oscillatory fluid or airfoil motion on resultant lift and drag.

Katzmayer's experiments which were performed in the aerodynamic laboratory of the Technical University of Vienna, may be divided into two series. In the first series, the angle of attack of the wing model was changed by oscillating the wing model about an axis parallel to the span and at right angles to the airflow. In the second series of experiments, the airfoils were stationary while the airflow itself was subjected to periodic oscillations. Here, for certain air velocities and frequencies, and considering thick airfoil sections, Katzmayer measured negative drag or positive propulsive force. This discovery, to be later known as "Katzmayer effect", helped to explain the propulsive mechanism of birds flying through the air.

¹ Platzer, M. F., Neace, K. S., and Pang, C. K., "Aerodynamic Analysis of Flapping Wing Propulsion", AIAA paper No. 93-0484, 31st Aerospace Sciences meeting, Reno, NV, January 11-14, 1993

Later, E. G. Richardson [8] used the "Katzmayr effect" to explain the locomotion of fish through water. In his paper, Katzmayr summarized his results to show: (1) the effect of flowing air, whose direction is undergoing constant periodical change, is quite favorable, (2) the wing section which exhibits favorable characteristics in a constant airflow, works better in an oscillating flow.

In 1935, Theodore Theodorsen [3] introduced the general theory of aerodynamic instability and the mechanism of flutter. In the first part of his paper, Theodorsen developed the velocity potentials due to flow around oscillating airfoil-ailerons. In the later part of the paper, he developed the differential equations of motions and determined the flutter speed.

The most relevant work with respect to the present research is that by I. E. Garrick [5], who applied the work of Theodorsen [3] to obtain a closed form analytical expression for the propulsive force generated by an oscillating airfoil. An airfoil oscillating in pure plunge or flapping motion was shown by Garrick to have a propulsive force throughout the entire range of reduced, k , while for an airfoil oscillating in pitch, propulsive force can only be achieved for a specified range of reduced frequency, k , where k must be greater than 2.0.

In 1942, W. Schmidt [14] recognized that the Knoller-Betz or Katzmayr effect applies to both a flapping airfoil in uniform flow or a stationary airfoil in oscillating flow. He demonstrated experimentally that a stationary airfoil positioned in the wake of a flapping airfoil increases the propulsive efficiency to almost 100 percent throughout the whole frequency range because the stationary airfoil converts the vortical energy generated by the flapping airfoil into additional thrust. He also found that the mechanical limitations inherent in pure flapping motions could be overcome by an arrangement which he called the wave propeller.

H. Bosch [15] investigated the interference of two lifting surfaces in two-dimensional unsteady incompressible flow, using classical flat-plate theory. He showed that a harmonically flapping airfoil upstream of a stationary airfoil increases the propulsive efficiency to almost 100 %, thus confirming Schmidt's experimental findings. Bosch's analysis is limited to flat-plate airfoils oscillating about a zero incidence mean position.

In 1957, Loewy [4] developed a two-dimensional model for the unsteady aerodynamics of the blade of a hovering rotor. He derived an expression for the two-dimensional oscillatory lift deficiency function as a function of the reduced frequency, wake spacing and the ratio of the airfoil frequency of oscillation and the rotational speed.

The wake in hover or vertical flight consists of helical vortex sheets below the disk, one from each blade. Unsteady motion of the rotor blade will produce shed vorticity in the wake spirals.

In Figures (2.1A) through Figure (2.1D), from Ref. [4], Loewy illustrated the basic elements of the unsteady flow field of a helicopter rotor. A rotor in hovering or vertical flight produces a trailing tip vortex with a downward axial velocity that, if otherwise undisturbed, forms a contracting helix as shown in Figure (2.1A). If the inflow over the rotor disk is constant, then the fluid off the trailing edge of the blades makes a helical surface with horizontal radial elements as shown in Figure (2.1B).

If there is an oscillation in blade effective angle of attack, blade lift will alternate also, and as a result of these changes in lift, vortices will be shed continuously at the blade trailing edge. These vortices fall along the horizontal radial elements of the helical surface shown in Figure (2.1B), so long as the oscillations in angle of attack are small. Figure (2.1C) illustrates this local sheet of shed vorticity. It should be noted that vorticity is considered to be on the helical surface shown in Figure (2.1B); the vertical displacements from that surface shown in Figure (2.1C) represent the strength of the vorticity at a particular azimuthal and radial position [4].

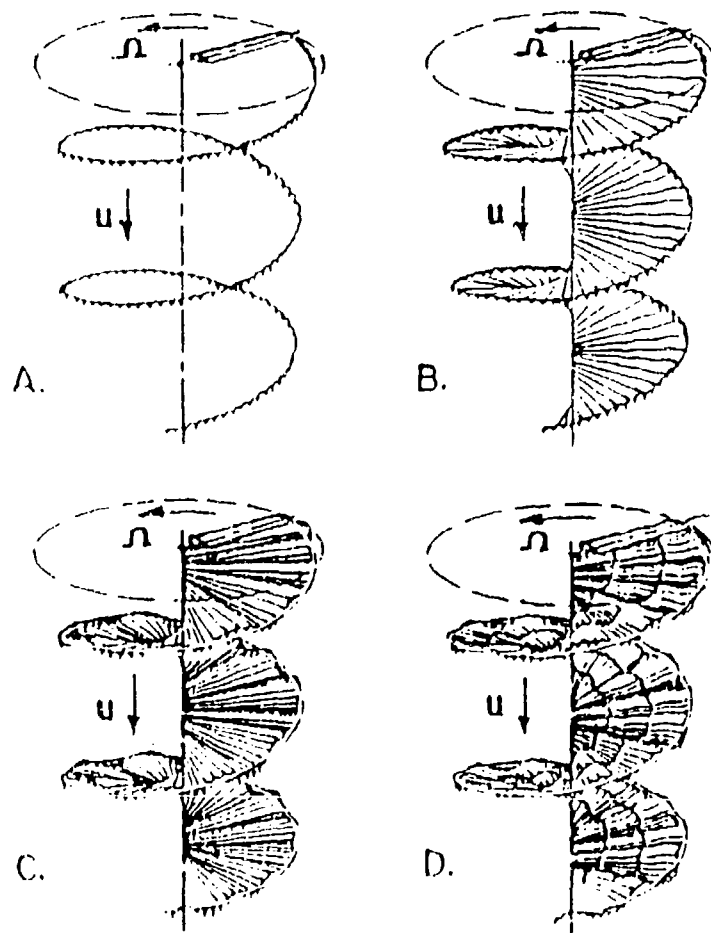


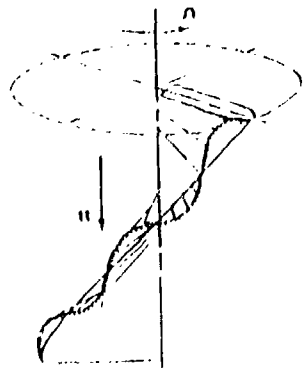
Figure (2.1) Loewy's Schematic Elements of Unsteady Rotor Flow Field

The variation in this vertical displacement (hence vortex strength) around the azimuth corresponds to the history of the motion of a given blade element at a fixed radius. Variation of shed vortex strength in the radial direction at any fixed azimuth angle is a function of the variation with blade span of (1) blade planform; (2) amplitude of oscillation of effective angle of attack, and (3) relative air velocity. Since (from the Helmholtz theorem) vorticity cannot begin or end in space, a variation of shed vorticity in the radial direction implies that there are trailing vortices at constant radii similar to and inboard of the tip vortex. These trailing vortices have been induced in Figure (2.1D).

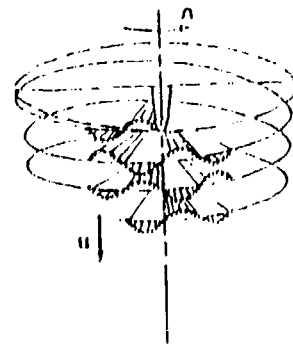
The schematic drawings, Figures (2.1A) through Figure (2.1D), Ref. [4], indicate the difficulty of attempting to obtain a complete representation of unsteady rotor aerodynamics. One means of simplifying the problem is to consider extreme "pitch" values for the helix. For the case of very high inflow velocity, u , in relation to Ω , and the opposite, where u is very low compared to Ω . This is shown in Figure (2.2).

When the vertical spacing between adjacent helical surfaces of shed vorticity is very large, then we expect that all shed vorticity beyond a small fraction of a revolution would be too far below the blade in question to have a significant effect. Under these conditions, it would be sufficient to account for only the attached vortex sheet within that fraction of a revolution, as in Figure (2.2A).

On the other hand, when the vertical spacing between the adjacent helical surfaces of shed vorticity is very small, all the sheets of shed vorticity tend to pile up on each other, and the effect of that vorticity close to the blade in question (shed by blade passes) is of more importance than that which exists beyond a reference azimuth angle on either side of the blade. This situation is depicted in Figure (2.2B), Ref. [4].



A. High Inflow



B. Low Inflow

Figure (2.2) Schematic Representation of Unsteady Rotor Flow Field.

With low rotor thrust values (low collective pitch) the wake remains near the rotor disk and therefore passes close to the following blades. Thus, the shed vorticity sheets below the rotor disk must be accounted for to correctly estimate the unsteady loads. For high inflow or high-speed forward flight the rotor wake will be convected away from the blades. The wake far from the blade section will have little influence, so emphasis is on modeling the wake near the blade. In the case of low inflow, this consists of vortex sheets that are nearly planar surfaces parallel to the disk plane [4].

Based on these considerations, a two-dimensional model for the unsteady aerodynamics of the rotor can be constructed. It is assumed that the chord, amplitude of the oscillation in effective angle of attack, and relative airspeed vary slowly enough with span so that what occurs aerodynamically at one blade radius station is essentially duplicated on either side of it.

The assumption means that the flow problem at a given blade section is two-dimensional. Furthermore, consistent with the idea that only the vorticity near the blade section has an important effect, one may allow the planar rows of vorticity to extend to infinity in the horizontal direction in order to achieve mathematical simplification. It should be stated that this is a first-order theory, so that such effects as that of the wake upon itself have been neglected. The oscillatory flow induced at the airfoil in the free-stream direction, for example, will affect the airfoil lift and moment as well as the vorticity shed at the trailing edge.

Since the shed vorticity is being accounted for as perturbations in the main flow, this component of induced velocity will be small compared to the free-stream velocity (except when the spacing approaches zero) and must react with small, first-order airfoil displacements. Because of the physical unrealities associated with the standard mathematical model representation of the problem (such as zero thickness of wake and airfoil, zero displacement of the wake from horizontal planes, and infinite velocities at the core of a vortex), the accuracy of results as the wake spacing goes to zero is questionable. The effect of the horizontal component of induced flow, therefore, has been neglected in Loewy's analysis.

Shown in Figure (2.3) is the two-dimensionalized model of unsteady rotor flow [4]. The portion of the circular surface which is determined by (1) a particular blade radius, (2) the azimuth angle on either side of the blade section (within which the shed vorticity is of importance), and (3) the vertical distance spanned by a given number of rows of vorticity, can be regarded as a plane, one in which the two-dimensional unsteady aerodynamic problem may be attacked.

This is shown in Figure (2.3 A), with an arrow indicating that the rows of vorticity under the rotor disc extend to infinity. Consistent with the idea that only the vorticity near the blade section has an important effect, one may allow the planar rows of vorticity to extend to infinity in the horizontal direction in order to achieve mathematical simplification. These final modifications are shown in Figure (2.3 B), which is a two-dimensional model, Ref. [4], of unsteady rotor aerodynamics for a single-bladed rotor operating at low inflow.

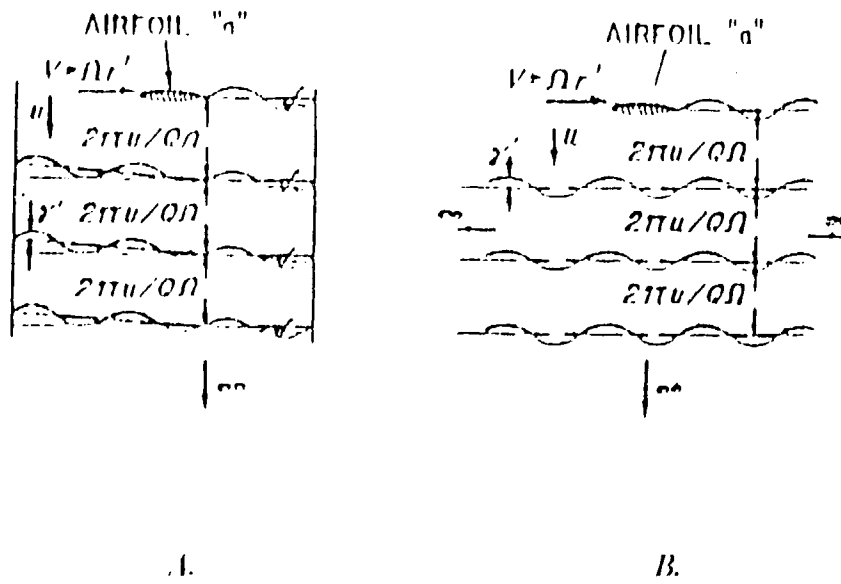


Figure (2.3) Two-dimensional Models of Unsteady Rotor Flow.

The general approach used by Loewy is the same as that of Schwarz [30]. Only the effects resulting from oscillatory motion of a thin airfoil are considered, and the airfoil itself is represented by continuous vorticity distributed along a straight line [9]. It may be also noted that the effect of viscosity in damping the shed vorticity could be accounted for by considering only a finite number of rows beneath the reference airfoil, or by multiplying the vortex strength by an experimental decay function related to the time through the rotational speed and the number of rotational cycles corresponding to a particular vortex row.

This has been omitted from the analysis since vortex decay time is long compared to the rotational periods of most rotors. An extension to Loewy's work is that by Shipman and Wood [29] in 1970. The authors present a method for determining rotor blade flutter in forward flight. Incompressible unsteady aerodynamic theory was applied where shed vorticity both in and below the plane of the rotor is accounted for. This was made possible by noting that the damping for rotor blade aeroelastic instability varies with velocity. Since the tangential velocity of any blade segment varies with azimuth, so will flutter damping¹.

It is assumed at the onset of flutter that oscillations will begin to build up prior to the blade reaching a critical azimuth position, then decay as the blade moves beyond this point. This build up and decay means that the vorticity shed due to the oscillations will be contained within a double azimuth region on either side of the critical azimuth position. Assuming this region to be small allows the wake system to be two-dimensional.

The lift deficiency function resulting from the two-dimensional wake model is compared with earlier results obtained for a helicopter in hover and fixed wings. In the limiting case when the advance ratio is very small, Shipman and Wood's lift deficiency reduces to Loewy's lift deficiency function. Also in the limit as the wake spacing is very large, this function reduces to Theodorsen's lift deficiency function.

¹ Shipman, K. W. , and E. R. Wood " A Two-Dimensional Theory for Rotor Blade Flutter in Forward Flight. " Journal of Aircraft, Vol. No. 8, Number 12, pp. 1008-1015. December 1971.

The theory was applied to bending torsion flutter for the tip segment of a rotor blade. The results followed the normal trends of having the flutter velocity decrease as the blade center of gravity was moved aft and of having the flutter velocity increase as the blade stiffness increased.

The previously shed wakes are destabilizing so that they reduce the flutter velocity. The buildup and decay produces wakes that are essentially centers of vorticity. Thus their position with respect to the reference blade will be sensitive to the advance ratio which determines the vertical spacing. It was found that as the wakes were brought closer by reducing the advance ratio and/or inflow ratio, the flutter speed is decreased [29].

The phenomenon of airfoil flutter is caused by energy extraction out of the wind stream by means of airfoils which are free to oscillate in pitch and plunge. As described by Duncan [19], this effect can be easily demonstrated in a wind tunnel if a device is built which allows to vary the phase relationship between pitch and plunge. Phase angles near 90 degrees produce maximum energy extraction so that the device operates as a flutter engine. McKinney and DeLaurier [20] demonstrated that this effect can be used to convert wind energy into mechanical energy. Scherer, McKinney and Delaurier used Theodorsen's flat-plate theory for performance estimates of the flapping foil propulsor and of the wingmill, respectively.

It was shown by W. Schmidt, that optimum energy extraction occurs for harmonically flapping airfoils upstream of a stationary airfoil. There is a need for aerodynamic analysis methods which enable systematic studies of the effect of airfoil geometry, incidence angle variation, amplitude of oscillation and airfoil interaction on the aerodynamic forces due to incompressible flow over airfoils or airfoil

combinations executing pitch or plunge motions. A panel method was developed in order to do parametric studies of these effects. In the past, a number of investigators have solved the steady flow problem using source and vortex paneling, the most prominent ones being Hess and Smith [21]. A few authors have extended this approach to the case of unsteady motion of single airfoils, notably Basu and Hancock [22] and Kim and Mook [23].

Basu and Hancock [22] presented a numerical method for the calculation of the pressure distribution, force, and moments on a two-dimensional airfoil undergoing an arbitrary unsteady motion in an inviscid incompressible flow. The method was applied to (i) a sudden change in airfoil incidence, (ii) an airfoil oscillating in high frequency and (iii) an airfoil passing through a sharp-edged gust.

Teng [24], developed a computer code for the numerical solution of unsteady inviscid incompressible flow over an airfoil. Pang [25] extended the work of Teng and developed a computer code to study unsteady airfoil interference effects. The technique uses the well known panel methods for steady flow and extends it to unsteady flow by accounting for the continuous shedding of vortices into the trailing wake.

III. DRAG REDUCTION DUE TO BLADE FLAPPING (KATZMAYR EFFECT)

A. INTRODUCTION

In this chapter, a discussion will first be presented of the physics of flapping airfoils which explains the bird's ability to generate a forward thrust by means of wing flapping. This will be followed by a description of two methods capable of predicting the pressure distributions, lift, pitching moment, and drag or thrust on airfoils which execute harmonic oscillations in plunge or pitch.

The first method is based on the generalization of the well-known steady-state panel method to the case of unsteady airfoil motion. It is based on the assumption of inviscid, incompressible flow. The second method is based on the classical Theodorsen theory for oscillating flat-plate airfoils in incompressible inviscid flow. The unsteady panel method permits the investigation of finite-thickness airfoils of arbitrary geometry which may execute rather general unsteady motions (ramp and oscillatory). In contrast, Theodorsen's analysis is restricted to thin airfoils (flat-plates) and to small amplitude oscillations. The chapter ends with a comparison of results computed by both methods.

B. THE PHYSICS OF FLAPPING AIRFOILS IN LOW-SPEED FLIGHT

The phenomenon of thrust generation due to wing flapping or due to steady flight in a sinusoidal gust can be explained in a rather elementary way. Consider the latter case of flight through a sinusoidal gust, as shown in Figure (3.1). The relative wind vector changes direction between a maximum positive and negative angle of attack. The resultant aerodynamic lift is perpendicular to the instantaneous wind vector. If we assume the viscous drag to be small, then it is easily seen that the sinusoidal gust generates a sinusoidally varying thrust.

A similar effect is generated if the airfoil executes a sinusoidally varying plunge motion (wing flapping) about an otherwise steady flight conditions. This explanation of thrust generation due to wing flapping or due to flight through a sinusoidal gust was first advanced by Knoller [10] and Betz [11]. Its experimental demonstration was accomplished by Katzmayr [7] and is therefore generally referred to as Katzmayr effect ¹.

Since it is well known that every change in airfoil incidence causes the shedding of a starting vortex, a more precise explanation of the Katzmayr effect has to take into account the continuous vortex shedding due to wing flapping or due to flight through a sinusoidal gust.

¹ Platzer, M. F., Neace, K. S. and Pang, C. K., "Aerodynamic Analysis of Flapping Wing Propulsion", page 1, AIAA paper No. 93-0484, 31st Aerospace Sciences meeting, Reno, NV, January 11-14, 1993.

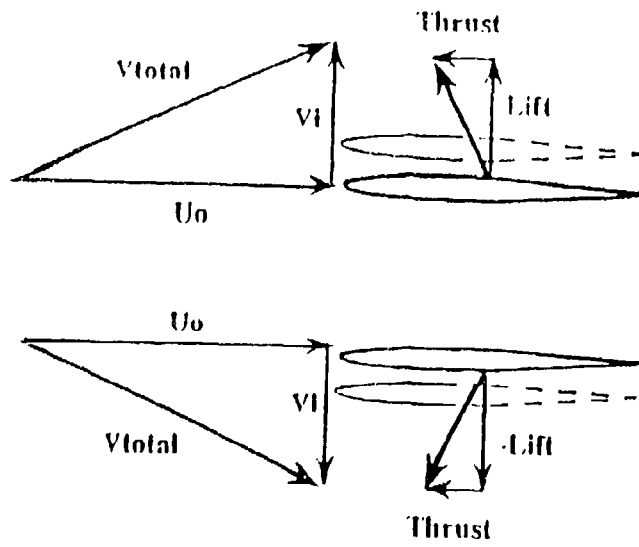


Figure (3.1) Propulsive force on plunging airfoil

Similarly, the quantitative prediction of the induced oscillatory forces (lift and thrust) had to await the development of a complete unsteady aerodynamic theory. Such a theory was first accomplished in the 1930's by Theodorsen [3] in the United States and by Küssner [16] in Germany. It can be found in the textbooks on aeroelasticity, for example the book by Bisplinghoff, Ashley, Halfman [41]. Therefore only the final formulas will be given here and the reader is referred to those texts for additional details. More recently, a second approach to the determination of the unsteady aerodynamic forces on oscillating airfoils became feasible with the advent of high speed computers and the development of efficient numerical solution methods. The fundamental building blocks of this method are presented in the next two sections.

C. PANEL CODE FOR STEADY INCOMPRESSIBLE INVISCID FLOW

In potential flow theory, the flow field around an airfoil may be represented by the velocity potential. Considering contributions from the free stream flow and the source and vorticity distribution, the total potential may be constructed:

$$\Phi = \Phi_F + \Phi_S + \Phi_V \quad (3.1)$$

where

$$\begin{aligned} \Phi_F &= U [x \cos(\alpha) + y \sin(\alpha)] \\ \Phi_S &= \int \frac{q(s)}{2\pi} \ln(r) ds \\ \Phi_V &= -\int \frac{\gamma(s)}{2\pi} \theta ds \end{aligned} \quad (3.2)$$

The source distributions $q(s)$ vary from panel to panel, while the vorticity strength $\gamma(s)$ is assumed constant for all panels. The value of representing the flow past an airfoil by surface singularity distributions lies in the fact that these singularity distributions automatically satisfy Laplace's equation, the governing flow equation for inviscid incompressible flow:

$$\Phi_{xx} + \Phi_{yy} = 0 \quad (3.3)$$

Since Laplace's equation is a linear homogeneous second order partial differential equation, the superposition principle used in Equation (3.1) holds. The boundary conditions include flow tangency at control points (mid-points of panels) and the Kutta condition at the trailing edge, requiring equal tangential velocities for the first and last panels. By evaluating the integrals along the airfoil surface, the potential may be determined at any point in the flow field. Each point is defined at a radius (r) and angle (θ) from a chosen reference point on the airfoil.

The reference point in this study is the leading edge. The airfoil is represented by a number of defined points, called nodes [34]. More points produce greater resolution and better accuracy. One hundred to two hundred points are usually sufficient, with the larger number used for more complicated airfoil shapes or more involved calculations. The lines connecting these nodes are the panels. There are $n+1$ nodes with first and last node overlapping.

Figure (3.2) depicts the panel geometry. Numbering starts at the trailing edge, then progresses along the lower surface, leading edge, and upper surface, and ends at the trailing edge. The unit normal vectors (n_i) are perpendicular to the panels and directed outward from the airfoil surface. The unit tangential vectors (t_i) are parallel to the panels and the positive direction is defined with increasing numbering (n to $n+1$). The panels may vary in length, with the exception of the first and last panels, which must be equal in order to use the Kutta condition at the trailing edge.

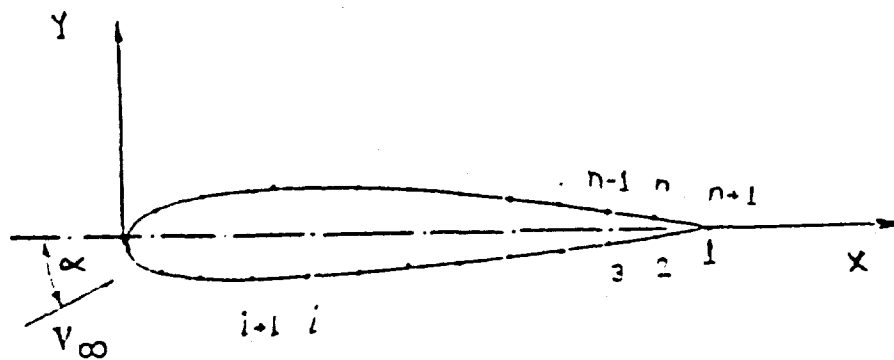


Figure 3.2 Panel Method Geometry

The required input consists of the number of nodes on the airfoil surface, the coordinates of the nodes referenced from the leading edge, and the angle of attack in degrees. The program produces normalized velocities and pressure coefficients at each control point as output. The use of influence coefficients leads to a straightforward procedure for programming the equations.

An aerodynamic influence coefficient is defined as the velocity induced at a field point by a unit strength singularity distribution on one panel. For the two-dimensional steady flow problem, the following influence coefficients are needed [34]:

A_{ij}^n : normal velocity component induced at the i^{th} panel control point by unit strength source distribution on the j^{th} panel

$$A_{ij}^n = \frac{1}{2\pi} \sin(\theta_i - \theta_j) \ln \frac{r_{ij} + 1}{r_{ij}} + \cos(\theta_i - \theta_j) \beta_{ij} \quad i \neq j \quad (3.4)$$

$$= 1/2 \quad i = j$$

A_{ij}^t : tangential velocity component induced at the i^{th} panel control point by unit strength source distribution on the j^{th} panel

$$A_{ij}^t = \frac{1}{2\pi} \sin(\theta_i - \theta_j) \beta_{ij} - \cos(\theta_i - \theta_j) \ln \frac{r_{ij} + 1}{r_{ij}} \quad i \neq j \quad (3.5)$$

$$= 0 \quad i = j$$

B_{ij}^n : normal velocity component induced at the i^{th} panel control point by unit strength vorticity distribution on the j^{th} panel

$$B_{ij}^n = \frac{1}{2\pi} \cos(\theta_i - \theta_j) \ln \frac{r_{ij} + 1}{r_{ij}} - \sin(\theta_i - \theta_j) \beta_{ij} \quad i \neq j \quad (3.6)$$

$$= 0 \quad i = j$$

B_{ij}^t : tangential velocity component induced at the i^{th} panel control point by unit strength vorticity distribution on the j^{th} panel

$$B_{ij}^t = \frac{1}{2\pi} \cos(\theta_i - \theta_j) \beta_{ij} - \sin(\theta_i - \theta_j) \ln \frac{r_{ij+1}}{r_{ij}} \quad i \neq j \quad \dots \dots \dots (3.7)$$

$$= 1/2 \quad \dots \dots \dots i = j$$

where the geometrical quantities, depicted in Figure (3.3) are defined by

$$r_{ij}^2 = (xm_i - x_j)^2 + (ym_i - y_j)^2 \quad xm_i = \frac{x_i + x_{i+1}}{2}$$

$$ym_i = \frac{y_i + y_{i+1}}{2} \quad \theta_i = \arctan \frac{y_{i+1} - y_i}{(x_{i+1} - x_i)} \quad \dots \dots \dots (3.8)$$

$$\beta_{ij} = \arctan \left(\frac{ym_i - y_{j+1}}{xm_i - x_{j+1}} \right) - \arctan \left(\frac{ym_i - y_j}{xm_i - x_j} \right)$$

The first boundary condition requires flow tangency at the control points :

$$(V^n)_i = 0 \quad i = 1, 2, \dots \dots \dots n \quad \dots \dots \dots (3.9)$$

In terms of influence coefficients (with $V_\infty = 1$),

$$\sum_{j=1}^n A_{ij}^n q_j + \gamma \sum_{j=1}^n B_{ij}^n + \sin(\alpha - \theta_i) = 0 \quad i = 1, 2, \dots \dots \dots n \quad \dots \dots \dots (3.10)$$

The second boundary condition is the Kutta condition, which states that the pressures on the lower and upper panels at the trailing edge must be equal if the flow is to leave the trailing edge smoothly.

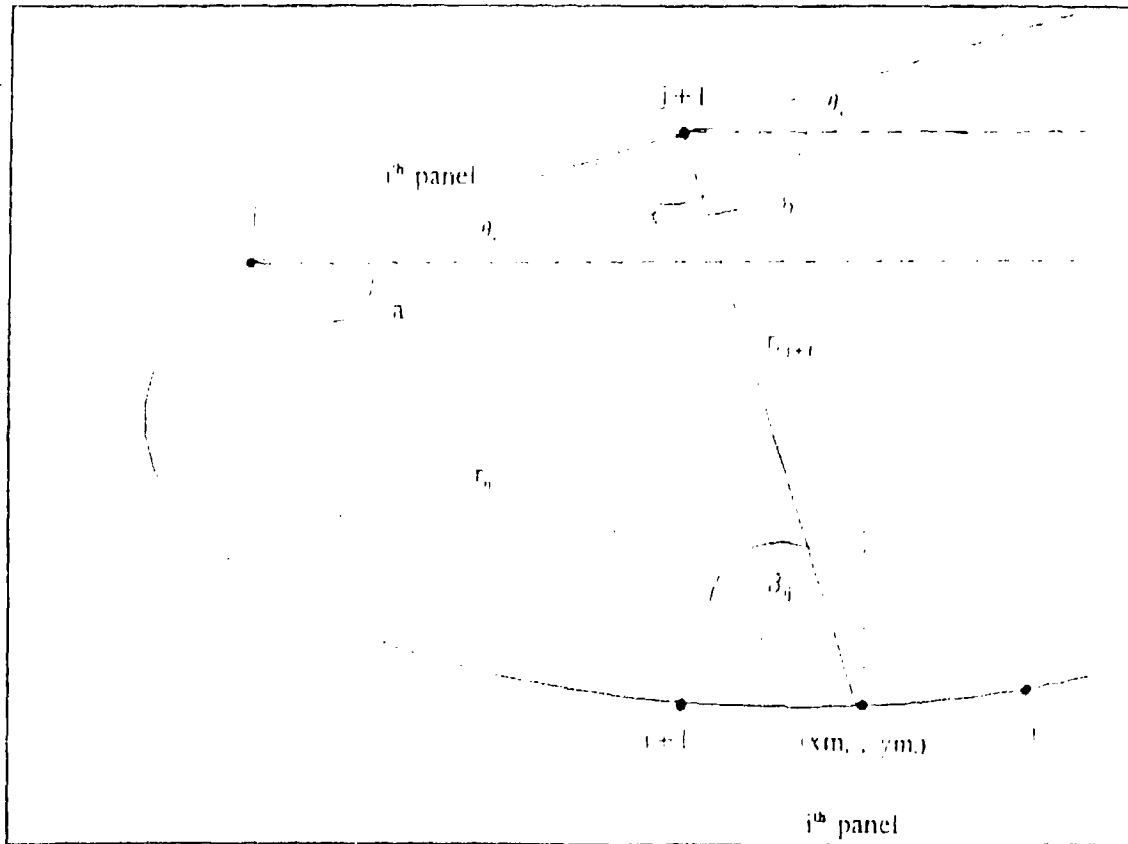


Figure (3.3) Relationship Between Geometrical Quantities

Using Bernoulli's equation, the pressure coefficient can be expressed as :

$$C_p = \frac{P - P_\infty}{\frac{1}{2} \rho V_\infty^2} = 1 - \left(\frac{V_{total}}{V_\infty} \right)^2 \quad (3.11)$$

The pressure equilibrium also implies equal velocities for incompressible flow. Since the normal velocities are taken to be zero, the boundary condition may now be stated as :

$$(V^t)_l = - (V^t)_u \quad (3.12)$$

where the negative sign is strictly due to the adopted convention of positive tangential velocities in the direction of increasing node numbering. Since the flow is positive to the right, the panel downstream of the front stagnation point will have negative values for computational purposes only. It is important to note that not all the lower surface panels have a reversed sign, only those downstream from the stagnation point. This is especially significant for non-symmetrical airfoils or any airfoil at an angle of attack.

In terms of influence coefficients, the normalized equation becomes

$$\sum_{j=1}^n [A_{ij}^t q_j] - \gamma \sum_{j=1}^n B_{ij}^t \cos(\alpha - \theta_j) = \sum_{j=1}^n [A_{ij}^t q_j] - \gamma \sum_{j=1}^n B_{ij}^t \cos(\alpha - \theta_j) \quad (3.13)$$

Equations 3.10 and 3.13 represent a linear algebraic system of $(n+1)$ equation and $(n+1)$ unknowns. The unknowns are the source strengths which vary from panel to panel (q_1, \dots, q_n) and the vorticity strength γ .

Expanding and rearranging Equation 3.10 for an example airfoil of $n = 73$ nodes and panels results in

$$\begin{aligned}
 A_{11}^n q_1 + A_{12}^n q_2 + \dots + \gamma (B_{11}^n + B_{12}^n + \dots + B_{1,73}^n) &= \sin(\alpha - \theta_1) \\
 A_{21}^n q_1 + A_{22}^n q_2 + \dots + \gamma (B_{21}^n + B_{22}^n + \dots + B_{2,73}^n) &= \sin(\alpha - \theta_2) \\
 A_{73,1}^n q_1 + A_{73,2}^n q_2 + \dots + \gamma (B_{73,1}^n + B_{73,2}^n + \dots + B_{73,73}^n) &= \sin(\alpha - \theta_{73})
 \end{aligned} \tag{3.14}$$

The equations now readily lend themselves to solution in matrix form. Recasting with simpler notation, the A_{ij}^n terms (coefficients of q_j) may be renamed a_{ij} and the sum of all B_{ij}^n terms in parentheses (coefficients of γ) renamed $a_{i,n+1}$, where $i = 1, 2, \dots, n$ and $j = 1, 2, \dots, n$. The terms on the right side of the equation may be renamed b_i . The $(n+1)$ equation, or in this example, the 74th equation comes from Equation 3.13 in a similar manner:

$$\begin{aligned}
 (A_{1,1}^1 + A_{73,1}^1) q_1 + (A_{1,2}^1 + A_{73,2}^1) q_2 + \dots + (A_{1,73}^1 + A_{73,73}^1) q_{73} \\
 - \gamma [(B_{1,1}^1 + B_{73,1}^1) + (B_{1,2}^1 + B_{73,2}^1) + \dots + (B_{1,73}^1 + B_{73,73}^1)] \\
 = \cos(\alpha - \theta_1) - \cos(\alpha - \theta_{73})
 \end{aligned} \tag{3.15}$$

The coefficient q_1 may be renamed $a_{74,1}$. All of the B^1 terms in the brackets together form the coefficient of γ , now renamed $a_{74,74}$. The entire right side of the equation constitutes the new term b_{74} .

Finally expressing this system can be written in concise matrix form

$$\begin{array}{ccccccc}
 a_{1,1} & a_{1,2} & \dots & a_{1,n+1} & q_1 & b_1 \\
 a_{2,1} & a_{2,2} & \dots & a_{2,n+1} & q_2 & b_2 \\
 \dots & \dots & \dots & \dots & \dots & \dots \\
 a_{n,1} & a_{n,2} & \dots & a_{n,n+1} & q_n & b_n \\
 a_{n+1,1} & a_{n+1,2} & \dots & a_{n+1,n+1} & \gamma & b_{n+1}
 \end{array} = \quad (3.16)$$

This system is solved in the program using a Gaussian Elimination subroutine. With the values of the q_i and γ known, the velocity at each panel control point may be calculated

$$V_i = \sum_{j=1}^n A_{ij}^1 q_j + \cos(\alpha - \theta_i) \gamma, \quad i = 1, 2, \dots, n. \quad (3.17)$$

The total velocity is equal to the tangential velocity due to taking the normal velocity to be zero

D. UNSTEADY PANEL CODE

The extension of this method to an airfoil experiencing a rapid change in angle of attack can be accomplished as follows. It is important to recall Prandtl's early flow visualization experiments which demonstrated the generation of a starting vortex off the trailing-edge whenever the angle of attack was changed. Hence continuous changes in angle of attack produce a continuous shedding of vorticity into the trailing wake. This shedding can be explained by the Helmholtz vortex theorem which requires that any change in the circulation around the airfoil must be matched by the appearance of an equal counter-vortex at the trailing edge in order to achieve constancy of the total circulation in the flow field.

The vortices shed from the trailing edge move with the fluid particles of the surrounding fluid and hence are swept downstream with a speed essentially equal to the free-stream speed. Therefore these vortices will stay close enough to the airfoil for a finite time to influence its pressure distribution. Any unsteady airfoil theory therefore must describe this vortex shedding process. It is this feature which distinguishes unsteady airfoil theory from its steady counterpart. The above considerations suggest that the airfoil can be modeled by similar source and vortex distributions as in the steady case.

¹Platzer, M. F. Class Lecture Notes, Naval Postgraduate School, Monterey,

California, Sep. 1993.

Hence source panels are again placed on the airfoil surface together with a single vortex distribution which is the same for each panel. An arbitrary change in angle of attack then is subdivided into small step changes such that a starting vortex is shed into the wake each time a step change occurs and the flow tangency and Kutta conditions are enforced at each time step.

In addition to the n airfoil panels a wake panel is assumed to be attached to the trailing edge such that, after each time step, the vorticity of the wake panel is assumed to be concentrated into a single point vortex which detaches from the airfoil and starts moving downstream with the free-stream velocity. As one wake panel detaches from the airfoil a new one is created and a wake of point vortices is created. As in the steady problem n unknown source strengths and one unknown vorticity strength on the airfoil are introduced.

In addition, there is now the unknown vorticity strength of the wake panel whose length and orientation are also unknown. Hence there are three additional unknowns which need to be determined by a proper set of equations: (a) the flow tangency conditions provides n equations, (b) the Kutta condition provides an additional equation, (c) the Helmholtz theorem provides an equation for the vorticity strength on the wake panel.

Therefore two more equations are needed to determine the length and orientation of the wake panel. These are obtained by making the following assumptions, i.e., (d) the wake panel is oriented in the direction of the local resultant velocity at its

mid-point. (c) the length of the wake panel is proportional to the magnitude of the local resultant velocity at its mid-point and to the time-step. The Kutta condition and the last two conditions are nonlinear equations and therefore necessitate an iterative solution procedure. Figure (3.4), from Ref. [25], shows the panel method representation for unsteady flow.

Vortex Shedding at Time Step t_k

Helmholtz's theorem

$$\Delta_k (\gamma_w)_k + \Gamma_k = \Gamma_{k-1}$$

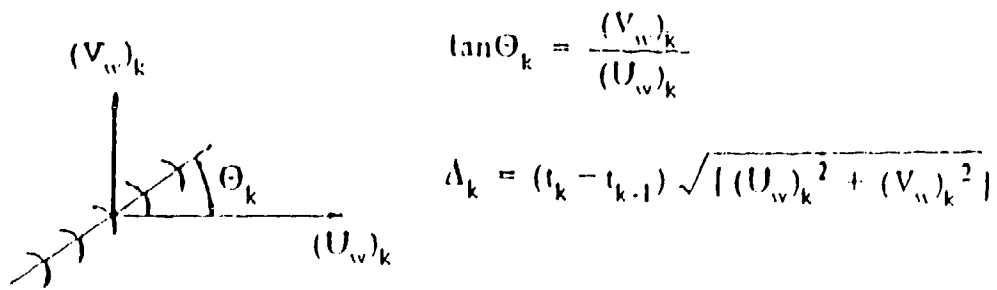
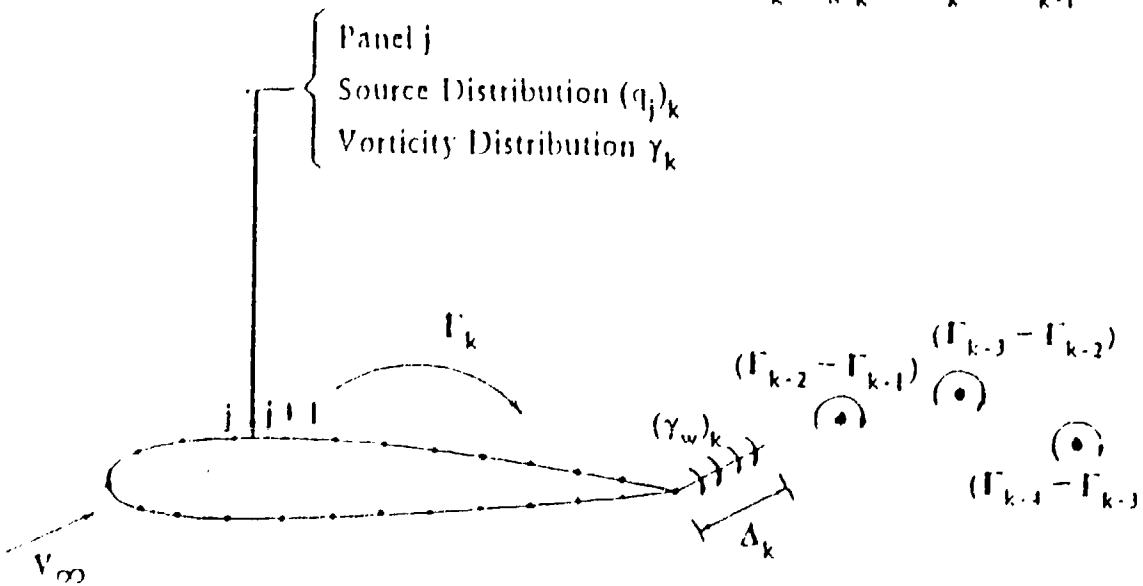


Figure (3.4) Panel Methods Representation for Unsteady Flow

5. THEODORSEN'S ANALYSIS

As stated before, Theodorsen's theory for oscillating flat-plate airfoils in inviscid incompressible flow is well documented. Therefore, we summarize here only the final formulas. The lift on an airfoil oscillating at frequency ω is given by

$$L = \pi \rho \omega^2 b^2 \{ L_{\eta} + (h_e/b) [L_{\alpha} - (1/2 - i) L_{\eta}] \} / U \quad (3.18)$$

where

$$L_{\eta} = (1 - i/2) C(k) / k,$$

$$L_{\alpha} = 1/2 - (i/k) [1 - 2 C(k)] - (2/k^2) C(k),$$

$$k = \omega b / U \quad (b \text{ is the semi-chord and "a" is the elastic axis })$$

$C(k)$ is the lift deficiency function and is given by

$$C(k) = \frac{H_1^{(2)}(k)}{H_1^{(2)}(k) - iH_0^{(2)}(k)} = F(k) - iG(k) \quad (3.19)$$

where $H_n^{(2)}(k)$ is the Hankel function of second kind and is given in terms of Bessel functions as $H_n^{(2)}(k) = J_n(k) - iY_n(k)$.

F. GARRICK'S PROPULSIVE FORCE ANALYSIS

Garrick [5] applied Theodorsen's theory to determine the thrust and drag generated by an airfoil which executes a sinusoidal motion in pitch or in plunge. He found the following formula for the average propulsive force :

$$P_x = \pi \rho b \omega^2 h_0^2 [a_1 h_0^2 + (a_2 - b_2) \alpha_0^2 + 2(a_3 - b_3) \alpha_0 h_0] \quad (3.20)$$

where $a_1 = F^2 + G^2$

$$a_2 = b^2 + a_1 [1 - k^2 + (1/2 - a)^2] - F/4 - (1/2 - a)F - G/k$$

$$a_3 = b + a_1 [-\sin(\varphi_2 - \varphi_0) + (1/2 - a) \cos(\varphi_2 - \varphi_0)] \\ - (F/2) \cos(\varphi_2 - \varphi_0) + (G/2) \sin(\varphi_2 - \varphi_0)$$

$$b_2 = b^2 [-a/2 - F/k^2 + (1/2 - a)(G/k)]$$

$$b_3 = (b/2) [(1/2 + G/k) \cos(\varphi_2 - \varphi_0) + (F/k) \sin(\varphi_2 - \varphi_0)]$$

For pure plunge, the average propulsive force is reduced to :

$$P_x = \pi \rho b \omega^2 h_0^2 [F^2(k) + G^2(k)] \quad (3.21)$$

For pure pitch, the expression for the average propulsive force is given by :

$$P_x = \pi \rho b^3 \omega^2 \alpha_0^2 [a_2 + b_2] \quad (3.22)$$

where a_2 and b_2 are defined in Equation (3.20).

The expression for the average drag in Equation (3.20) of Garrick's report 567 [5], was found to be in error. The correct expression as given in Garrick's subsequent review [32] is

$$D = \Lambda^2 C^2 \left[\frac{1}{k^2} + \frac{1}{2} + \frac{2\pi}{k} \left(\frac{1}{2} - F \right) + \frac{1}{2} + \frac{1}{2} + \frac{F}{k^2} + \frac{1}{2} + \frac{G}{k} \right] \quad (3.23)$$

where

$$C^2 = F^2 + G^2 \quad \text{and} \quad \Lambda = \pi \rho \omega^2 b^3$$

G. COMPARISON OF RESULTS

In a recent thesis, Riester [43] presented a detailed comparison with Theodorsen's predictions of the lift and pitching moment computed with the unsteady panel code. Generally, good agreement was found, thus lending credence to the reliability of the panel code. In the present work, we are interested in the prediction of the thrust and drag forces generated by an oscillating airfoil. Calculations were performed to ascertain the panel code's capability. Figures (3.5) to (3.7) show the comparison between Garrick's predictions and the panel code results. These figures present plots of the average propulsive force coefficient vs the non-dimensional plunging amplitude of oscillation, HBAR (HBAR = h/c), for three reduced frequencies, $k = 0.1, 1$ and 2 . The two methods are in good agreement for small plunge amplitudes. As might be expected, the agreement starts to deteriorate with increasing plunge amplitude. The panel code was applied to an NACA 0009 airfoil using 100 panels.

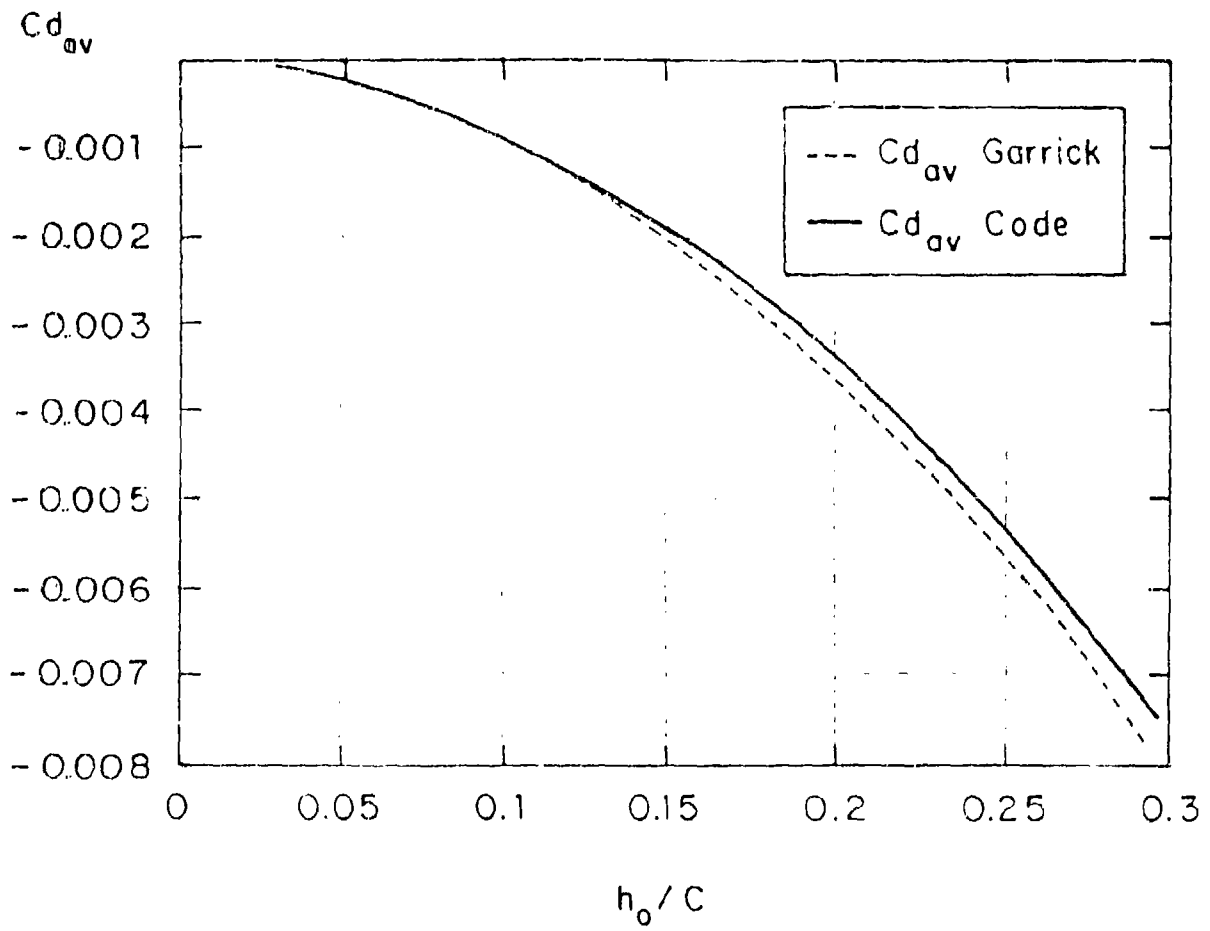


Figure (3.5) Comparison of Panel Code Results with Garrick ($k=0.1$)

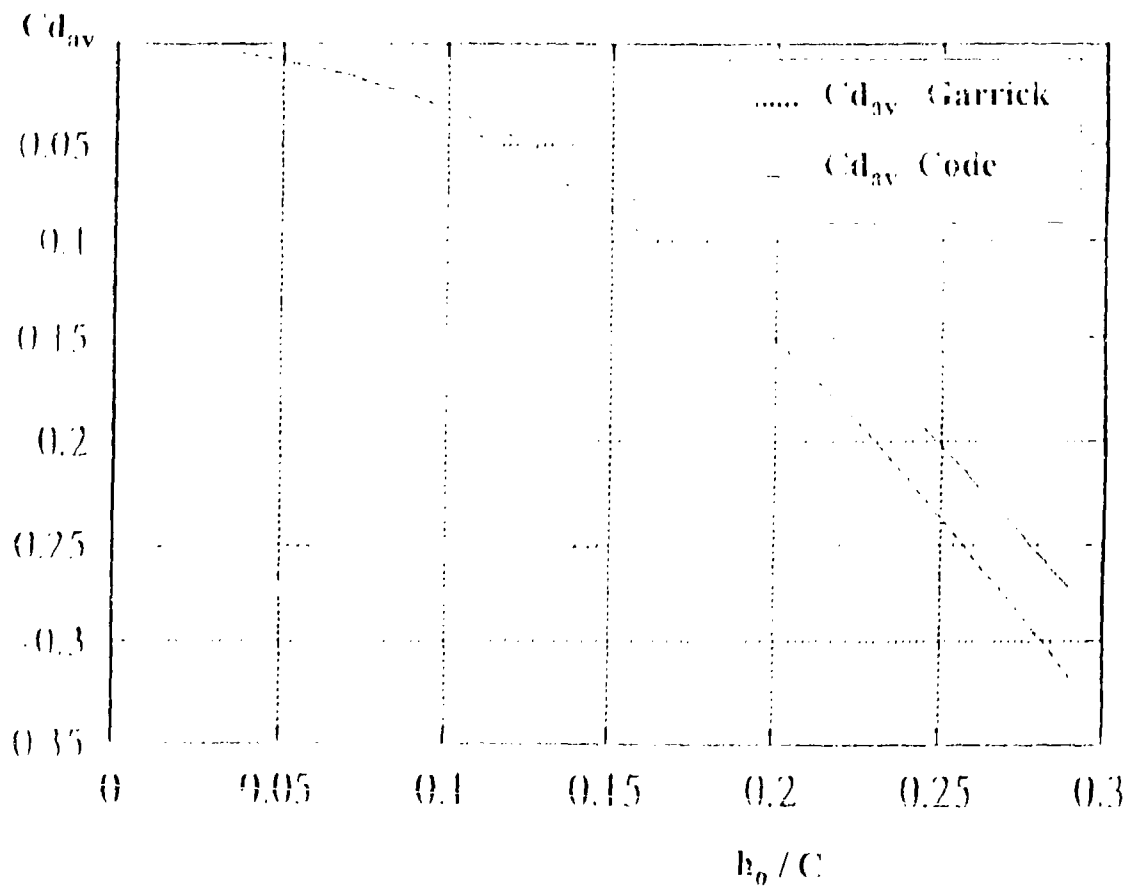


Figure (3.6) Comparison of Panel Code Results with Garrick ($k = 1$)

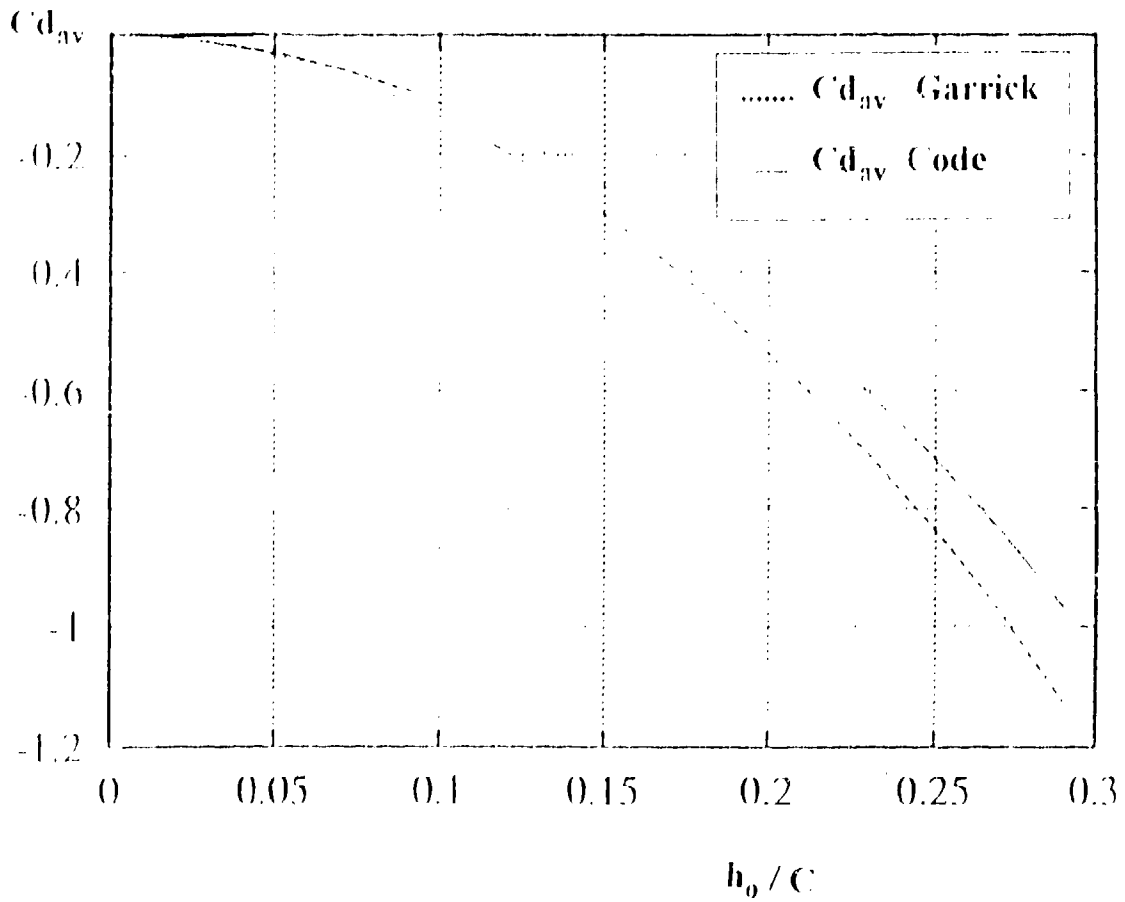


Figure (3.7) Comparison of Panel Code Results with Garrick ($k = 2$)

II. ESTIMATED POWER REDUCTION DUE TO HHC FOR OH-6A HELICOPTER

The ultimate objective of this research was to determine the effect of unsteady aerodynamics on the measured power values for the OH-6A helicopter. We are especially interested in knowing whether these effects could produce the power changes recorded during the NASA - Army open loop flight tests in the flight regime from hover to 100 knots.

In order to estimate the change in torque due to propulsive force (foot-pounds per blade) due to HHC, the blade span was divided into sections. Assuming hover conditions, the reduced frequency at each blade section was calculated. The panel code was used to compute the propulsive force coefficient, C_d , at each blade section assuming pure plunge motion with a plunging amplitude of 1". The blade deflections, obtained from Wood et al [27], were then used to estimate the real value of the plunging amplitudes at each blade segment.

Finally, the net blade torque could be calculated by considering the propulsive force at each blade section and multiplying this value times the rotor radius, then summing over the length of the blade. Table 3.1, from Ref. [42], shows the OH-6A helicopter parameters that were used to estimate the propulsive forces. The most important parameters are: number of blades, $Q = 4$, rotor radius (ft), $R = 13.2$, blade chord (ft), $c = 2b = 0.57$, rotor speed (rad/sec), $\Omega = 49.2$, and helicopter weight (lb), $G = 2550$.

TABLE 3.1 THE OH-6A HELICOPTER ROTOR PARAMETERS :

Rotor radius (ft)	13.2
Number of blades	4
Rotor speed (rad/sec)	59.26
Blade chord (ft)	0.57

Table (3.2) shows, at each blade section r/R , the reduced frequency, $k(r)$, local speed, $U(r)$, the computed average propulsive force, $P_{sh}(r)$ and the torque, $T_{sh}(r)$, due to the propulsive force at each blade section. Summing the estimated torque at each blade section, the resultant torque due to the propulsive force per blade was found to be 8.11 ft-lb assuming a pure plunging motion with constant plunging amplitude of 1" at each blade section. Wood et al [27], applied Garrick's equation and considered the effect of the second to twelfth harmonic loads. He found, for 2 P harmonic (HHC "on" 180 degree phase at 60 knots), that the power gained is about 11.3 horsepower. For more detail, the reader is referred to table 2 of Ref. [27]. Figures 3.3 to 3.11 show the blade deflections for several harmonics used by this reference. Shown in Figure (3.12) is the average drag coefficient, C_{dav} , versus reduced frequency as obtained with the panel code for a plunging amplitude of 1". The airfoil used was NACA 0015 (OH-6A airfoil). The propulsive force, P_{sh} , is given by :

$$P_{sh} = 0.5 \cdot \rho \cdot U^2 \cdot C \cdot dr \cdot C_d \quad (3.24)$$

and the torque, T_{sh} , at each blade section is given by:

$$T_{sh} = P_{sh} \cdot r \quad (3.25)$$

where U is the local speed at each section, C_d is the propulsive force coefficient as obtained by the unsteady panel code and r is the radial distance of each blade section. For the OH-6A, the angular frequency, $\Omega = 50.26$ rad/sec, therefore the power per blade is found to be 0.74 horsepower as given by :

$$P = T_{sh} \cdot \Omega \quad (3.26)$$

TABLE 3.2 LOCAL REDUCED FREQUENCY, $K_p(r)$, PROPULSIVE FORCE, $P_{sh}(r)$ AND TORQUE, $T_{sh}(r)$.

r/R	$k(r/R)$	$U(r/R)$	$P_{sh}(r/R)$	$T_{sh}(r/R)$
[--]	[--]	[ft / sec]	[lbf]	[ft-lb]
0.1	0.863	66.4	0.0618	0.122
0.2	0.4315	132.8	0.0798	0.26
0.3	0.2877	199.2	0.9530	0.44
0.4	0.258	265.6	0.108	0.64
0.5	0.173	332.0	0.118	0.86
0.6	0.144	398.4	0.127	1.09
0.7	0.1233	464.8	0.134	1.32
0.8	0.1079	531.2	0.139	1.56
0.9	0.0959	597.6	0.144	1.81

$$\sum T_{sh} = 8.1 \text{ ft-lb}$$

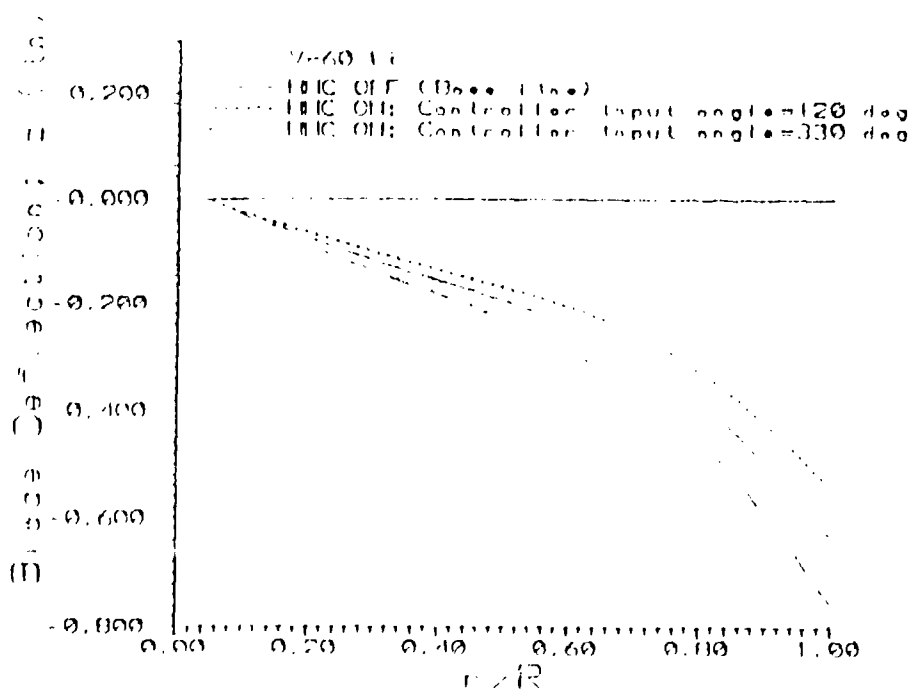


Figure (3.8) Blade Deflection vs Radial Station at 2P

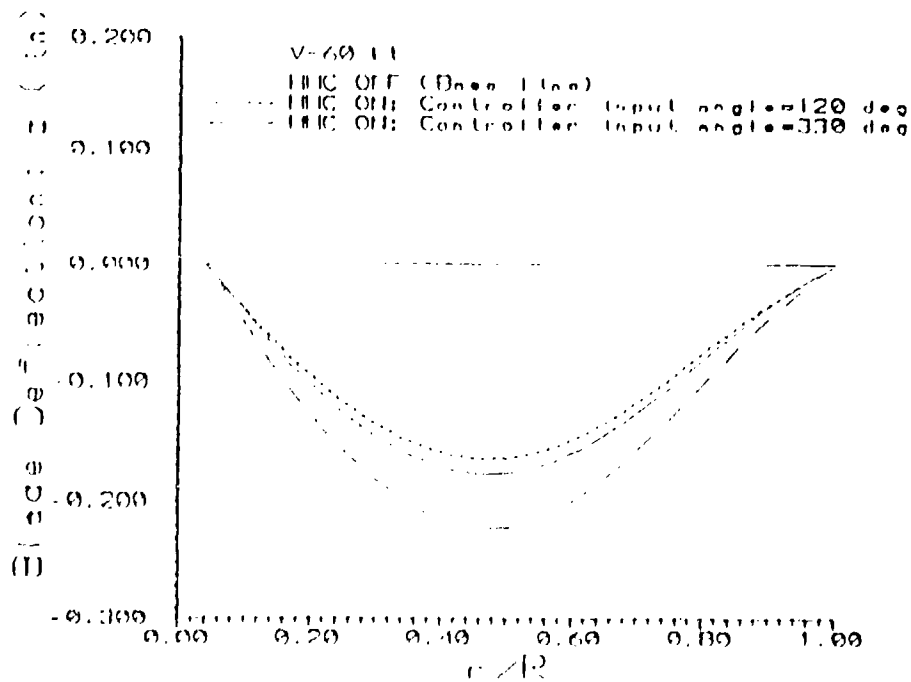


Figure (3.9) Blade Deflection vs Radial Station at 3P

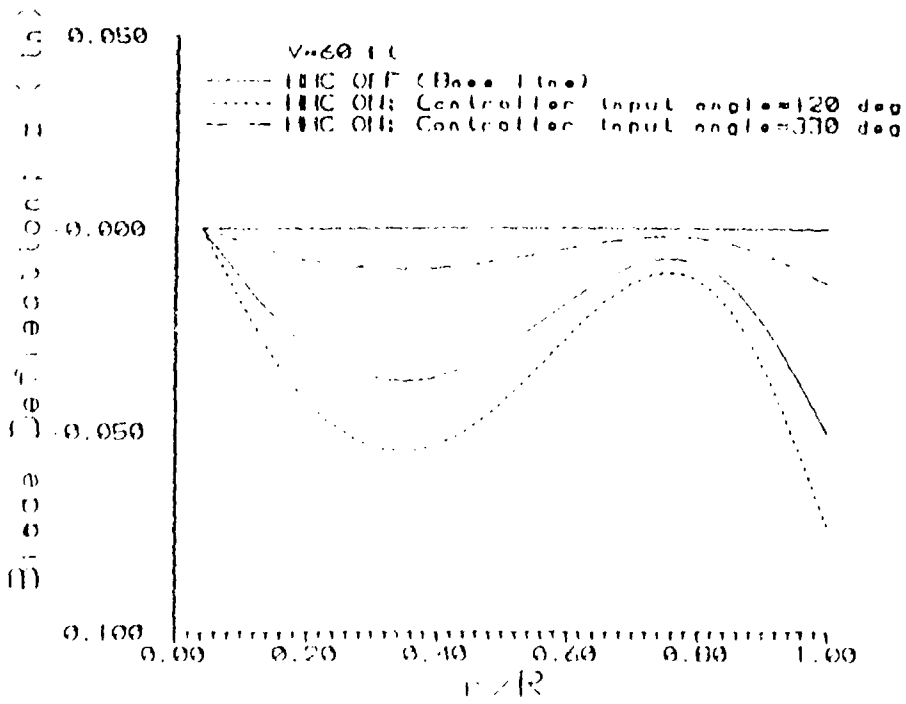


Figure (3.10) Blade Deflection vs Radial Station at 4P

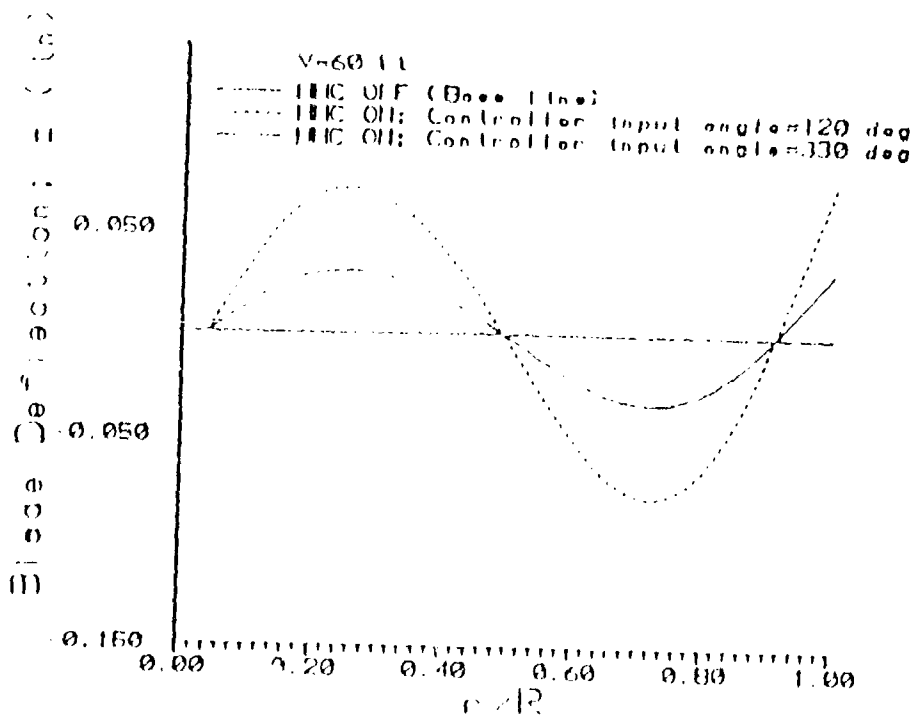


Figure (3.11) Blade Deflection vs Radial Station at 5P

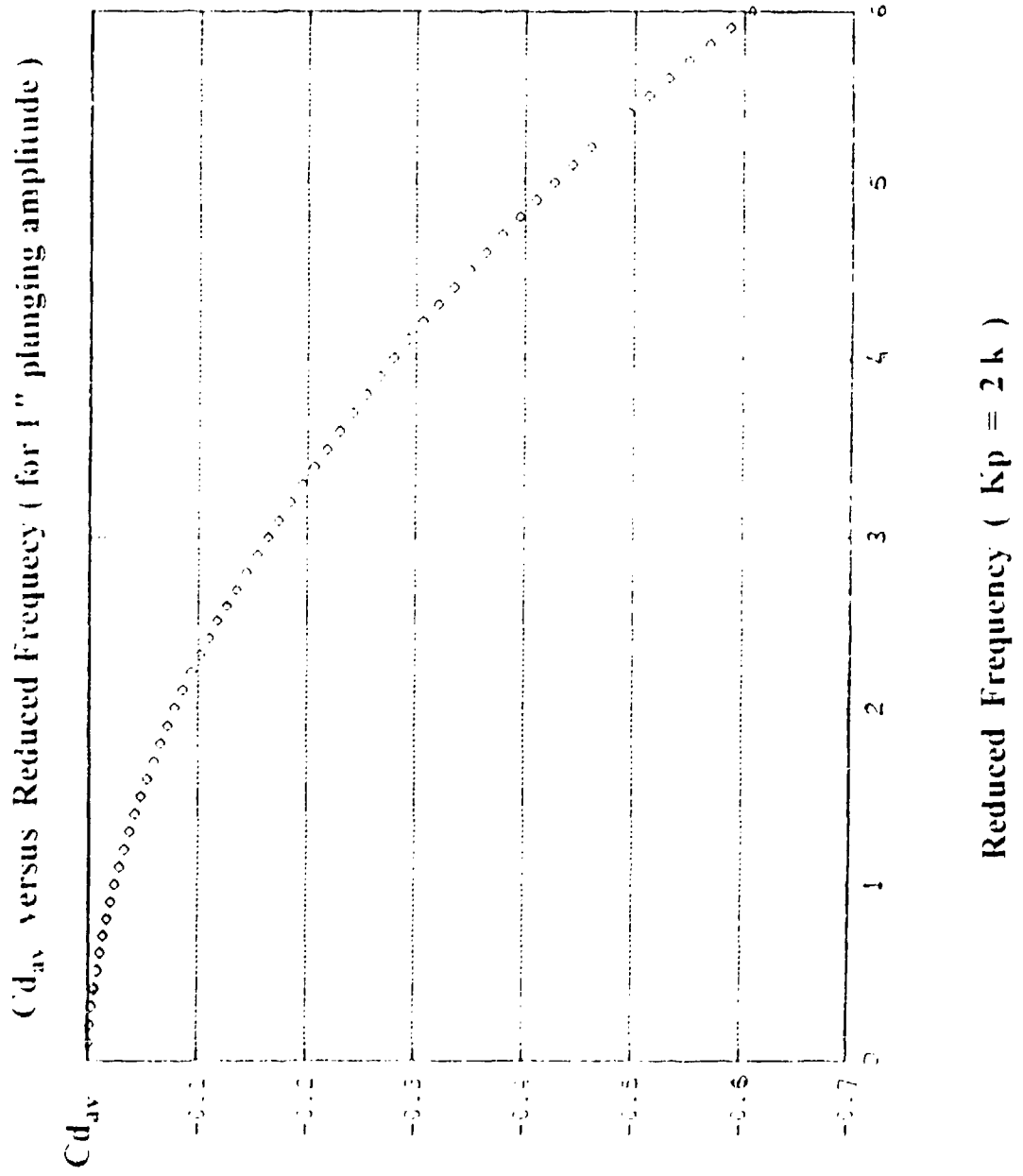


Figure (3.12) $C_{d_{av}}$ vs k_p (Plunging Amplitude 1")

TABLE 3.3 : $C_{d_{av}}$ versus REDUCED FREQUENCY K_p at $h_{bar} = 1''$

$k_p = 2k$	$C_{d_{av}}$
0.1	-0.0004937
0.2	-0.0018445
0.3	-0.003588
0.4	-0.0056899
0.5	-0.008108
0.6	-0.01082
0.7	-0.01363
0.8	-0.01724
0.9	-0.02057
1	-0.02457
1.1	-0.029702
1.2	-0.033156
1.3	-0.0379
1.4	-0.04291
1.5	-0.04822
1.6	-0.05382
1.7	-0.05972
1.8	-0.06592
1.9	-0.07241
2	-0.079203
2.1	-0.08633

IV. ANALYSIS OF WAKE INTERFERENCE EFFECTS

A. INTRODUCTION

The results of Chapter III show that propulsive forces, generated solely by plunge oscillations of an airfoil are insufficient to explain the power reduction observed and measured on the OH-6A helicopter. Therefore, in this chapter, we examine whether the power reduction might be caused by favorable wake interference effects due to the wakes shed from preceding blades.

To this end, the extension of the unsteady panel code to the case of two airfoils [25] was adopted and applied to the study of the wake interference effects between two helicopter blades. Wake interference effects were studied in the 1950's by Loewy [4] by extending Theodorsen's analysis. Loewy treats an infinite number of layers of shed vorticity placed beneath the rotor at a given wake spacing and develops a modified lift deficiency function. His interest was in the possibility of wake-induced blade flutter, which restricted his analysis to the determination of lift and pitching moment changes due to wakes shed from preceding blades. A closer inspection of Loewy's paper suggests that it should be possible to use the same approach to examine drag and propulsive force changes on the reference blade due to wakes shed from neighbouring blades.

Further, it is desirable to carry this one step further and investigate the case of a single wake shed from the preceding blade which interferes with the wake shed from the reference blade¹. This case allows a direct comparison with the unsteady two-foil panel code.

Also, there are regimes of helicopter flight where only the first layer of shed vorticity is of consequence. In the following sections we first describe the two-foil panel code and Couch's modification of the Loewy analysis. This is followed by a presentation and comparison of the major results.

B. UNSTEADY TWO-FOIL PANEL CODE

The extension of the single airfoil code (previously described) to the case of two airfoils requires no new building blocks. However, the two-foil analysis requires the introduction of five frames of reference, namely two moving local frames of reference which are attached to the two airfoils, two frozen local frames of reference, and the inertial frame of reference. Furthermore, it requires the satisfaction of the two Kutta conditions which are coupled non-linearly. The solution requires an iterative procedure to compute the two vorticity distributions.

¹ A detailed development of this theory is derived and presented in a recent NPS thesis by Mark Couch, Ref. [40].

It also necessitates the creation of a subroutine which transforms all coordinates in either of two local frames of reference to the global frame of reference. Finally, it requires the extension of the influence coefficient concept to include the effect of the second airfoil with its own wake and it requires the introduction of an additional influence coefficient, namely that on the wake element due to the wake element from the other airfoil. If each airfoil is modelled with N panels, then this produces a $2N \times (N+3)$ matrix which is subsequently solved by Gauss elimination.

Pang [25] was only able to verify this code by comparing the computed pressure distributions with previous work by Giesing [53]. Hence it was necessary to further evaluate the code by comparing its output with other known solutions before applying it to the oscillatory blade interference problem. These comparisons are given in section C.

The main parameters used in this code are: the airfoil type, number of panels, N , the relative locations of the two airfoils, initial angle of attack, amplitudes of oscillation (pure pitch, pure plunge or both), frequency of oscillation for each airfoil, the pivot points (for pitch cases), rise time (for ramp motions). These input parameters are in the file "fort.1"

This program produces an extremely large amount of output to the screen. It is convenient to write the output to a file on a Unix based machine during program runs. The output file can get very large for long program runs (when the time history is long)

For this reason, the logical variable "output" was added to the input file in two modes "true" or "false". When this variable is set to "false", the screen output is not printed and the required outputs are redirected to output files.

The following list describes the output files and the data they contain:

- fort.2: This is for user supplied airfoil coordinates, if desired.
- fort.3: This file contains the global coordinates of AF1 at each time step.
- fort.4: This file contains the global coordinates of AF2 at each time step.
- fort.7: This file contains the lift, moment, and drag coefficients for both airfoils.
- fort.8: This file contains the pressure coeff. for AF1 at each time step.
- fort.9: This file contains the pressure coeff. for AF2 at each time step.
- fort.10: This file contains the first airfoil's core vortex (wake) positions.
- fort.11: This file contains the second airfoil's core vortex (wake) positions.
- fort.12: This file contains the angle of attack at each time step.
- fort.13: This file contains the y-axis translational motion at each time step.

C. LOEWY'S ANALYSIS

Loewy [4] developed a two dimensional model for the unsteady aerodynamics of the blades of a hovering rotor, including the effect of the shed wakes. Figure (4.1), from reference [40], shows his two-dimensional model of the helical wakes. The wake in the case of a multi-bladed rotor in hover consists of helical vortex sheets below the disk, one from each blade.

Assuming sinusoidal motion, the downwash over the reference airfoil, V_1 and its vorticity (either bound or shed) may be written respectively as

$$V_1 = \bar{V}_1 e^{i\omega t} \quad \gamma_1 = \bar{\gamma}_1 e^{-i\omega t} \quad (4.1)$$

where the barred quantities are complex. The induced velocity at a point z on the airfoil resulting from an element of vorticity of strength $\gamma_{1,d}$ at a general point in the wake is given by [4]

$$dw(x,t) = \frac{\gamma_{1,d}(x-\xi) d\xi}{2\pi \left\{ (x-\xi)^2 + (nQ + q)^2 (h)^2 \right\}} \quad (4.2)$$

where Q is the total number of blades and h is the vertical distance between successive rows of vorticity, n is the number of revolution index, and q is the number of blades index as shown in Figure 4.1. The wake spacing, h is defined as [4]:

$$h = \frac{2\pi u}{bQ\Omega} \quad (4.3)$$

where u is the inflow velocity (time-averaged normal to the disk).

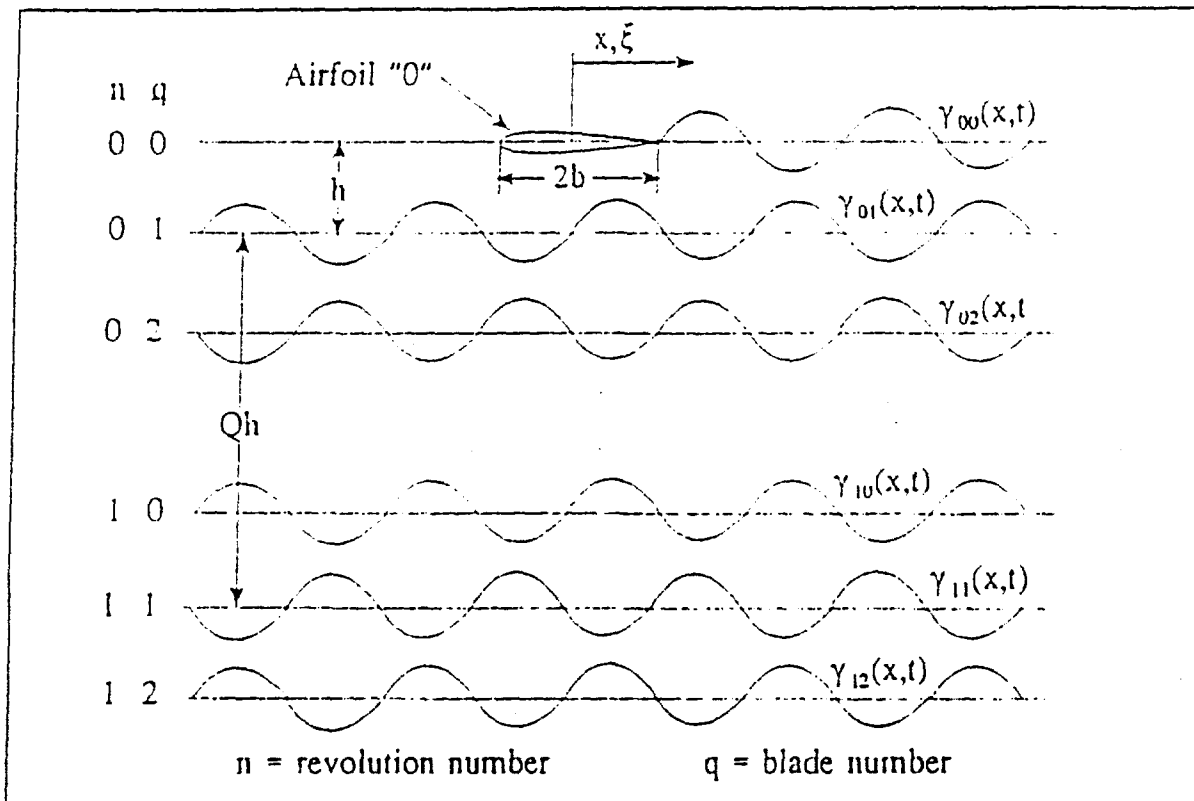


Figure (4.1) Aerodynamic Unsteady Model for a Multi-Bladed Rotor.

The total downwash over the airfoil can be expressed conveniently by summing the integrals involving the bound vorticity and the row of vorticity in the plane of the reference blade with those for the rows of vortices below the plane of the rotor :

$$w(x,t) = -\frac{1}{2\pi} \left[\int_1^1 \frac{\gamma_a(\xi) d\xi}{x-\xi} + \int_1^{\infty} \frac{\gamma_{00}(\xi) d\xi}{x-\xi} + \sum_{q=1}^{Q-1} \sum_{n=0}^{\infty} \int_{-\infty}^{\infty} \frac{\gamma_{nq}(\xi)(x-\xi) d\xi}{(x-\xi)^2 + (nQ+q)^2 h^2} + \sum_{n=1}^{\infty} \int_{-\infty}^{\infty} \frac{\gamma_{n0}(\xi)(x-\xi) d\xi}{(x-\xi)^2 + n^2 Q^2 h^2} \right] \quad (4.4)$$

The first two terms on the right-hand side of this integral equation are those that arise in the classical unsteady airfoil theory of Theodorsen [3], the third and fourth terms contribute the influence of all the vorticity below the plane of the rotor disc. Loewy solved the integral equation using Sohngen's inversion formula [31], and obtained his lift deficiency function, $C(k, m, h)$, which is given by :

$$C(k, m, h) = F(k, m, h) - i G(k, m, h) \quad (4.5)$$

where k is the reduced frequency (defined by $\omega b/U$), m is given by the ratio ω/Ω , h is the wake spacing defined before, and the real and imaginary parts of Loewy's lift deficiency function, F, G are given by [4]:

$$F(k, m, h) = \frac{J_1 \alpha A - (Y_1 + \beta J_1) B}{A^2 + B^2}$$

$$-G(k, m, h) = \frac{(Y_1 + \beta J_1) A + J_1 \alpha B}{A^2 + B^2}$$

where

$$A = J_1 \alpha + Y_0 - J_0 \beta \quad , \quad -B = Y_1 + J_1 \beta - J_0 \alpha$$

and

$$\alpha = \frac{e^{kh} - e^{-kh}}{e^{kh} - 2 \cos(2\pi m) + e^{-kh}} \quad , \quad \beta = \frac{2 \sin(2\pi m)}{e^{kh} - 2 \cos(2\pi m) + e^{-kh}}$$

Here it can be seen that as the spacing between rows of vorticity, h , becomes infinite, F' approaches F and G' approaches G . Also as k tends to infinity, $C'(k,m,h)$ approaches $C(k)$. When h is zero, all the vorticity lies in the plane of the airfoil, singularities result, and the meaning of any obtained results, physically speaking, is not clear [4]. Loewy [4], and Couch [40] showed plots for F' and G' versus reduced frequency k . Loewy treats an infinite number of wakes and Couch explores a finite number including the special case of a single wake. These plots show the effects due to wake phasing, m , and wake spacing, h . A case of special interest is the wake shedding from one preceding blade only. For this case Loewy's lift deficiency function, C' , reduces to the following lift function, C^* , obtained by Wood and Couch [40]:

$$C^* = F^* - i G^* \quad (4.6)$$

where
$$F^* = \frac{J_1(1+2\hat{\alpha}_N)A_N - (Y_1 - 2J_1\hat{\beta}_N)B_N}{A_N^2 + B_N^2}$$

$$G^* = -\frac{(Y_1 - 2J_1\hat{\beta}_N)A_N + J_1(1+2\hat{\alpha}_N)B_N}{A_N^2 + B_N^2}$$

$$A_N = J_1(1+2\hat{\alpha}_N) + Y_0 - 2J_0\hat{\beta}_N, \quad B_N = -Y_1 + 2J_1\hat{\beta}_N + J_0(1+2\hat{\alpha}_N),$$

$$\hat{\alpha}_N = \sum_{n=1}^N e^{-nkh} \cos 2\pi mn, \quad \hat{\beta}_N = \sum_{n=1}^N (-e^{-nkh} \sin 2\pi mn)$$

The propulsive force coefficient can be calculated and the results, obtained by Wood and Couch [40], using F^* and G^* are:

For pure plunge :
$$C_{p_r} = \pi k^2 \bar{h}_0^2 \left\{ (F^*)^2 + (G^*)^2 \right\}$$

For pure pitch :
$$C_{p_r} = \pi k^2 \alpha_0^2 \left\{ (F^*)^2 + (G^*)^2 \left[\frac{1}{k^2} + \left(\frac{1}{2} - a\right)^2 \right] + \frac{1}{2} \left(\frac{1}{2} - a\right) - (F^*) \left(\frac{1}{2} - a + \frac{1}{k^2}\right) - \left(\frac{1}{2} + a\right) \frac{(G^*)}{k} \right\}$$

D. EVALUATION OF THE TWO-FOIL PANEL CODE

Several analyses are available in the aerodynamic literature which permit a limited evaluation of the two-foil panel code. These are

1. Ground Effect on Airfoil Lift in Steady Flight

S. Tomotika et al [44] analyzed the ground effect on a 2-D flat plate using the method of conformal transformations. Figure 4.2 a shows the panel code results. Figure 4.2 b reproduces Tomotika results. It is seen that the two methods are in good agreement. Figure 4.3 a and Figure 4.3 b show the comparison between the result obtained by Wegley [46] for a 10% thick RAE101 airfoil in ground effect and the panel code prediction for a NACA 0010 at zero angle of attack. The two results are again seen to be in good agreement considering the fact that the RAE101 airfoil (whose coordinates are not known) was approximated by a NACA 0010 airfoil.

2. Biplane Effect

Glauert [45] defined a factor B which gives the lift reduction on the airfoil in an unstaggered biplane configuration compared to the lift on a monoplane at the same incidence. Table 4.1 gives the correction factor for several non-dimensional biplane spacings. It is seen from this table and from Figure (4.4) that the two results are again in reasonable agreement.

C/C_{l0} vs h/c

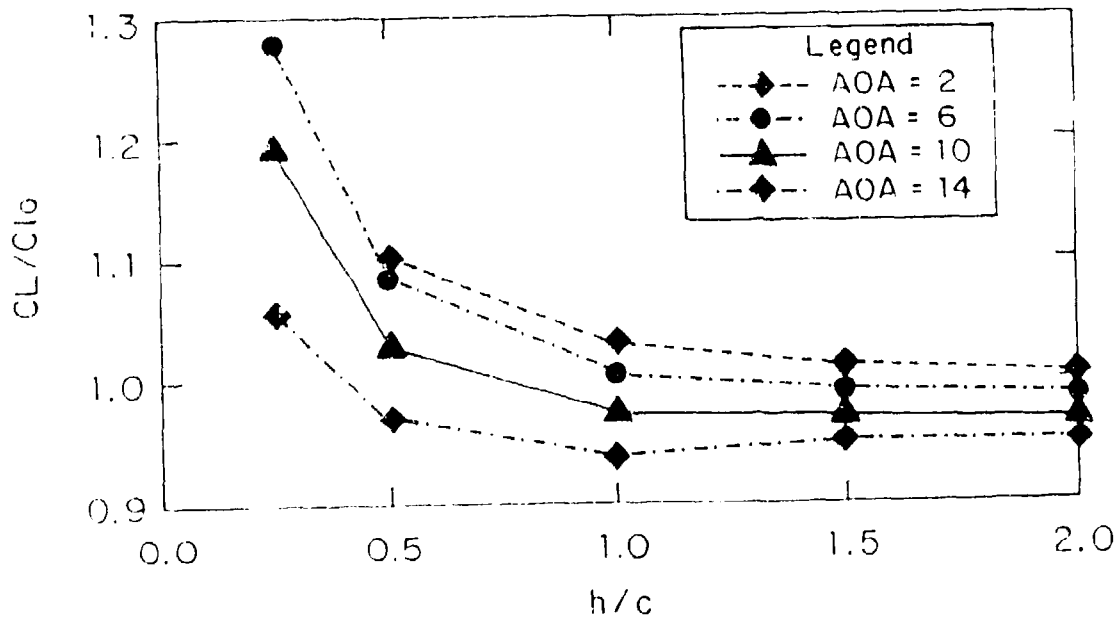


Figure 4.2 a C/C_{l0} vs h/c (Panel Code)

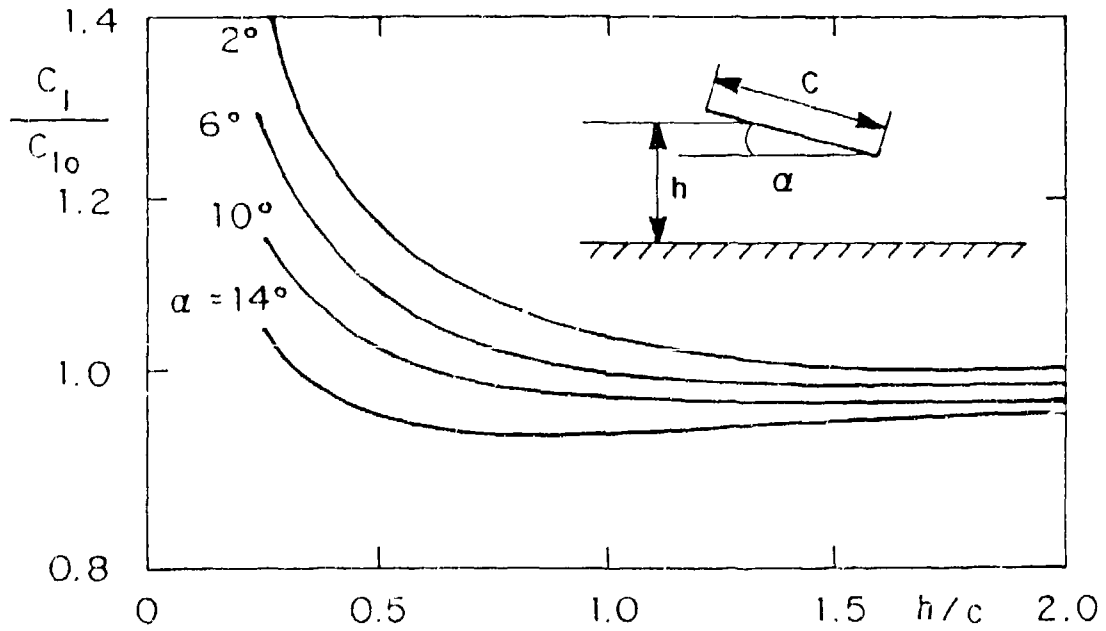


Figure (4.2 b) C/C_{l0} vs h/c (From Ref. [44])

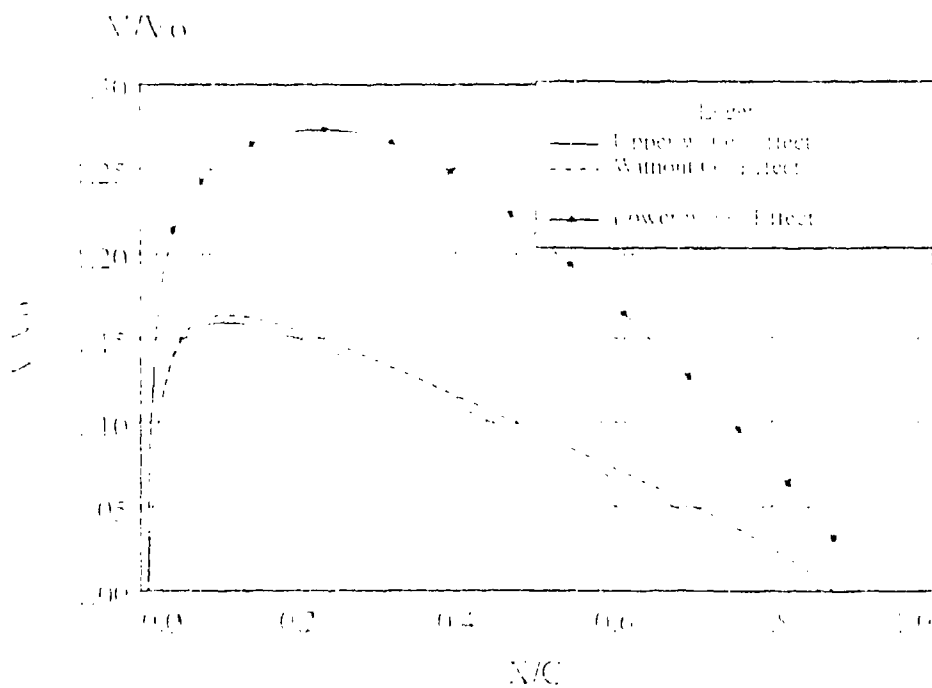


Figure (4.3 a) Local Velocity Distribution, V_a/V vs X/C (Panel Code)

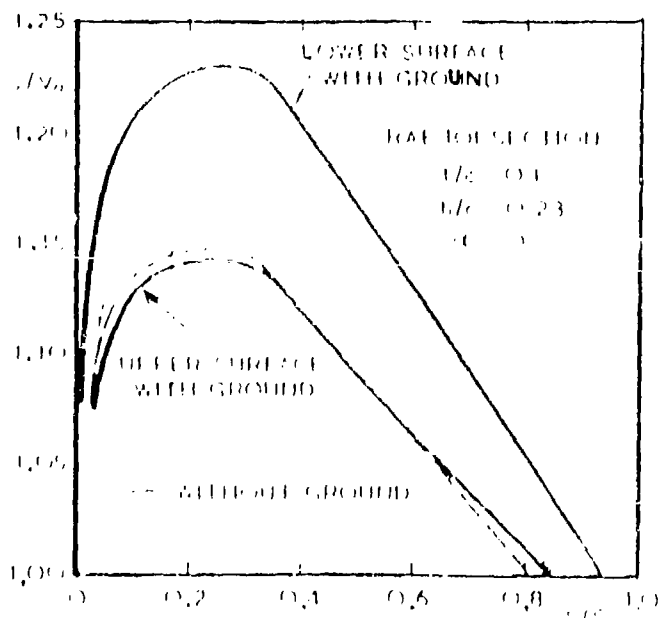


Figure (4.3 b) Local Velocity Distribution, V_a/V vs X/C (after Wegicy [46])

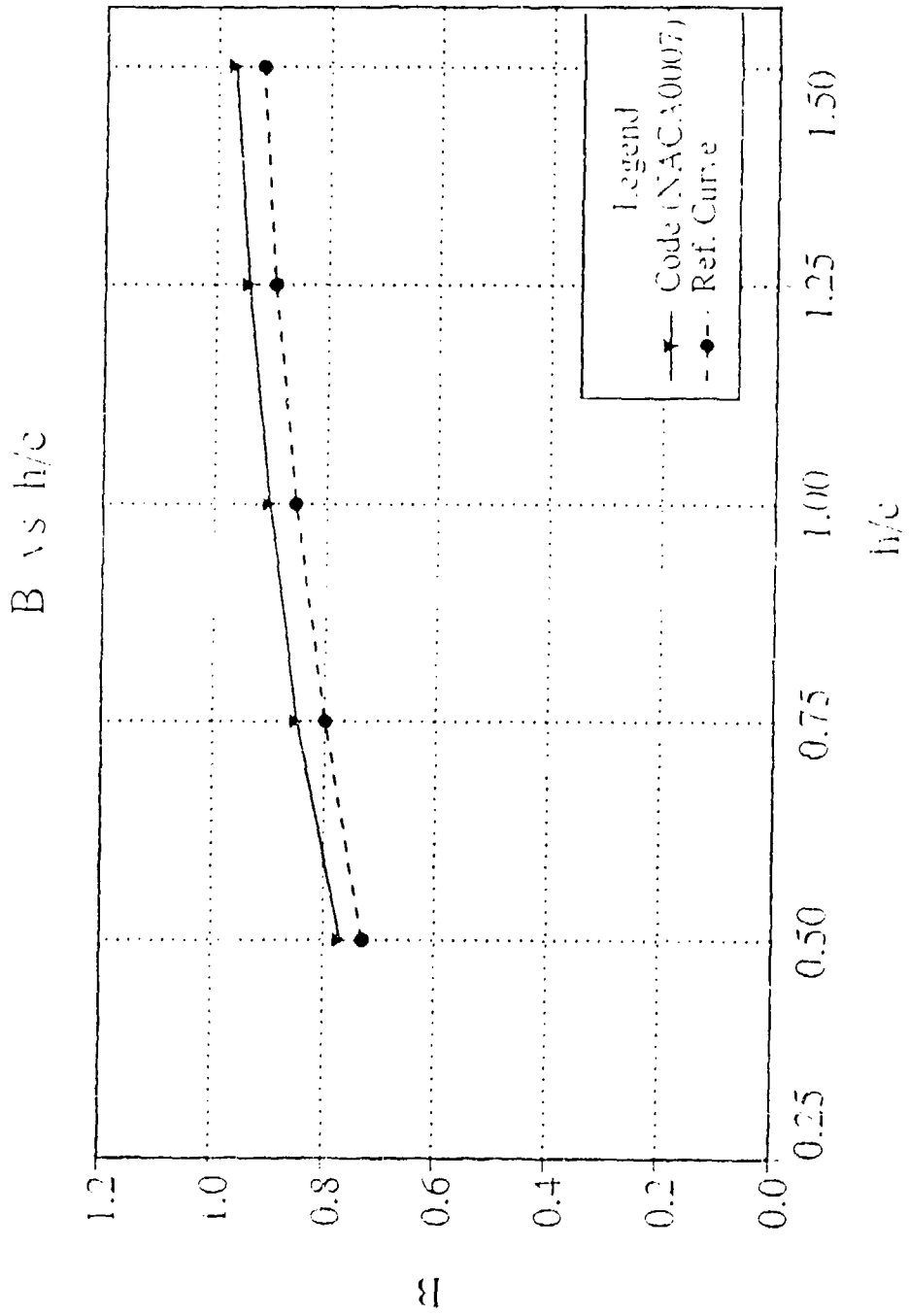


Figure (4.4) Correction Factor, B vs the Chord-gap Ratio h/c

TABLE 4.1 CORRECTION FACTOR FOR A BIPLANE

h/c	B (Code)	B (ref. [45])
0.50	0.770	0.730
0.57	0.847	0.800
1.00	0.902	0.855
1.25	0.942	0.895
1.50	0.97	0.920

Another ground interference study is due to Bagley [46]. As can be seen from the comparison of the panel code (Figure 4.5 a) with his predictions (Figure 4.5 b), in ground effect, the lift is reduced over the upper surface and increased over the lower surface. As the airfoil approaches the ground, the flow between the airfoil and ground is reduced and hence the pressure is increased.

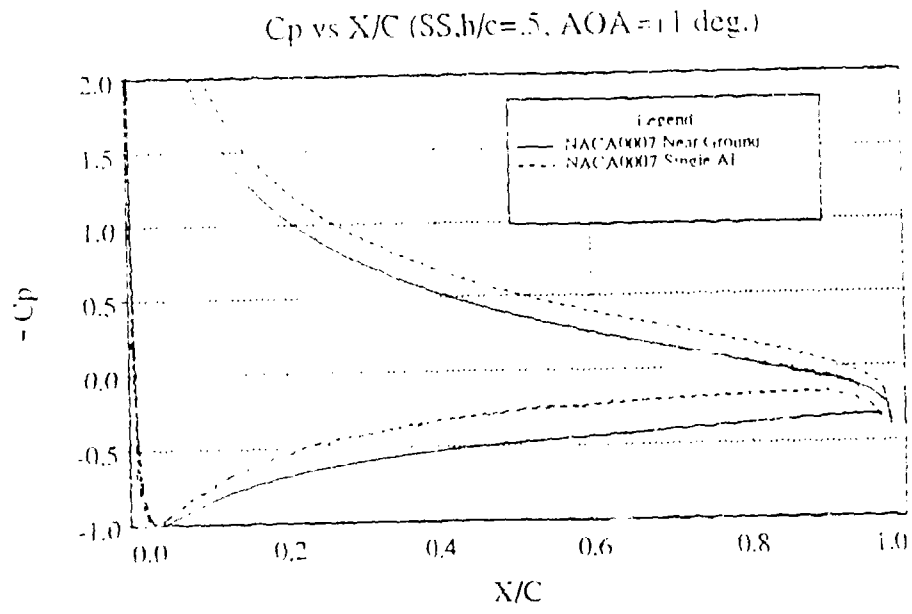


Figure (4.5 a) Pressure Distribution vs X/C (Panel Code)

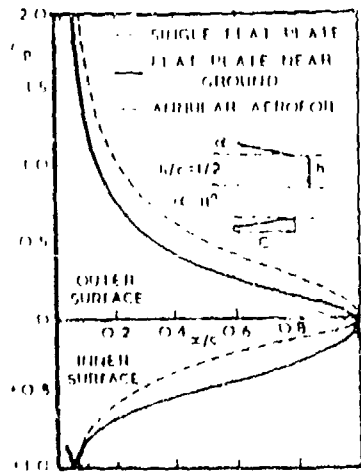


Figure (4.5 b) Pressure Distribution vs X/C (Bagley)

E. ANALYSIS OF OSCILLATORY BLADE INTERFERENCE EFFECTS

Having determined in Chapter III that pure flapping of a single helicopter rotor blade is unlikely to produce a drag reduction sufficient to explain the OH-6A HHC power reductions [1], solely due to the Katzmayr effect, we investigate in this section the possibility of favorable blade/wake interference effects. Consider the arrangement of the two airfoils shown in Figure (46). The wake shed from airfoil #2 impinges airfoil #1, if the vertical spacing between the two airfoils falls below a certain value, depending on the amplitude of oscillation of airfoil #2. This case cannot be analyzed with the unsteady panel code because the vortices start to penetrate the second airfoil or because the wakes shed from the two airfoils come in contact with each other, as shown in Figure (47).

On the other hand, if the vertical non-dimensional spacing is two or more no problems occur. A second important parameter is the horizontal spacing between the two airfoils. This parameter controls the phasing between the two wakes. Hence the unsteady two-foil code permits the analysis of Loewy's arrangement for the special case of two wakes. This case is considered by Wood and Couch [40] in closed form and presented in Ref. [39]. Furthermore, the single airfoil case is recovered if the vertical spacing is chosen to be large because the effect of the first airfoil on the second must diminish with increasing distance between the two foils.

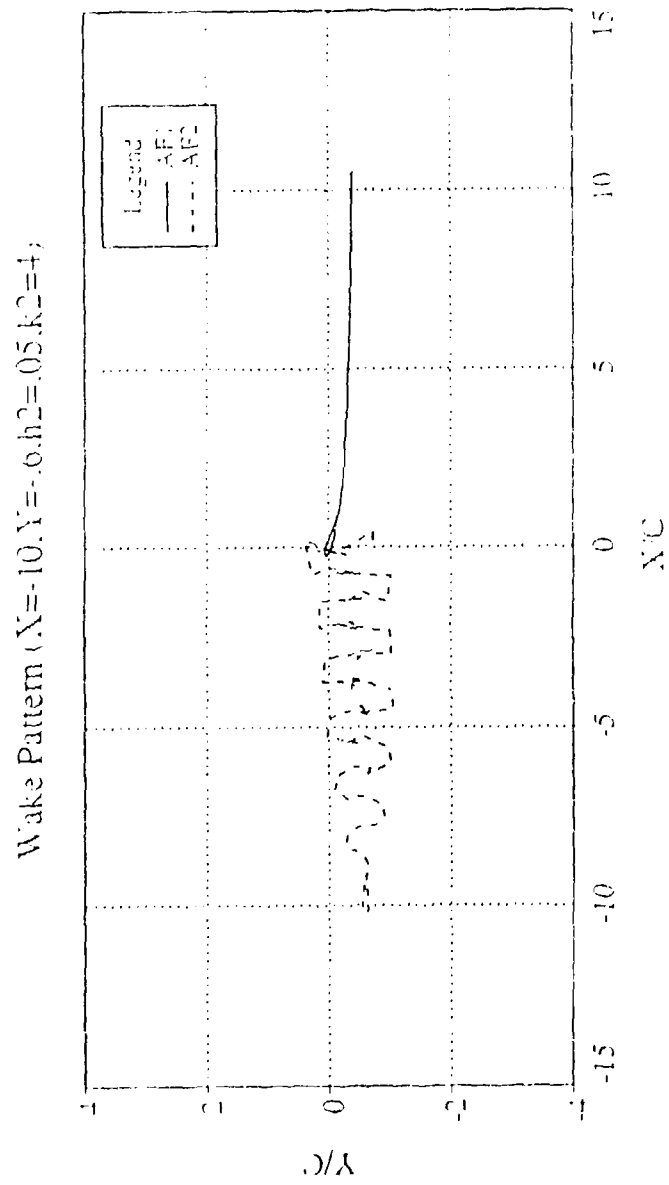


Figure (4.6) Wake Pattern (Airfoil # 2 Plunging at High reduced Frequency and Close to Airfoil # 1)

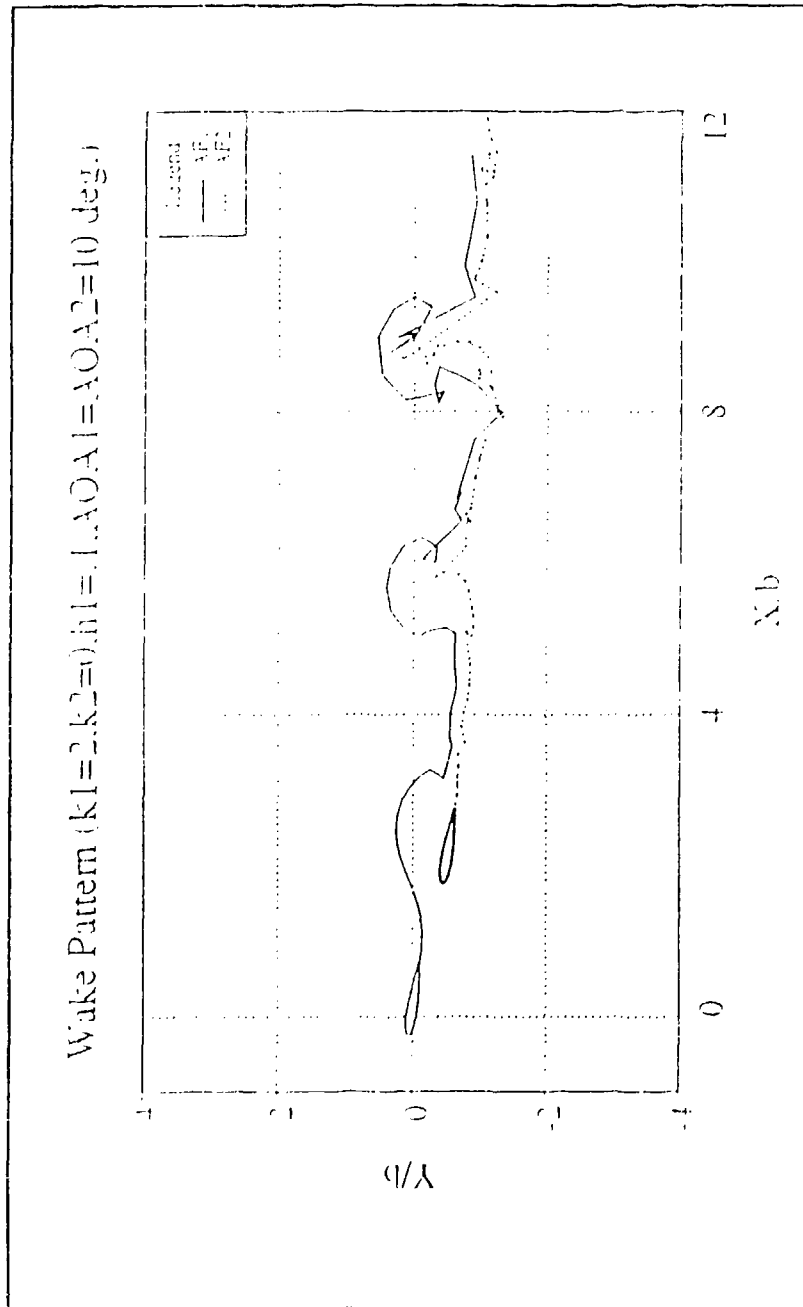


Figure (4.7) Wake Interference Between Two Plunging Airfoils in Close Proximity

Figure (4.8) and Figure (4.9) show the computed lift and drag (thrust) coefficient for airfoil # 1 in the presence of airfoil # 2. Both airfoils are oscillating in plunge with an amplitude of 0.14 and a reduced frequency of 0.0617. The vertical spacing between the two airfoils is 200. In this case the lift and thrust coefficients are found to be identical to the ones obtained from the single airfoil code, thus showing that a distance of 200 is sufficient to recover single airfoil results.

In Figures (4.10) to (4.21), on the other hand, the vertical spacing is reduced to 2. For these calculations, the time step is .3 to .5 time units. The plunging amplitude is again 0.14, the reduced frequency is 0.0617. The twelve figures 4.10 to 4.21 show four different cases of phasing between the two wakes. In Figures (4.10) to (4.12), the wake pattern, lift and drag are shown for zero phasing, $m = 0$, Figures (4.13) to (4.15) show a phase of $m = 0.20833$, Figures (4.16) to (4.18) show the case of $m = 0.25$, and Figures (4.19) to (4.21) show the case of $m = 0.5$.

A closer inspection of these figures reveals the strong effect of the wake phasing. For $m = 0$, airfoil # 1 experiences a reduction in thrust compared to the single foil, whereas for $m = 0.5$ airfoil # 1 experiences a significant increase in thrust. These results are summarized in Figure (4.22) where the single airfoil results are also shown as well as the predictions by Wood and Couch [40] when specialized to the case of two interfering wakes only. The agreement between the two predictions is encouraging.

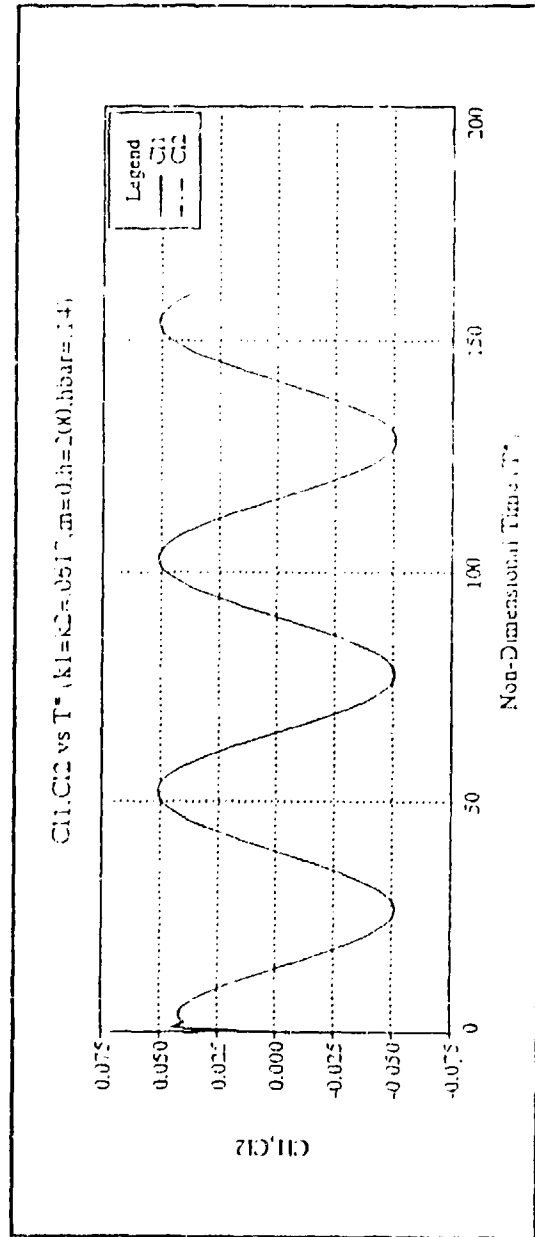


Figure (4.8) ($C1$ vs T^* (plunge, $m = 0$, $h = 200$))

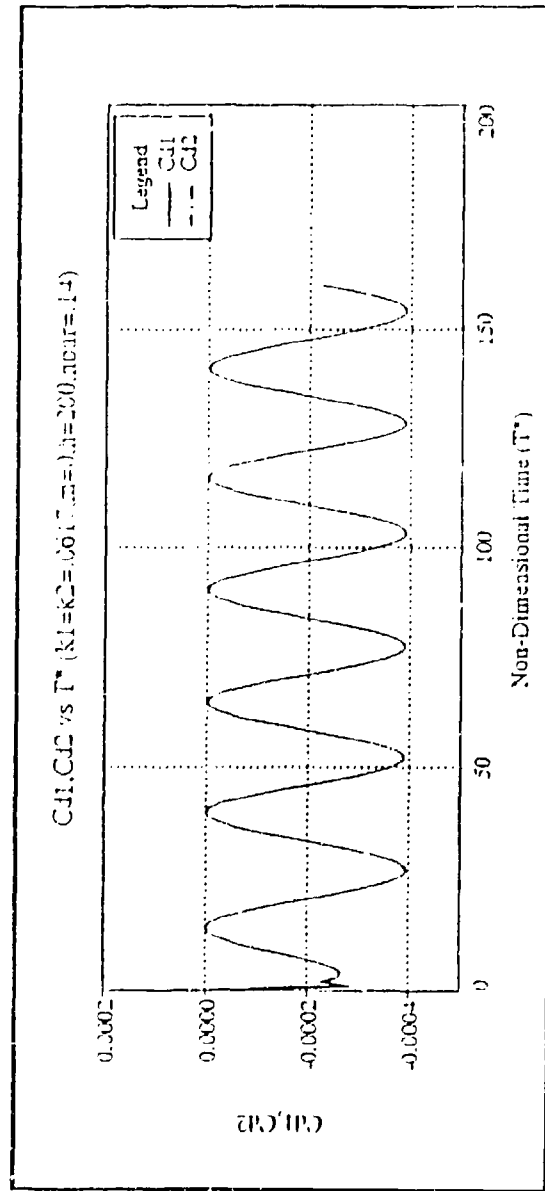


Figure (4.9) Cd vs T^* (plunge, $m = 0$, $h = 200$)

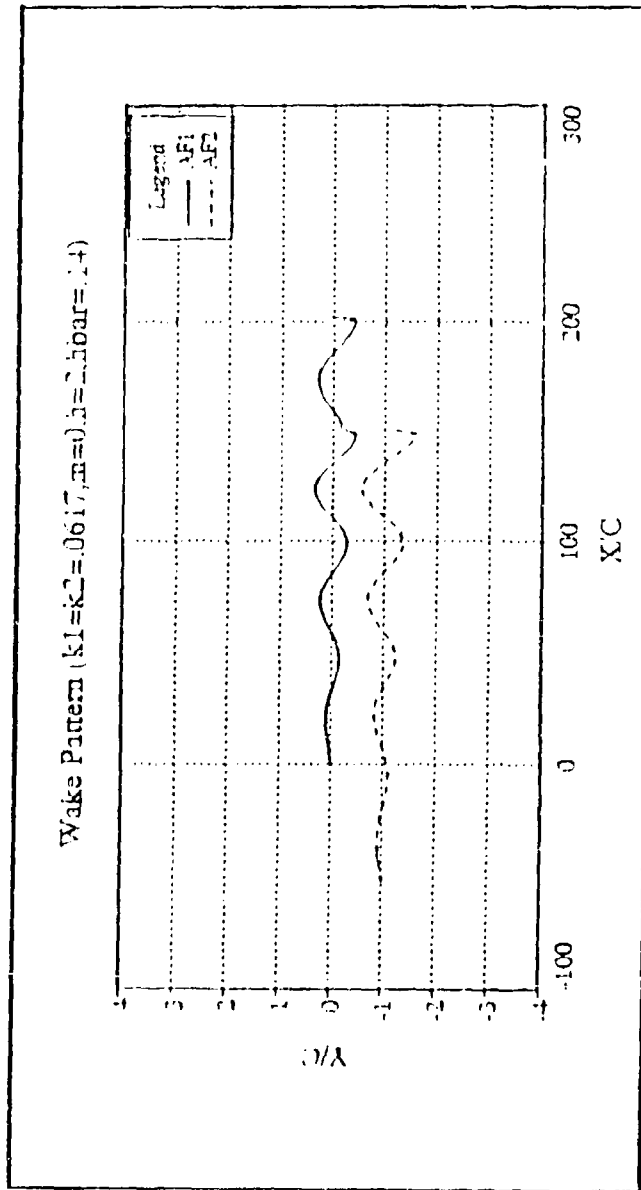


Figure (4.10) Wake Pattern (plunge, $m = 0, h = 2$)

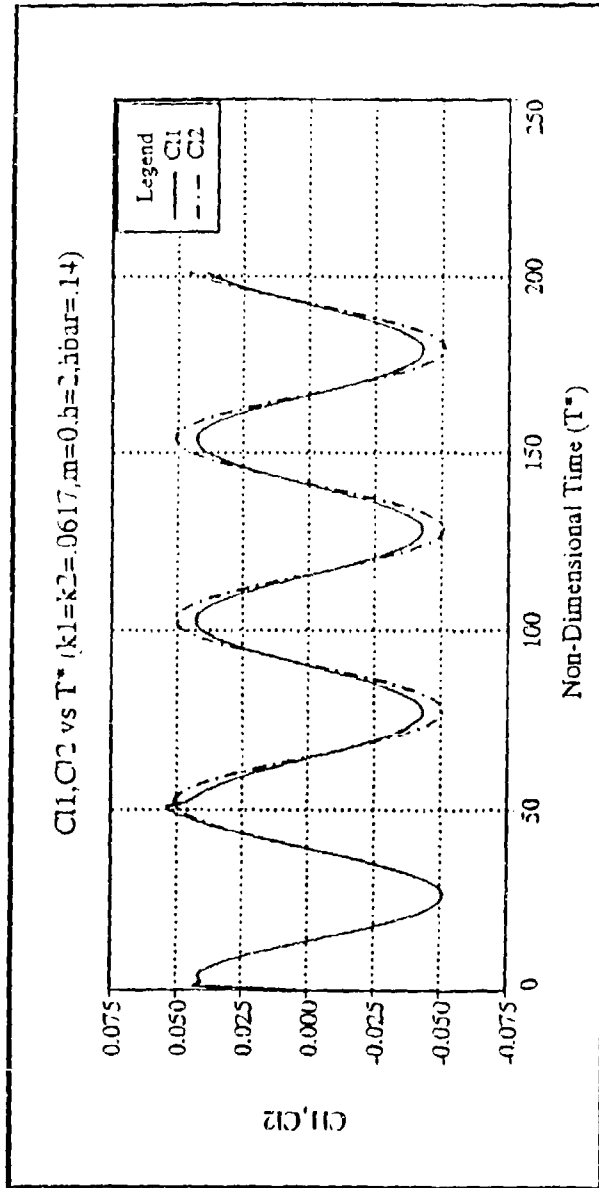


Figure (4.11) $C1$ vs T^* (plunge, $m = 0$, $h = 2$)

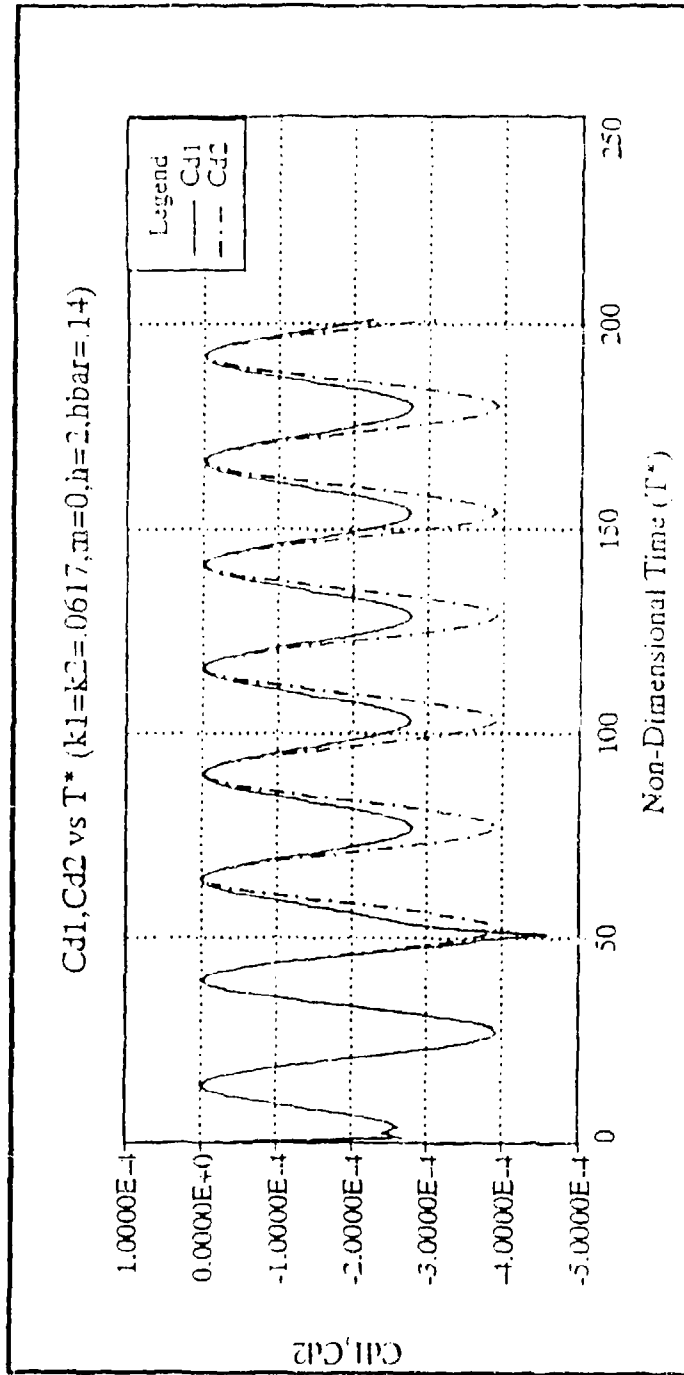


Figure (4.12) Cd vs T^* (plunge, $m = 0, h = 2$)

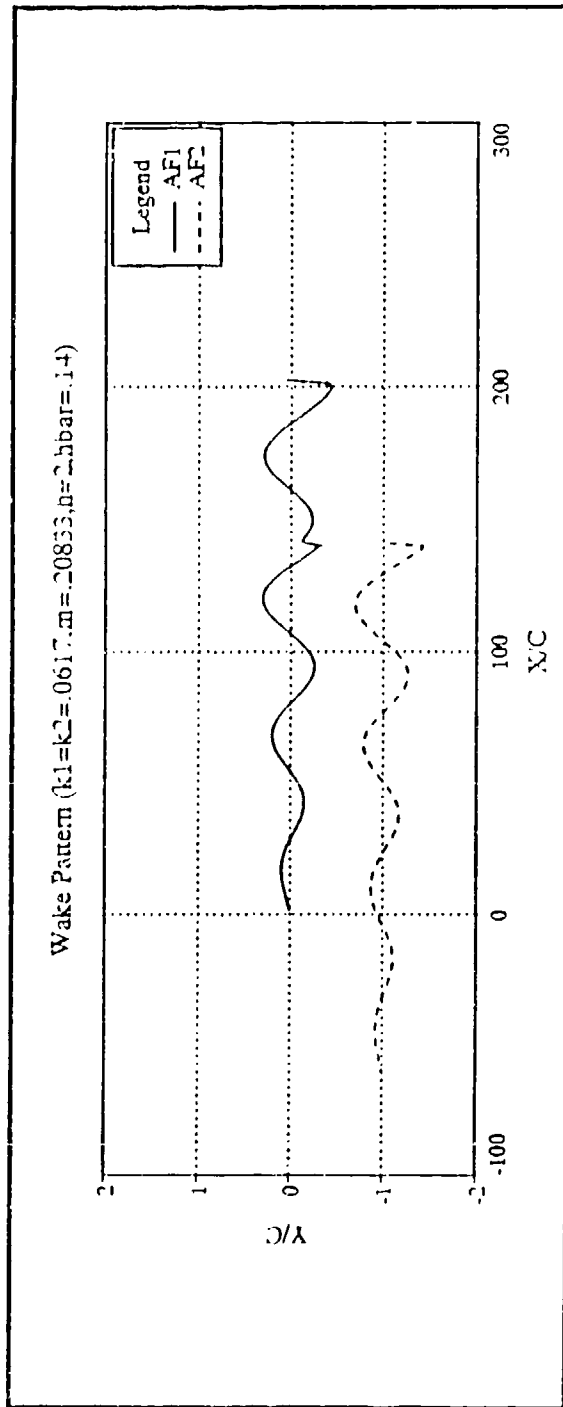


Figure (4.13) Wake pattern (plunge, $m = 0.20833$, $h = 2$)

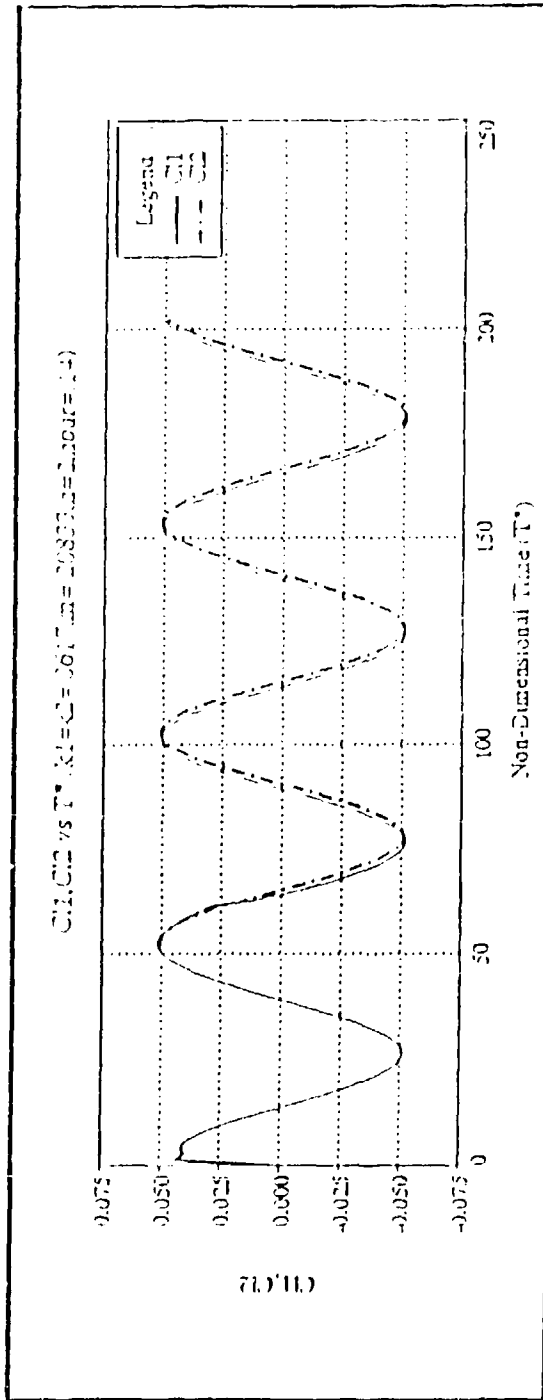


Figure (4.14) C1 vs T* (plunge, m = 0.20833, h = 2)

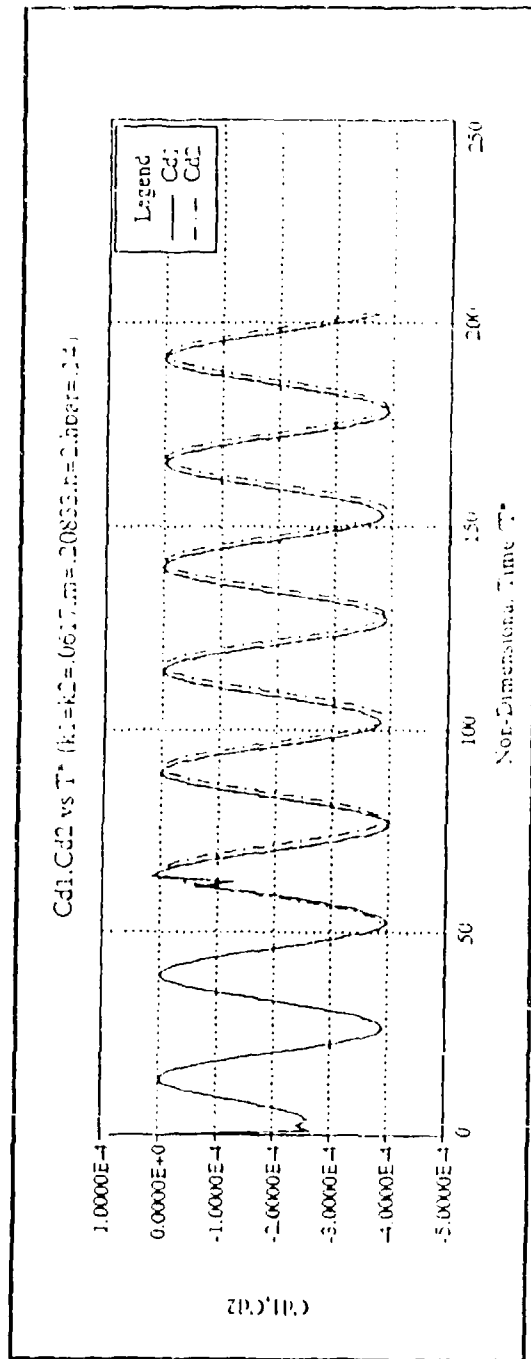


Figure (4.15) Cd vs T* (m=0.20833 , h = 2)

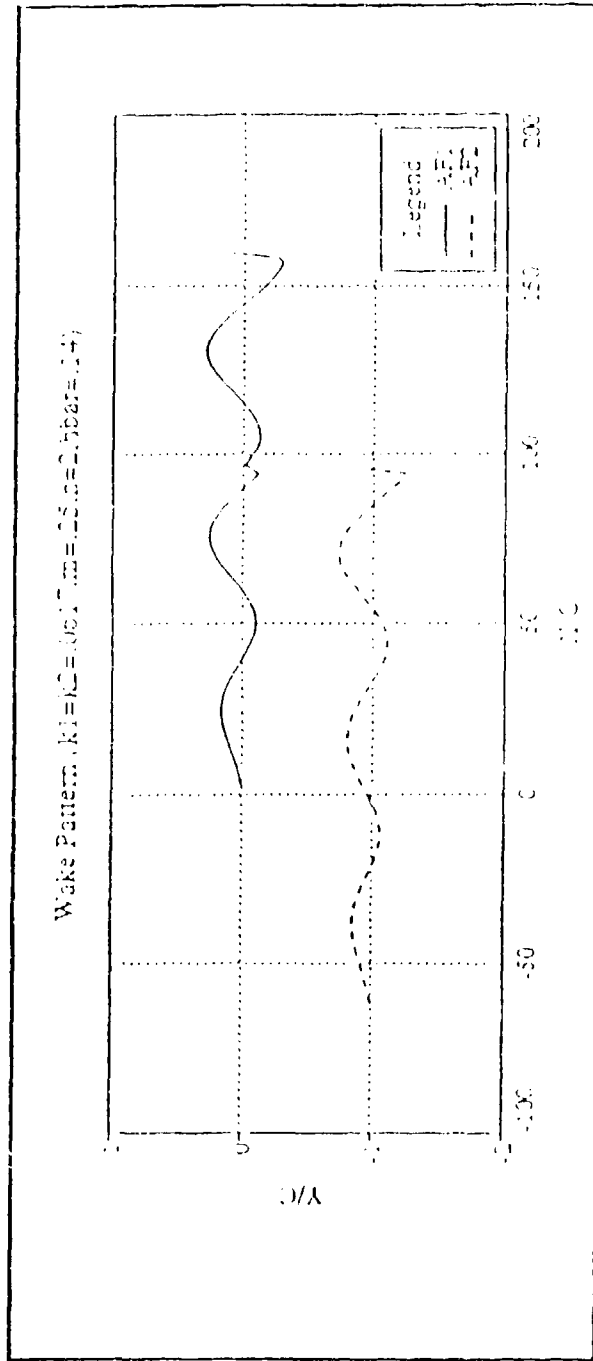


Figure (4.16) Wake pattern (plunge, $m = 0.25$, $h = 2$)

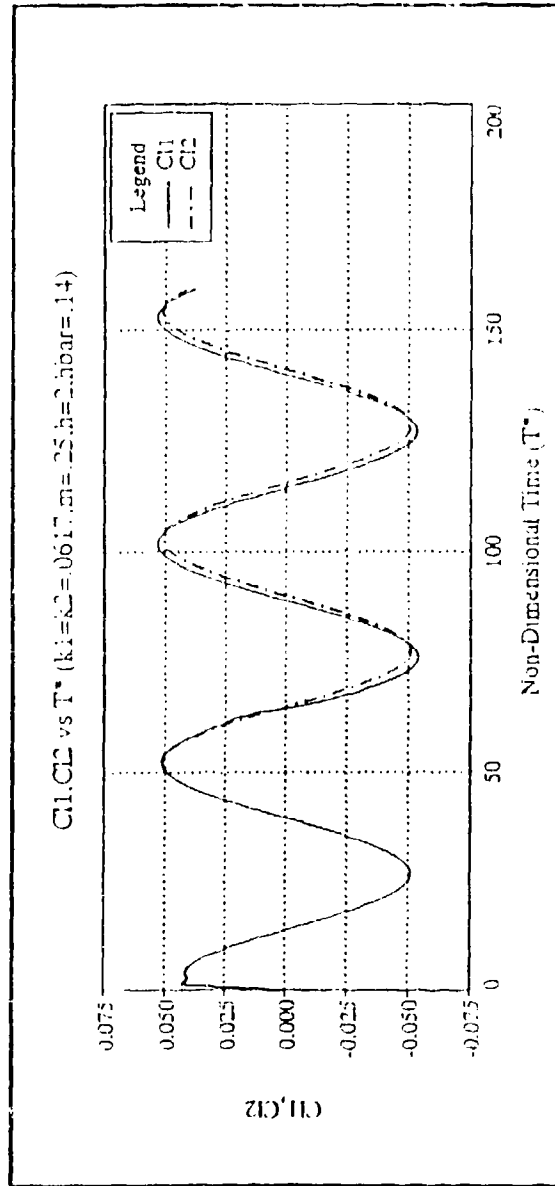


Figure (4.17) $C1$ vs T^* (plunge, $m = 0.25$, $h = 2$)

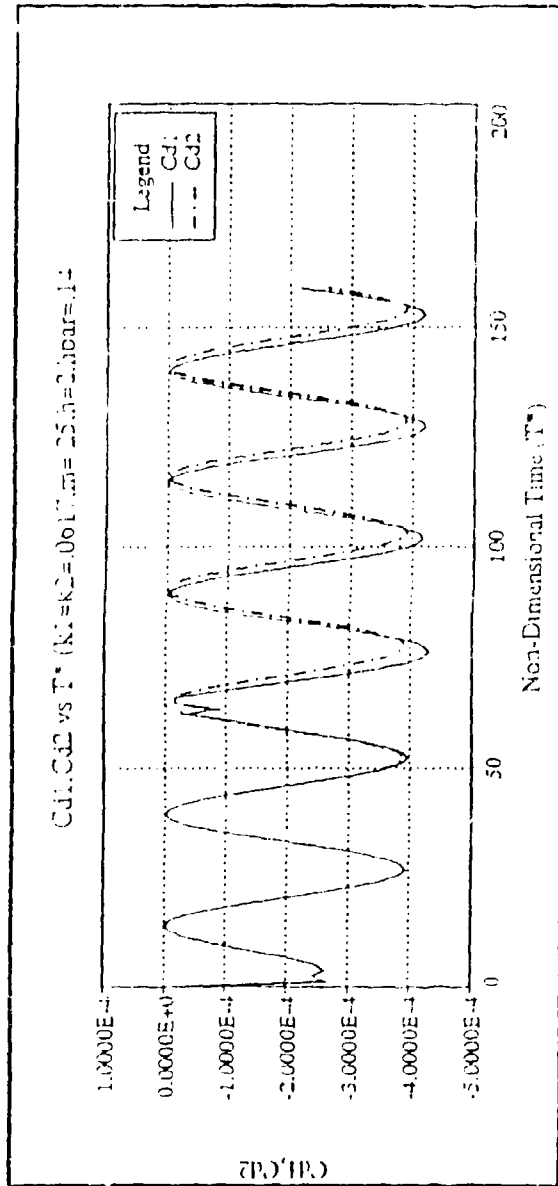


Figure (4.18) Cd vs T* (plunge, $m = 0.25$, $h = 2$)

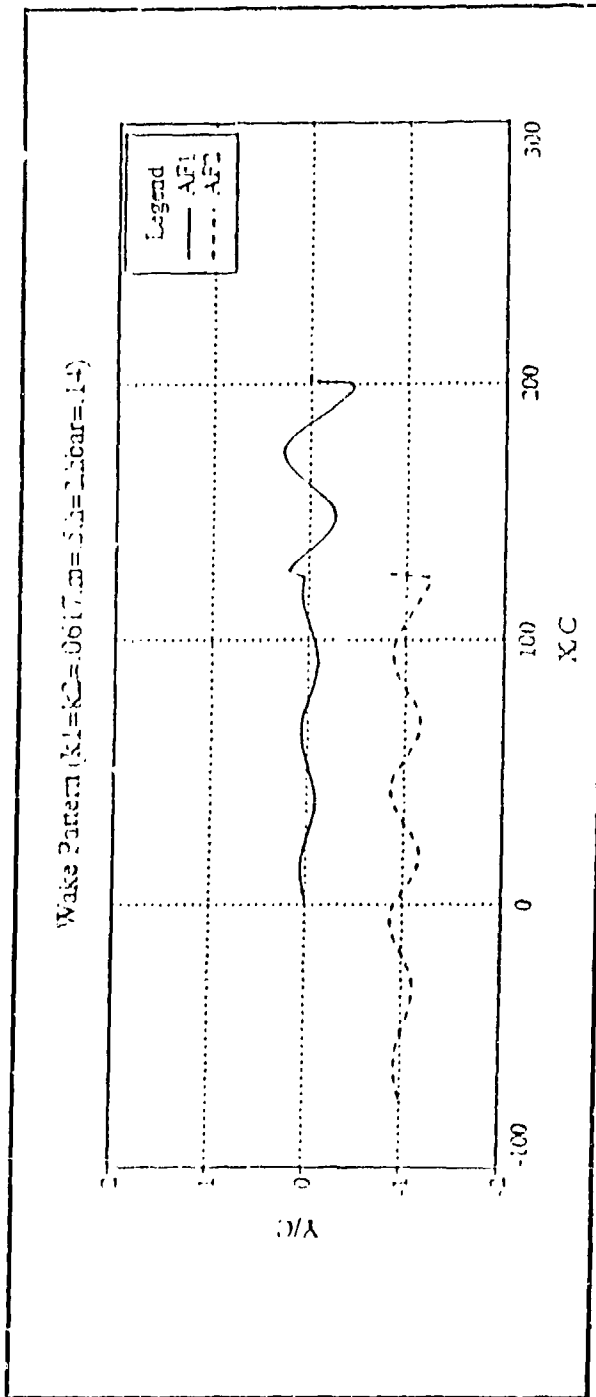


Figure (4.19) Wake pattern (plunge, $m = 0.5$, $h = 2$)

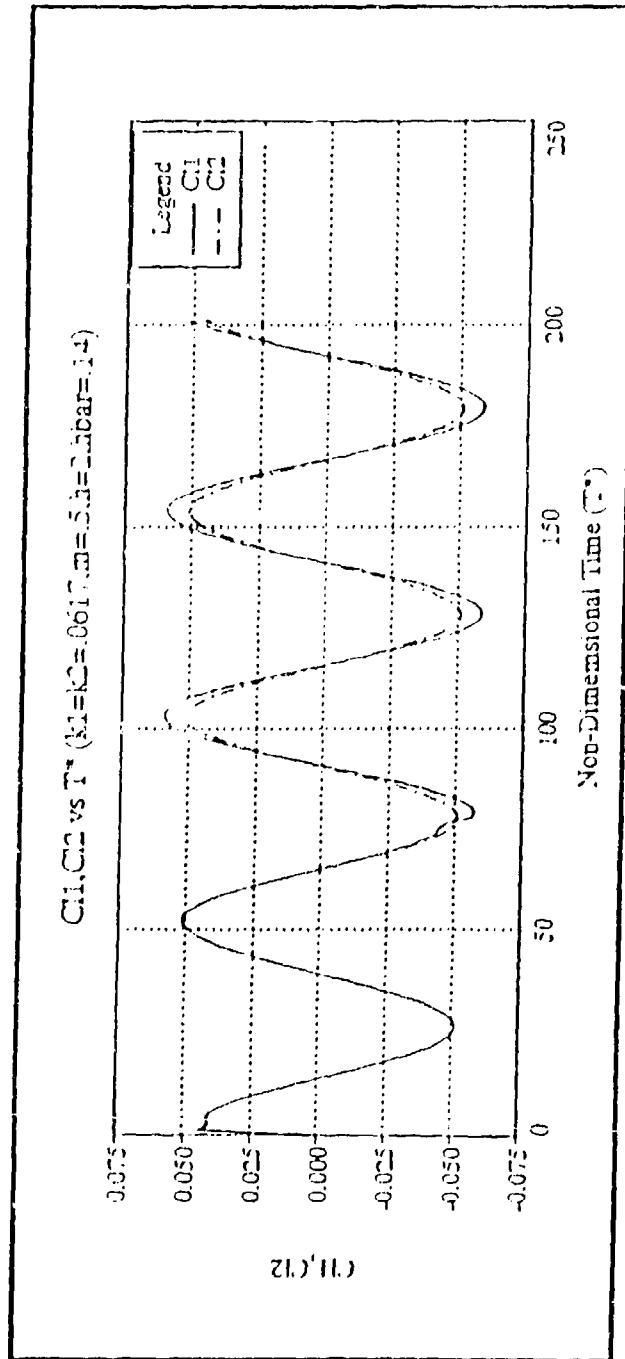


Figure (4.20) C_l vs T^* (plunge, $m = 0.5$, $h = 2$)

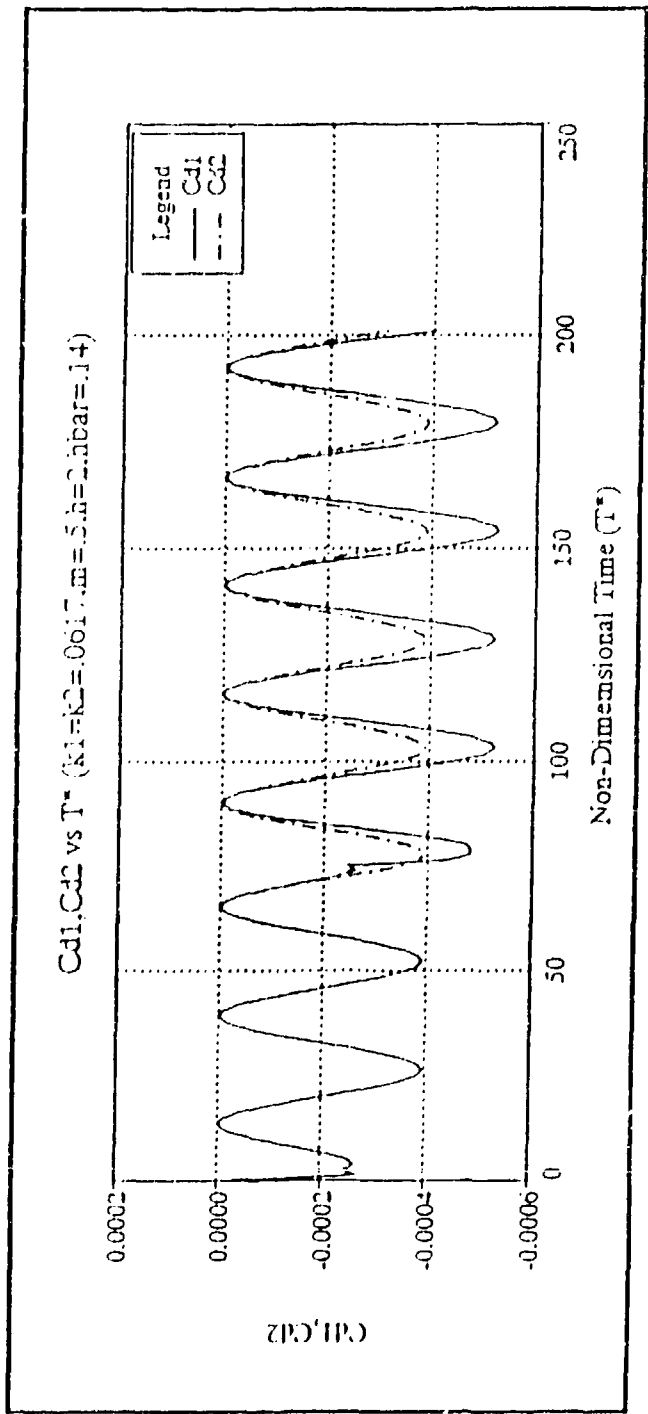


Figure (4.21) Cd vs T* (plunge, m = 0.5 , h = 2)

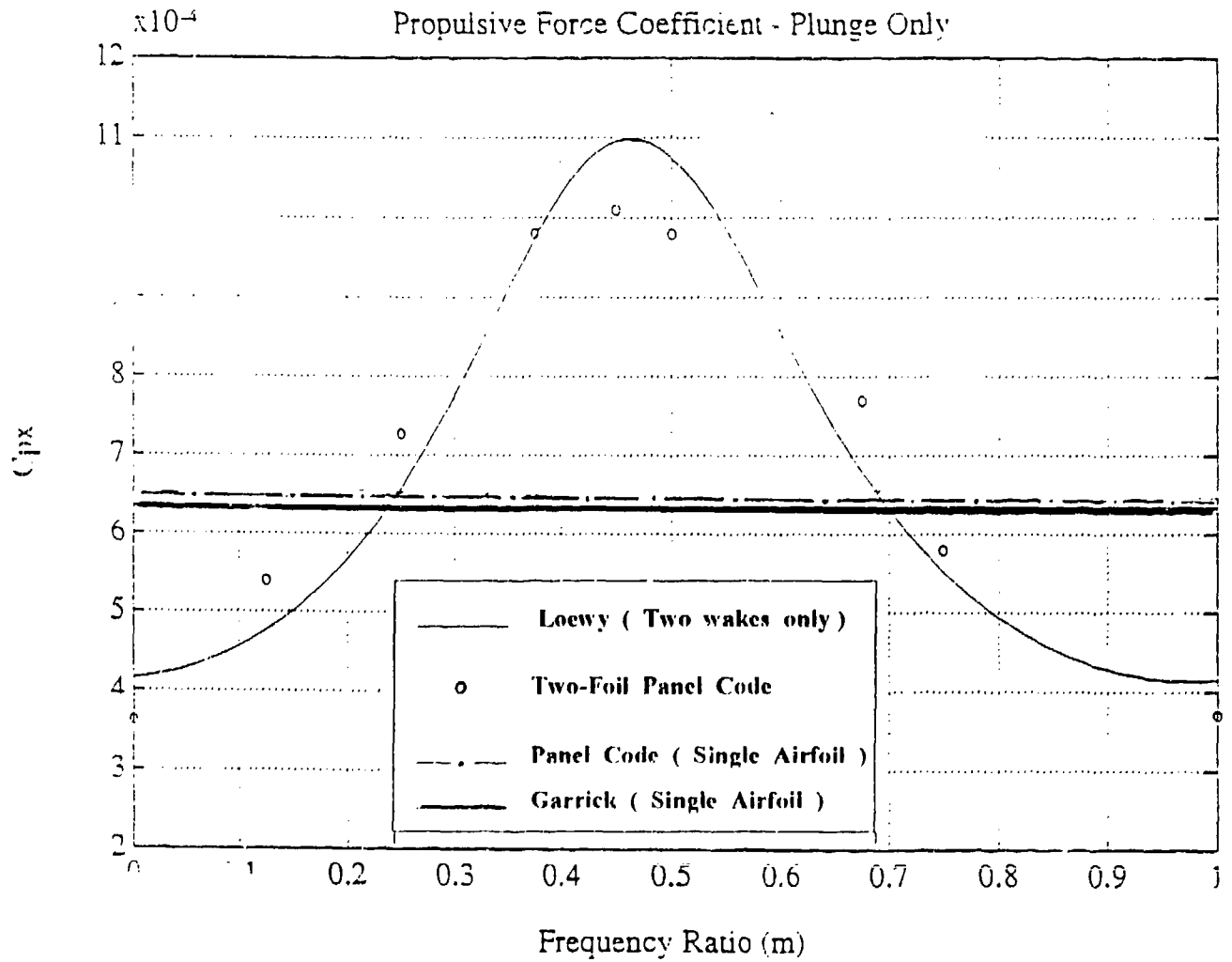


Figure (4.22) Average Propulsive Force Due to Plunge Versus Wake Phasing, m

Similar results are obtained for the pitch case. The airfoils studied are again NACA 0007 foils, pitching about the quarter-chord point with an amplitude of 1 degree and a reduced frequency of 0.0617. Figures (4.23) to (4.32) display the same phasing values as in the plunge case. These figures and the summarizing Figure (4.33) show again that values of m near zero and one produce increased drag compared to the single airfoil case, but values of m near 0.5 produce thrust, whereas the single airfoil produces drag. Both analyses, the analysis by Wood and Couch [40] for the special case of two wakes only and the panel code, produce similar trends. However, the quantitative agreement is not as good as in the plunge case. The precise reason is not sufficiently understood at this time. It appears that the resolution of the suction peaks over the leading edge and therefore the computation of the thrust is more sensitive in the pitch case than in the plunge case. Furthermore, it must be remembered that Loewy's analysis for an infinite number of wakes and that by Wood and Couch [40] for two wakes are based on the flat-plate assumption, whereas the panel code requires a minimum blade thickness in order to obtain accurate results. A further evaluation of the panel code can be done for the drag produced by a single airfoil pitching about the leading edge. In this case the analytical theory of Garrick [5] and the computational results of Bosch [15] are available. It can be seen from Figure (4.34) that the trends are again in agreement, but the code results deviate from Garrick's and Bosch's results with increasing frequency. These deviations must be attributed to the geometry differences (flat plate versus NACA 0007) and the higher amplitude used in the panel code. Note that the pitching airfoil starts to develop thrust only at a reduced frequency greater than about 1.8.

Wake Pattern ($k_1 = k_2 = 0.0617$, $\alpha_o = 1^\circ$, Wake Spacing, $h = 2$, $m = 0$)

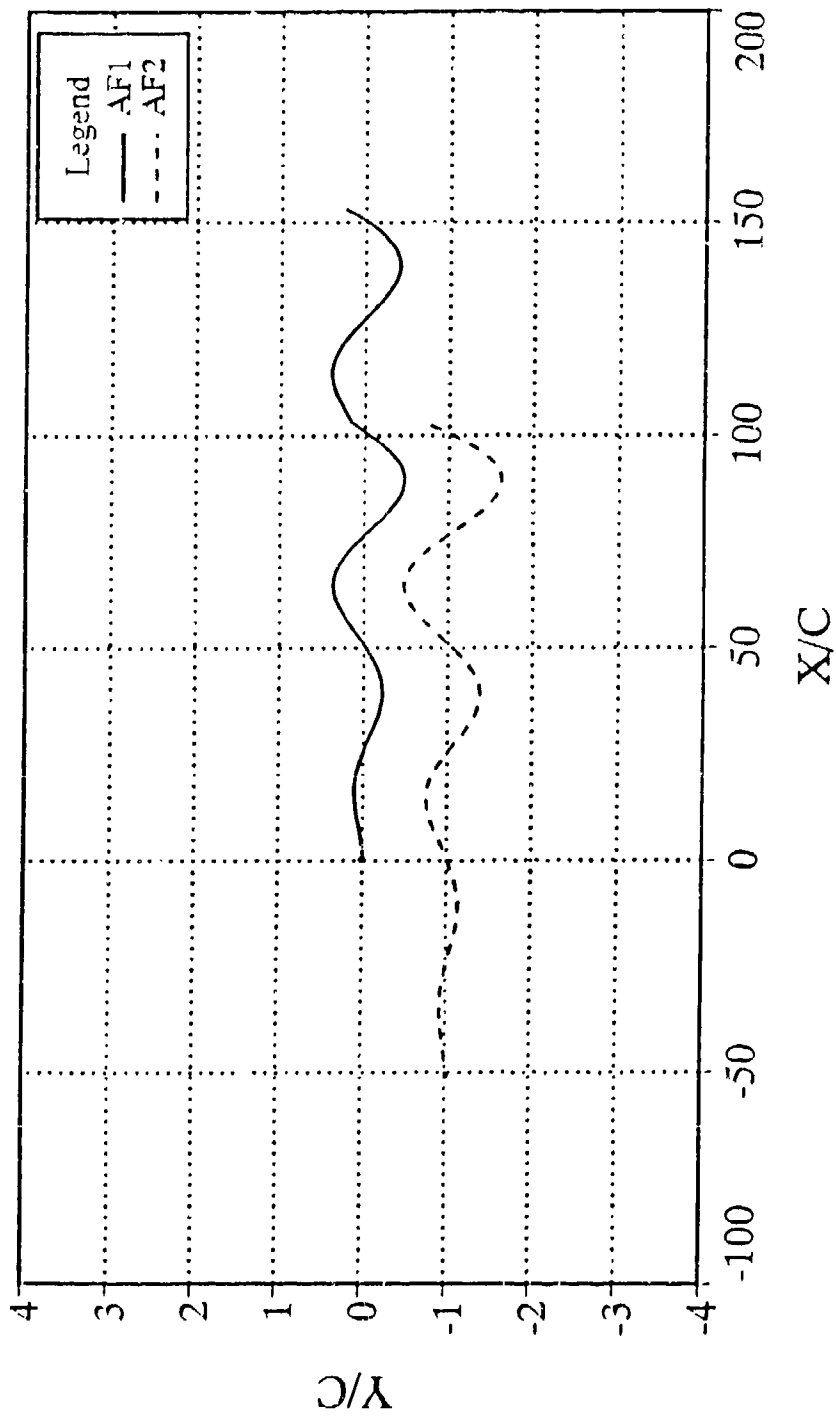


Figure (4.23) Wake pattern (pitch, $m = 0$, $h = 2$)

Cl vs T* (k1 = k2 = 0.0617, $\alpha_0 = 1^\circ$, Wake Spacing, h = 2, m = 0)

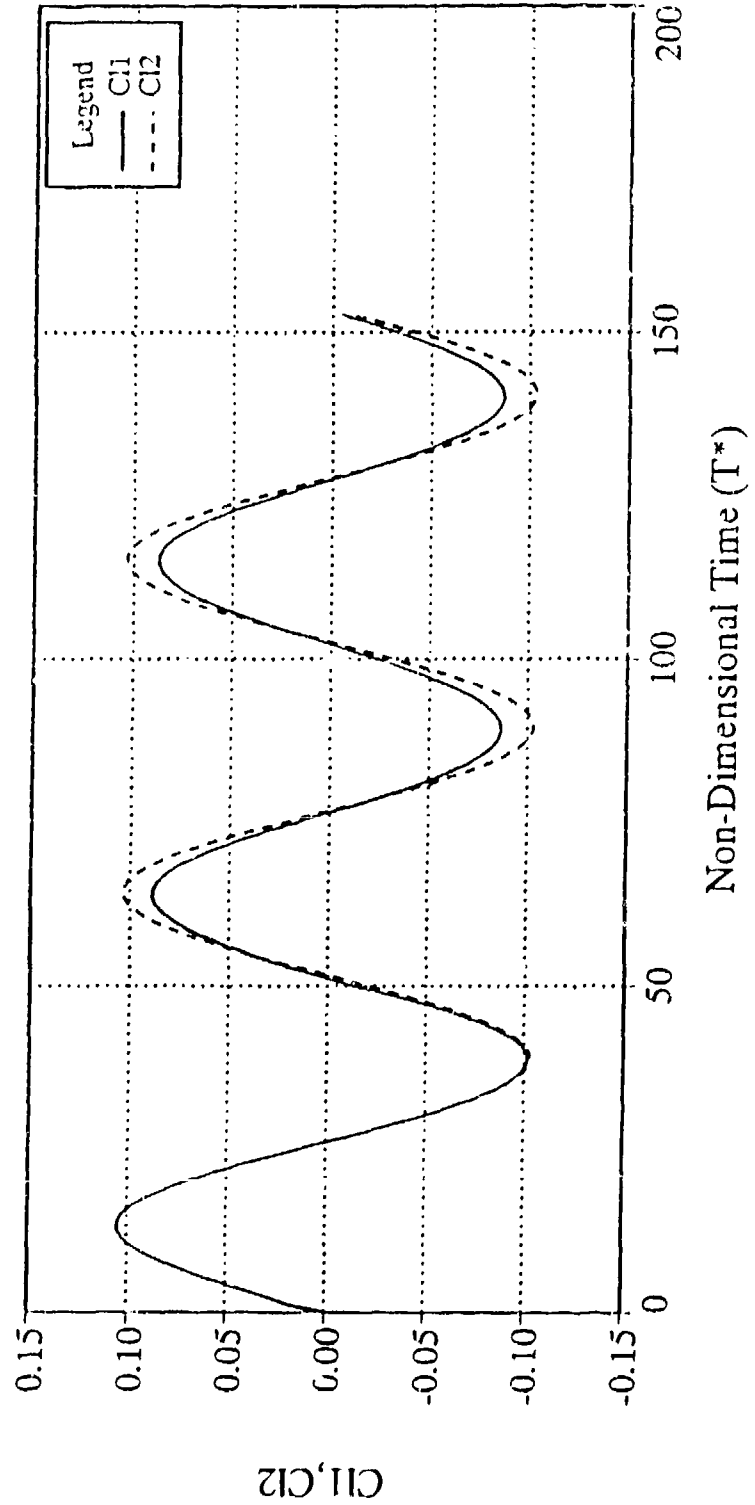


Figure (4.24) Cl vs T* (pitch, m = 0, h = 2)

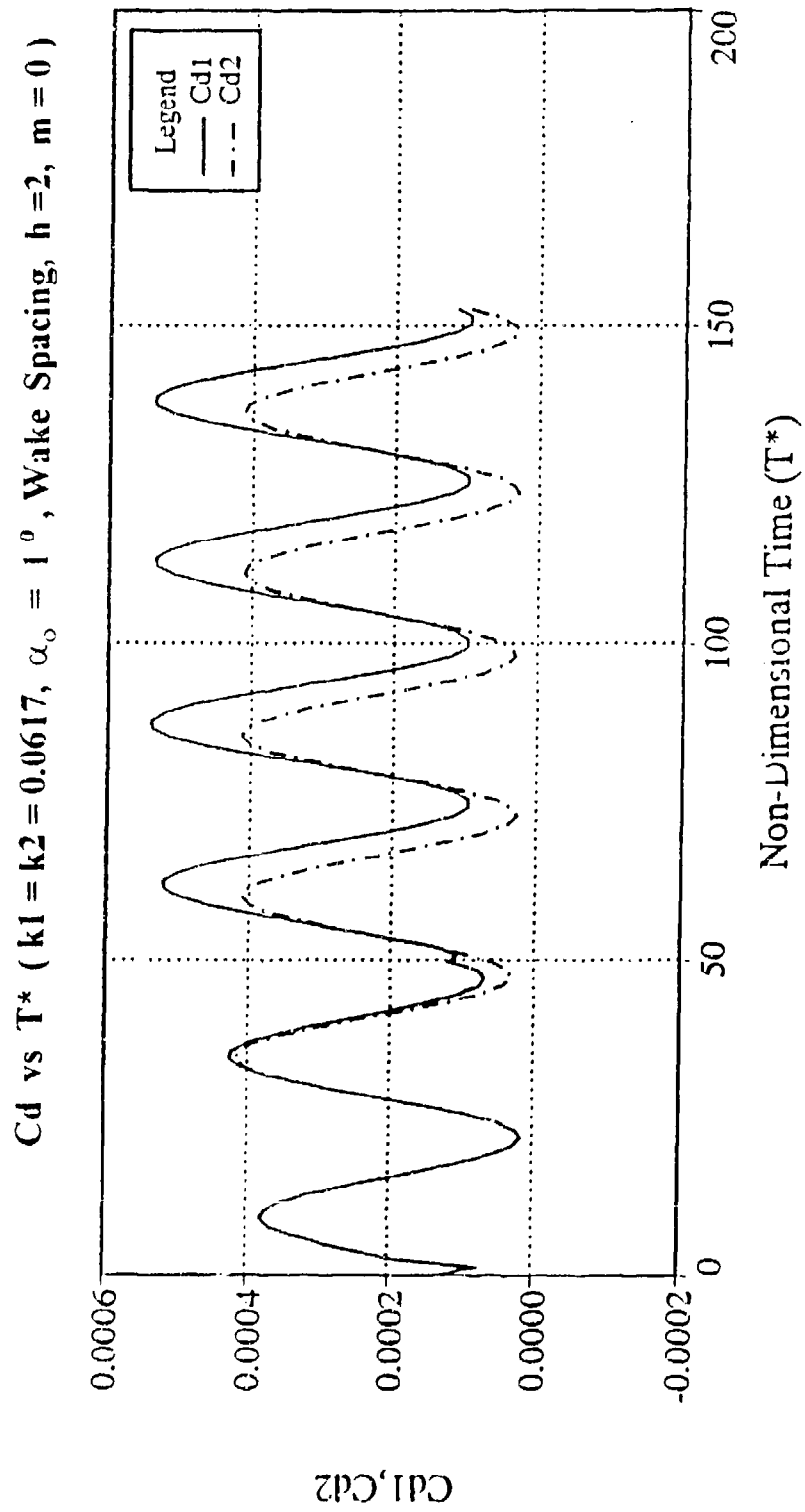


Figure (4.25) C_d vs T^* (pitch, $m = 0$, $h = 2$)

CI vs T^* ($k1 = k2 = 0.0617$, $\alpha_0 = 1^\circ$, Wake Spacing, $h = 2$, $m = 0.20833$)

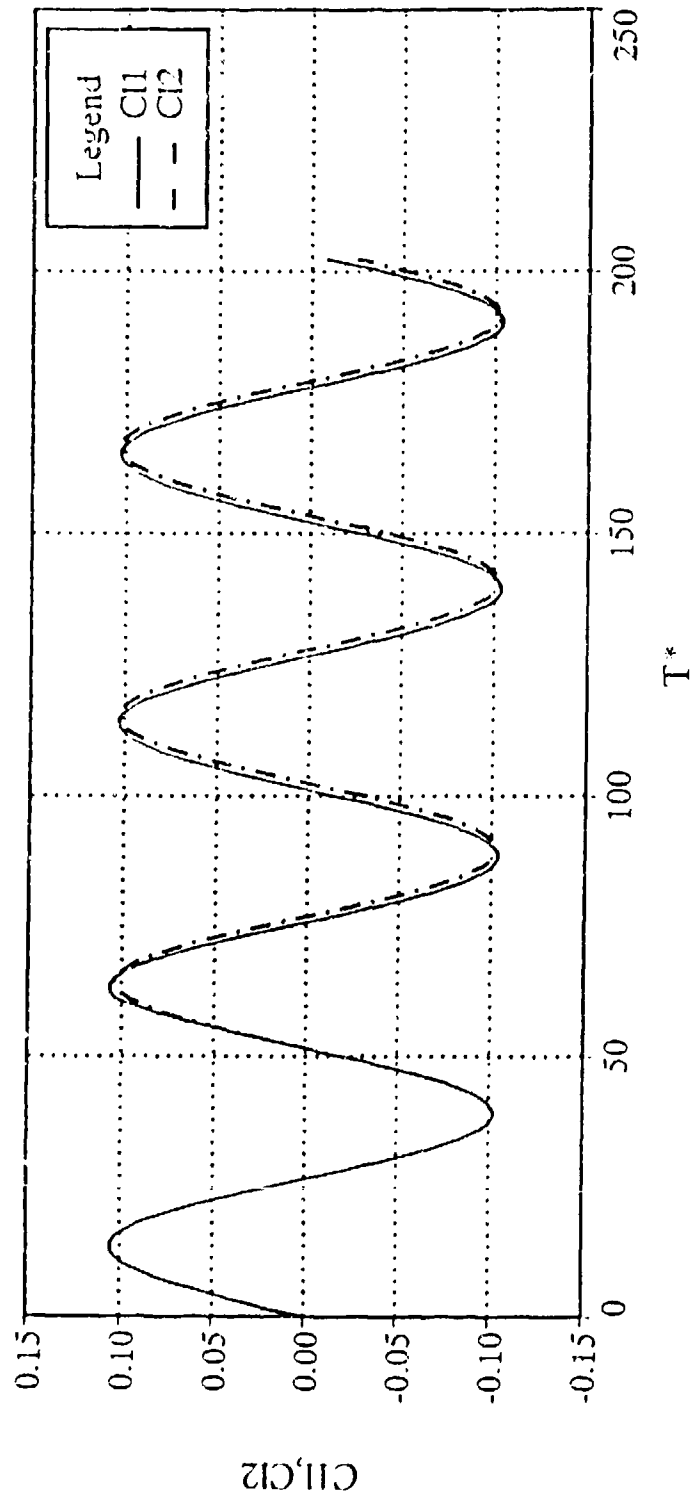


Figure (4.26) CI vs T^* (pitch, $m = 0.20833$, $h = 2$)

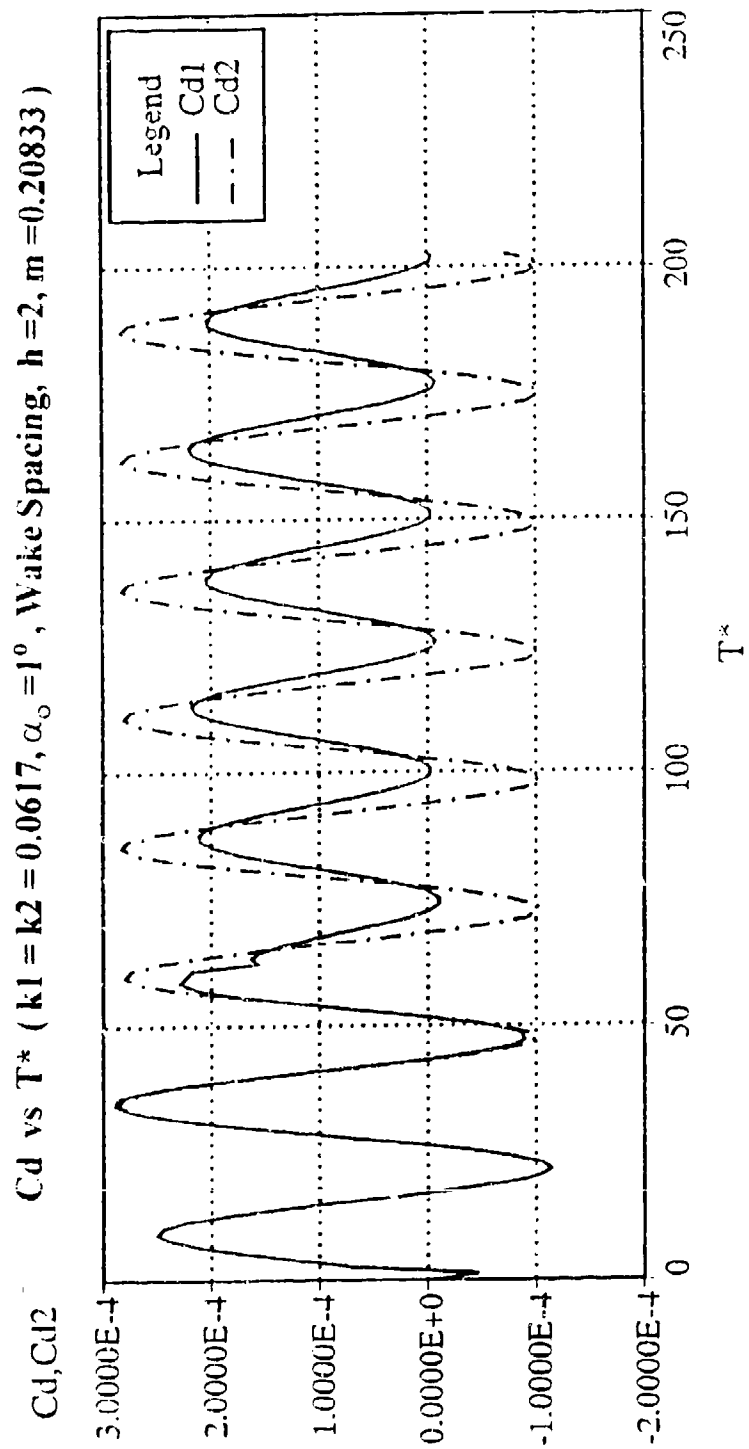


Figure (4.27) C_d vs T^* (pitch, $m = 0.2083, h = 2$)

CI vs T^* ($k1 = k2 = 0.0617$, $\alpha_0 = 1^\circ$, Wake Spacing, $h = 2$, $m = 0.25$)

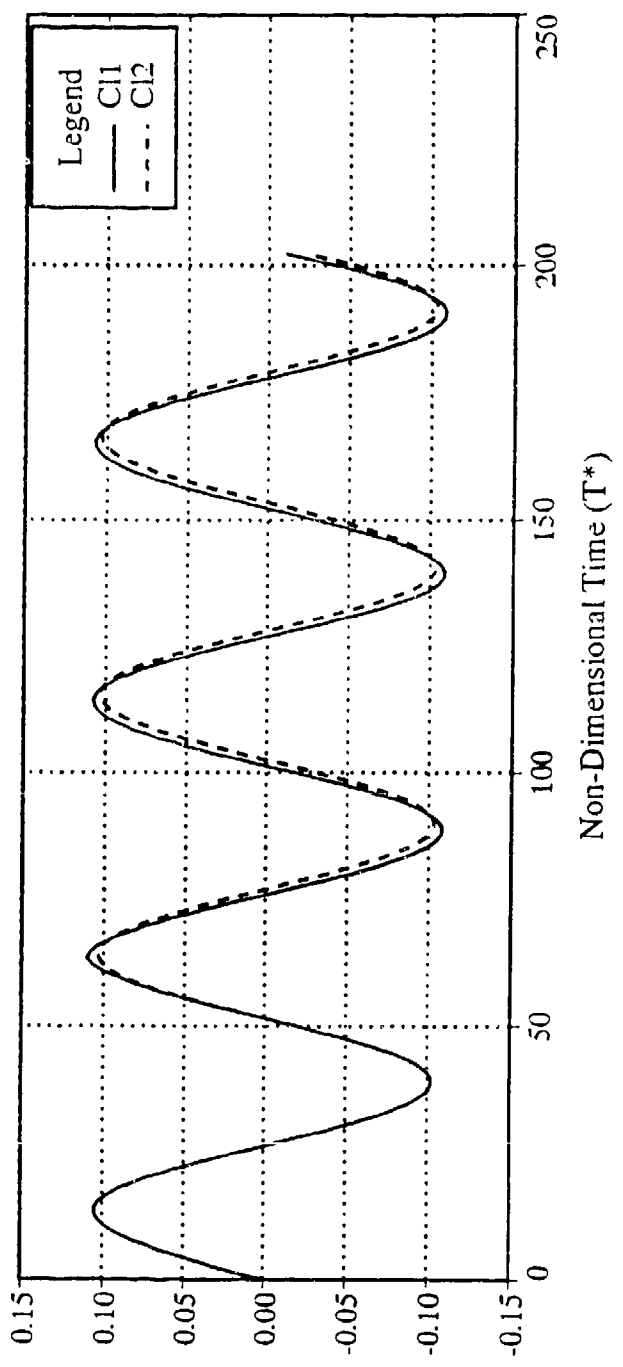


Figure (4.28) CI vs T^* (pitch, $m = 0.25$, $h = 2$)

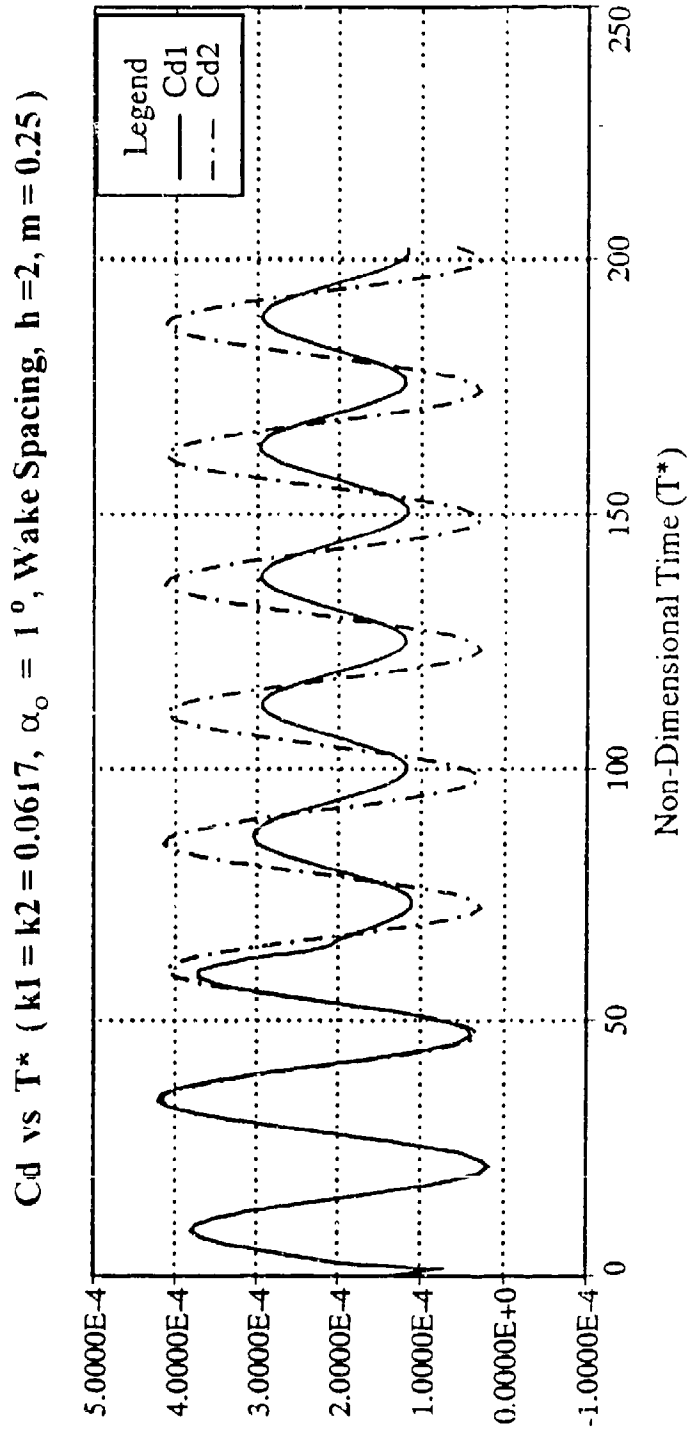


Figure (4.29) Cd vs T* (pitch, m = 0.25 , h = 2)

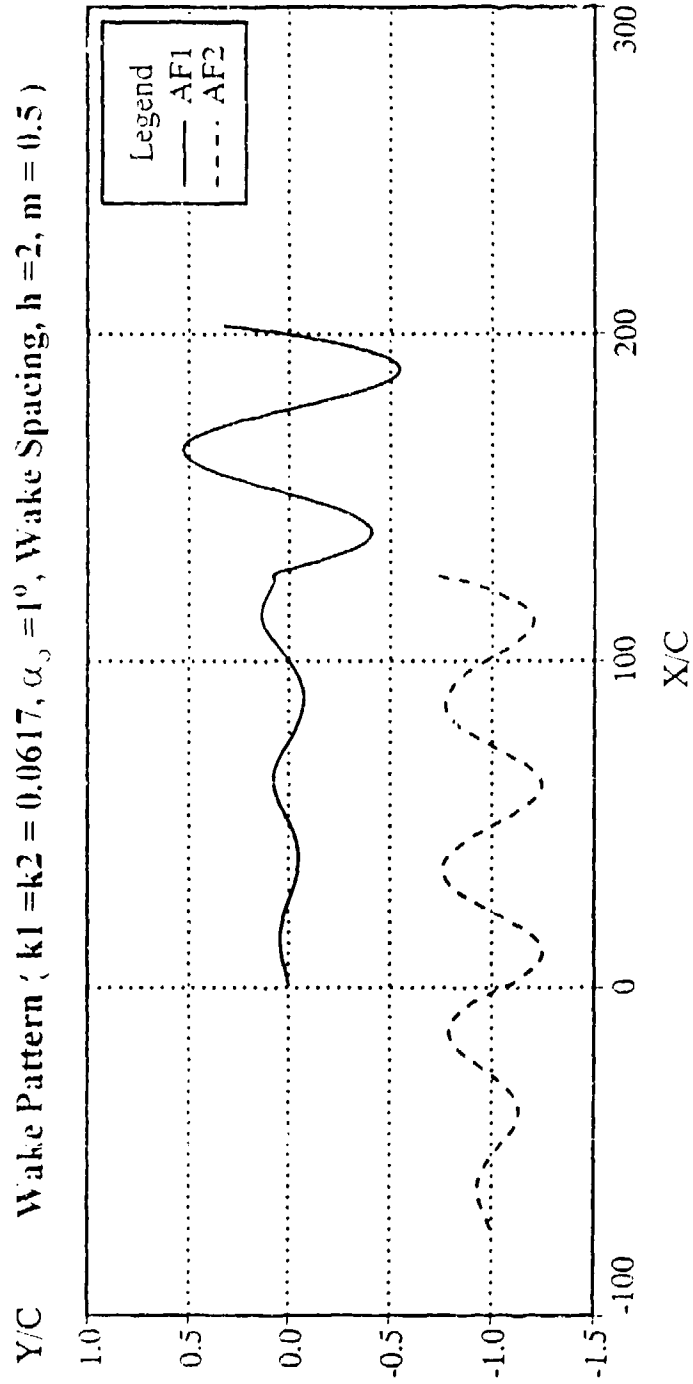


Figure (4.30) Wake pattern (pitch, $m = 0.5$, $h = 2$)

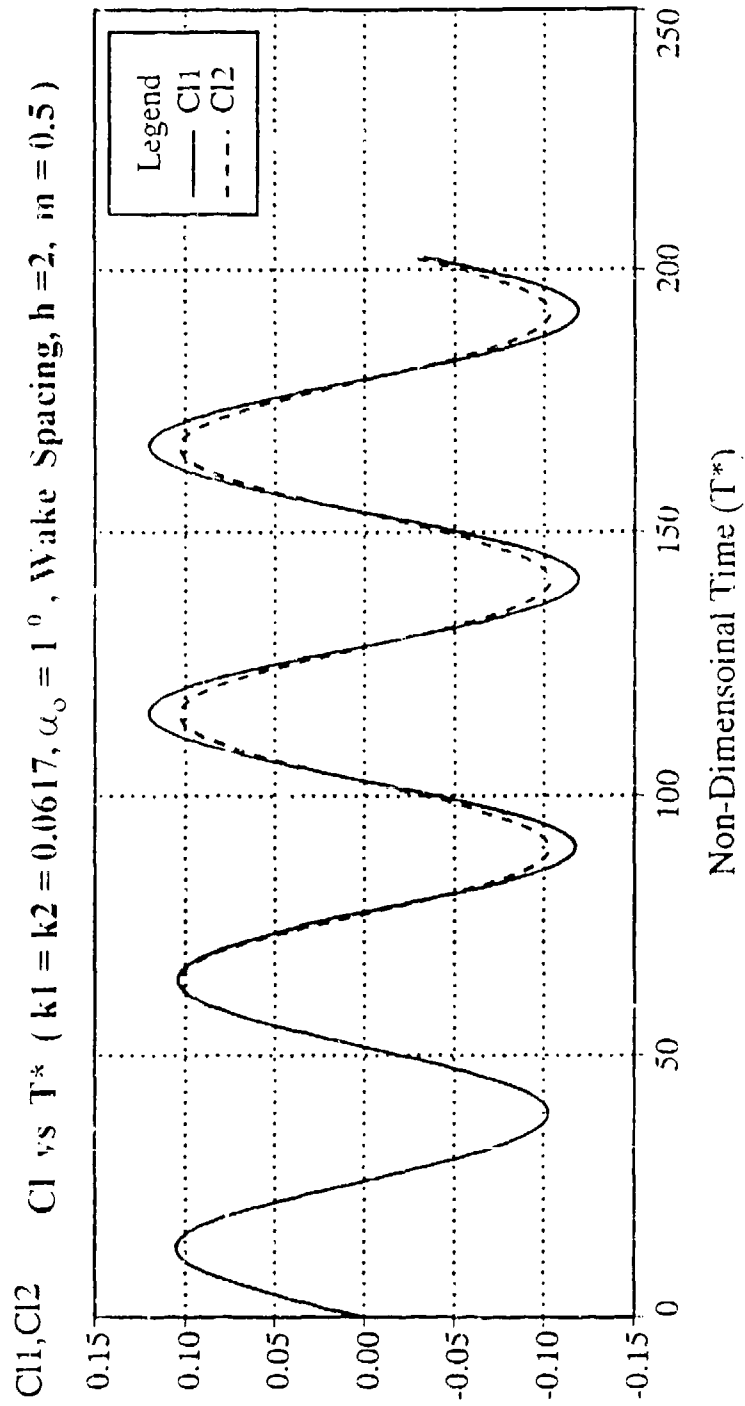


Figure (4.31) Cl vs T^* (pitch, $m = 0.5$, $h = 2$)

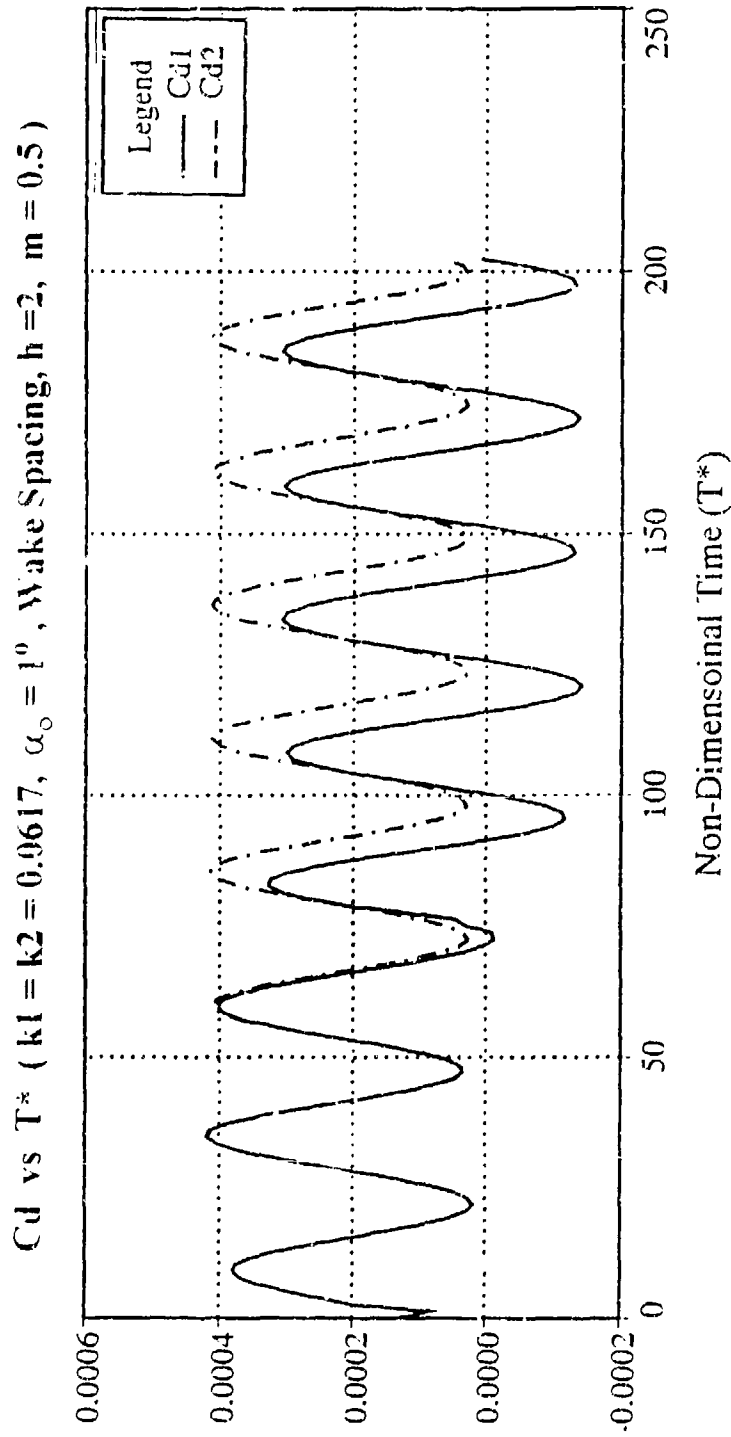


Figure (4.32) C_d vs T^* (pitch, $m = 0.5$, $h = 2$)

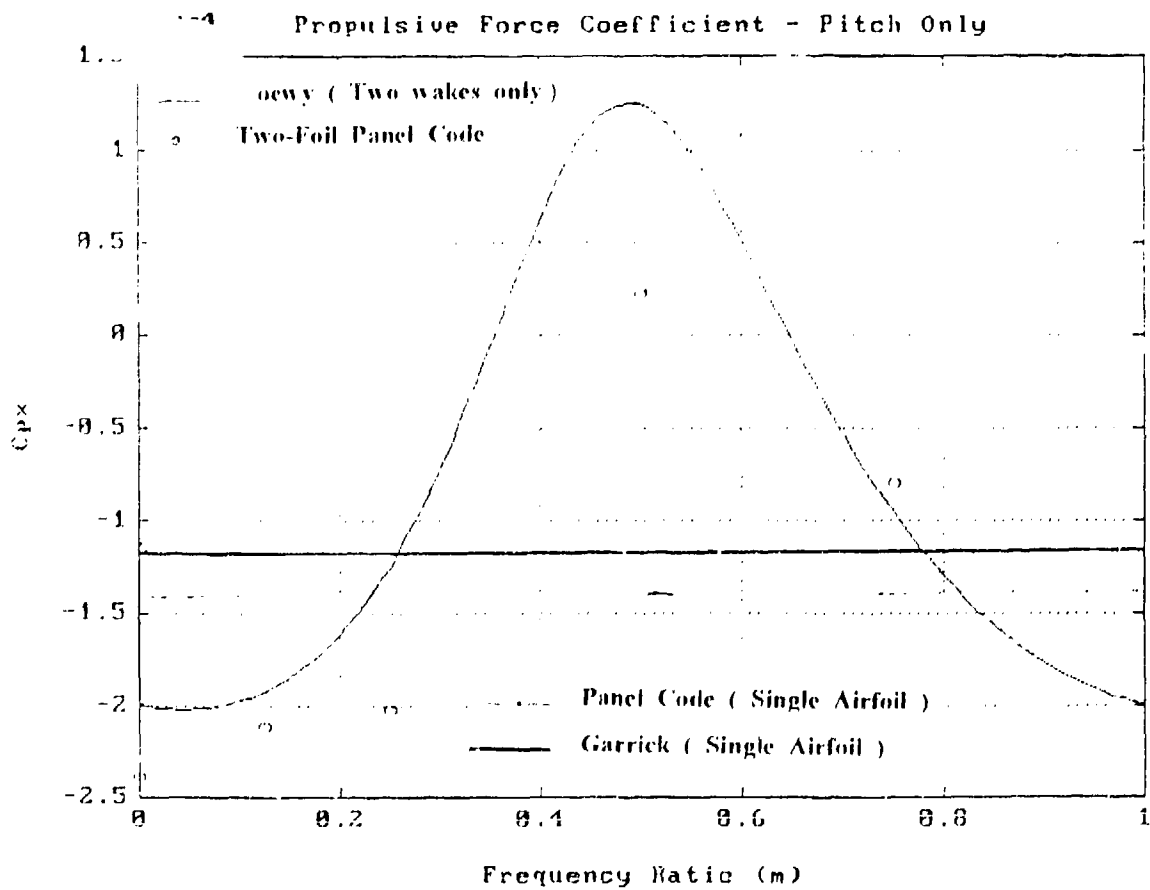


Figure (4.33) Average drag vs wake phasing (pitch only)

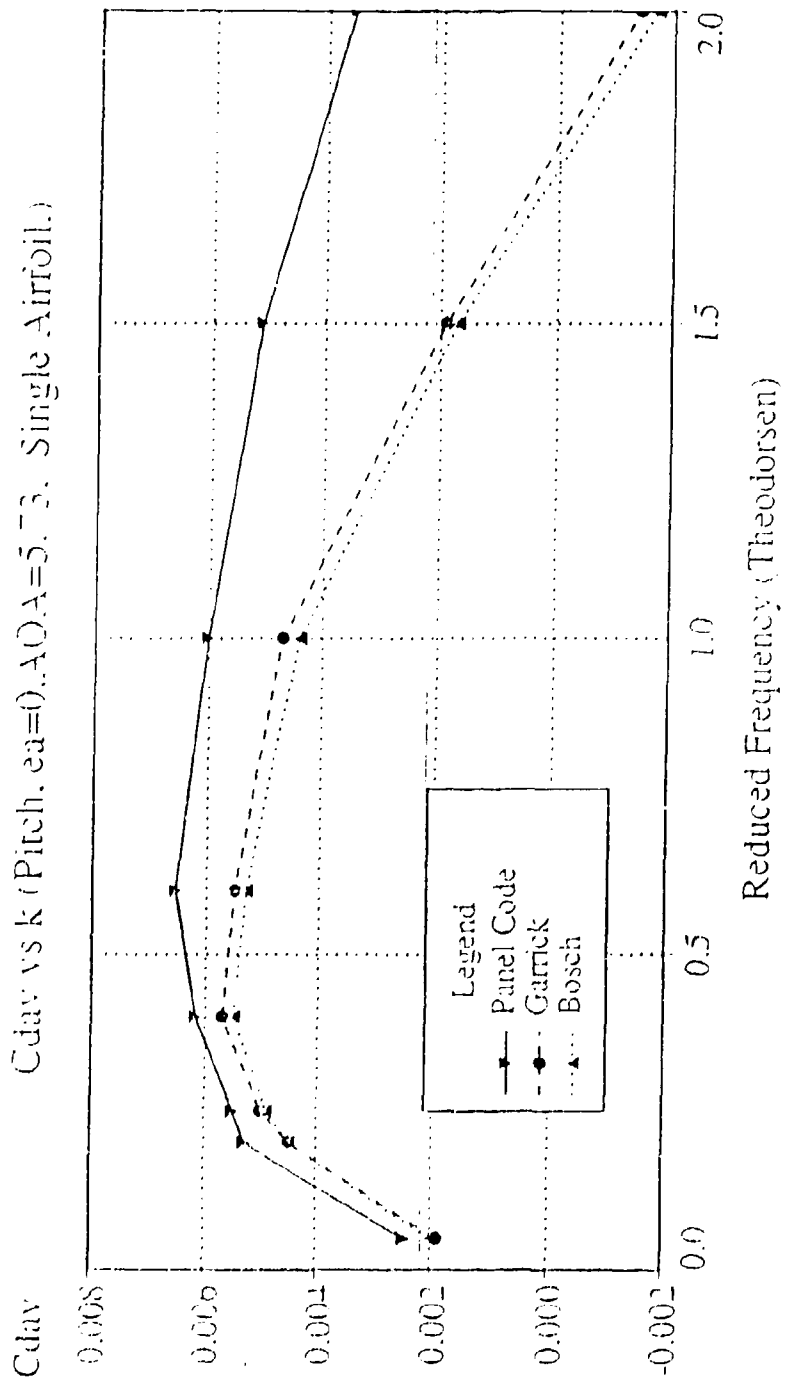


Figure (4.34) Average drag versus reduced frequency (single airfoil)

V. PROPULSIVE EFFICIENCY AND FLUTTER ANALYSIS

A. INTRODUCTION

In the previous two chapters it was shown that a single airfoil which performs harmonic plunge oscillations generates a certain amount of forward thrust (Katzmayr effect) and that this thrust may be enhanced by the oscillatory wake shed from the preceding blade if the frequency ratio or phasing m is in the range $0.2 < m < 0.7$ approximately 0.5. It was also shown that a similar enhancement occurs for pitching blades. However, pitching airfoils develop thrust only for relatively high values of reduced frequency, $k > 0.6$ by Garrick results [5].

Furthermore, it is well known that a pitching airfoil may develop negative aerodynamic damping and thus experience single-degree-of-freedom flutter. As shown by Loewy [4], the possibility of flutter is enhanced by wake interference. This is an effect known as wake-induced flutter. It is therefore of interest to study the effect of various parameters on propulsive efficiency and on flutter instability in more detail.

B. PROPULSIVE EFFICIENCY

The propulsive efficiency is defined as the ratio of the average work of propulsion to the work required to maintain the oscillation. If this factor is zero or negative, we expect energy to be extracted from the air and fed to the oscillating system. For a flat plate performing a flapping motion given by $h(t)$, where $h(t) = h_0 e^{i\omega t}$ the result for the horizontal force per unit span, averaged over one cycle, is given by [42].

$$D = -\pi\rho b\omega^2 h_0^2 [F^2(k) + G^2(k)] \quad (5.1)$$

where $F(k)$ and $G(k)$ are the real and imaginary parts of the Theodorsen lift deficiency function $C(k)$. For the case of pitching motion, the average horizontal force per unit span length is given by the following equation. (5.2):

$$\bar{D} = -\pi\rho b^3 \omega^2 \alpha_0^2 \left\{ [F^2 + G^2] \left[\frac{1}{k^2} + \left(\frac{1-a}{2}\right)^2 \right] + \left[\frac{1}{2} - F \right] \left[\left(\frac{1-a}{2}\right) - \frac{F}{k^2} - \frac{G}{K} \left(\frac{1+a}{2}\right) \right] \right\}$$

where α_0 is pitch amplitude and (a) is the position of axis of rotation. $a = -1$ corresponds to the leading edge, $a = +1$ is the trailing edge. The propulsive efficiency then is given by :

$$\eta = -\frac{\bar{D}U}{W} \quad (5.3)$$

W is the average work required to maintain the oscillation. For pitch, it is given by [42]:

$$W = \pi\rho b^3 \omega^2 U \alpha_0^2 \left\{ \frac{1}{2} \left(\frac{1-a}{2}\right) - \left(a + \frac{1}{2}\right) \left[F \left(\frac{1-a}{2}\right) + \frac{G}{k} \right] \right\} \quad (5.4)$$

For plunge, it is given by

$$W = \pi \rho b^2 h_a^2 \omega^3 \frac{1}{k} F(k) = \pi \rho b h_a^2 \omega^2 U F(k) \quad (5.5)$$

Then the efficiency factor, η , can be expressed as, for plunge :

$$\eta_h = \frac{F^2(k) + G^2(k)}{F(k)} \quad (5.6)$$

and for pitch :

$$\eta_a = \frac{F^2 + G^2}{k^2} \left[\frac{1}{2} + \left(\frac{1-a}{2} \right)^2 + \frac{1}{2} - F \left(\frac{1-a}{2} \right) \frac{F}{k^2} - \frac{G}{k} \left(\frac{1+a}{2} \right) \right] \quad (5.7)$$

$$\frac{1}{2} \left(\frac{1-a}{2} \right) - \left(a + \frac{1}{2} \right) \left[F \left(\frac{1-a}{2} \right) + \frac{G}{k} \right]$$

Figure (5.1) shows the propulsive efficiency of a single plunging airfoil as a function of reduced frequency. Slowly flapping airfoils reach very high values of efficiency, approaching one. As the frequency of flapping is increased, the efficiency falls to 50 percent. Pitching airfoils, on the other hand, start out with an efficiency of no more than 50 percent at high frequency of oscillation which quickly falls to zero and to negative values with decreasing frequency. A negative propulsive efficiency means that no work is required to maintain the oscillation, but instead energy is extracted from the airstream. This implies a loss of damping and thus the possibility of single-degree-of-freedom flutter in pitch.

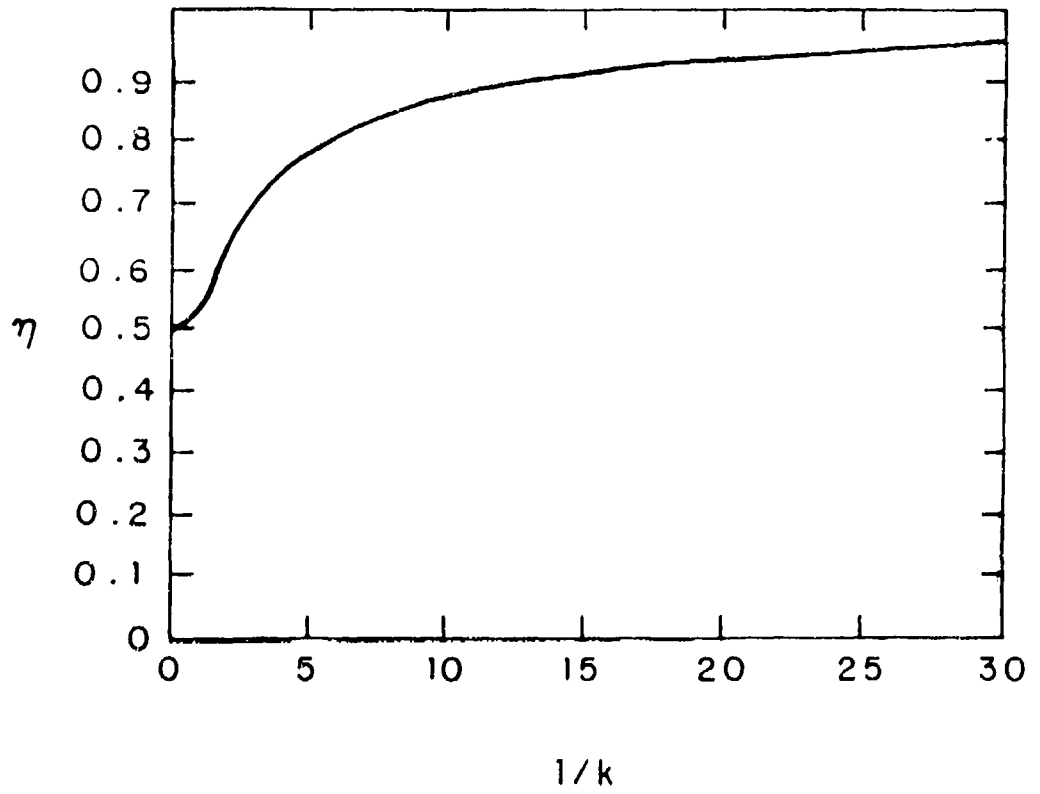


Figure (5.1) Propulsive Efficiency η versus $1/k$ for a plunging airfoil

Figure (5.2) shows the propulsive efficiency of an airfoil which pitches about the leading edge. The efficiency quickly drops to negative values as the frequency is reduced. As seen in Figure (5.2), infinitely large negative values are reached as the inverse frequency approaches 24, corresponding to a reduced frequency of 0.038. This is the flutter condition, as will be explained in more detail in the next section.

Similar trends are found for other pitch axis locations, as seen in Figure 5.3 (pitch axis is at the quarter chord and mid-chord point). The three quarter chord point is an exception. Here the propulsive efficiency is minus one at very high reduced frequency, which falls to larger negative values with decreasing frequency (Figure 5.4). However, it is interesting to note that a small shift of the pitch axis of only 0.5 % in either direction restores the efficiency to 0.5 for large frequencies, from which it starts to drop with decreasing frequency.

These results show that there is a fundamental difference between airfoil plunge and pitch motions. Plunge oscillations of a single airfoil always produce thrust, and the efficiency decreases as the frequency is increased. Pitch oscillations, on the other hand, produce thrust only at relatively high values of reduced frequency, $k > 0.6$. This possibility of single-degree-of-freedom in pitch flutter is discussed in more detail in the next section.

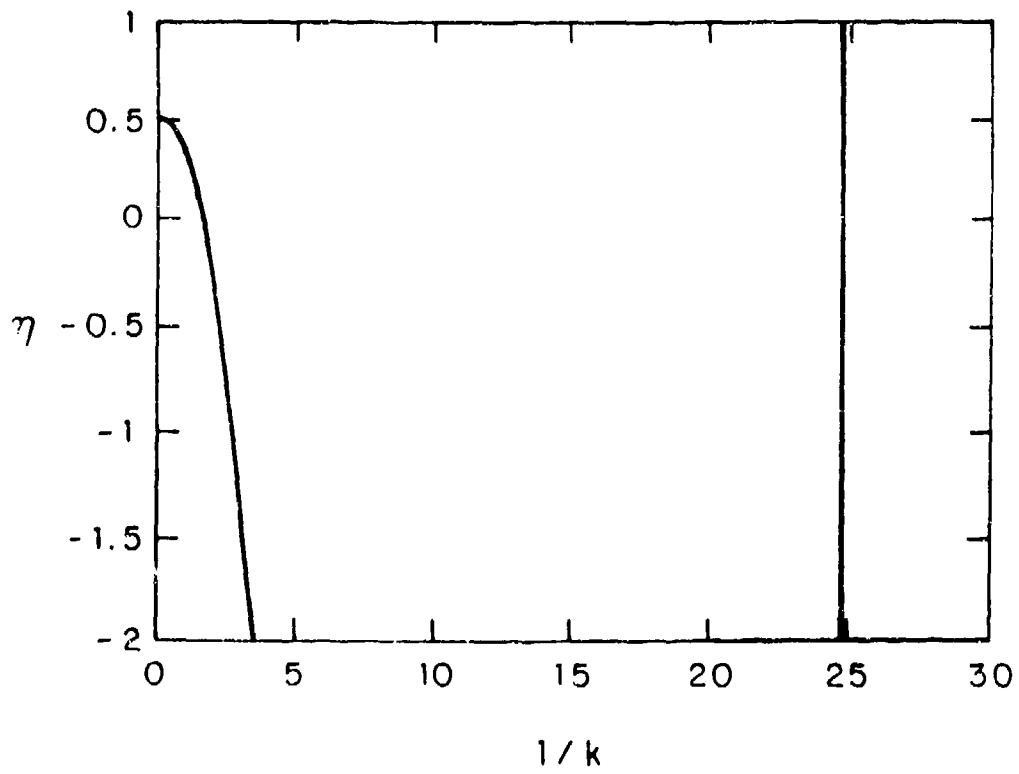


Figure (5.2) Propulsive Efficiency η versus $1/k$ for an airfoil pitching about the leading edge

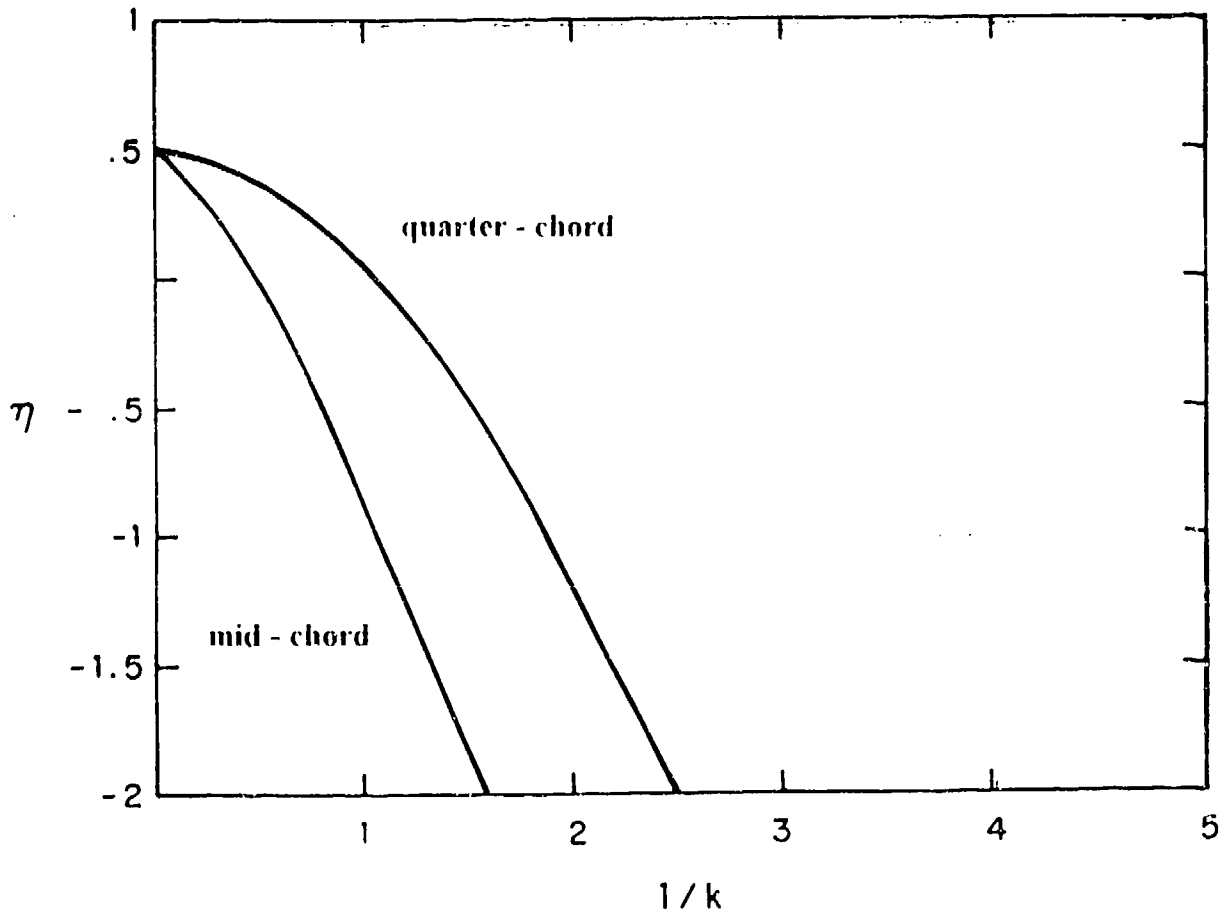


Figure (5.3) Propulsive Efficiency η versus $1/k$ for an airfoil pitching about the quarter - chord point and mid - chord point

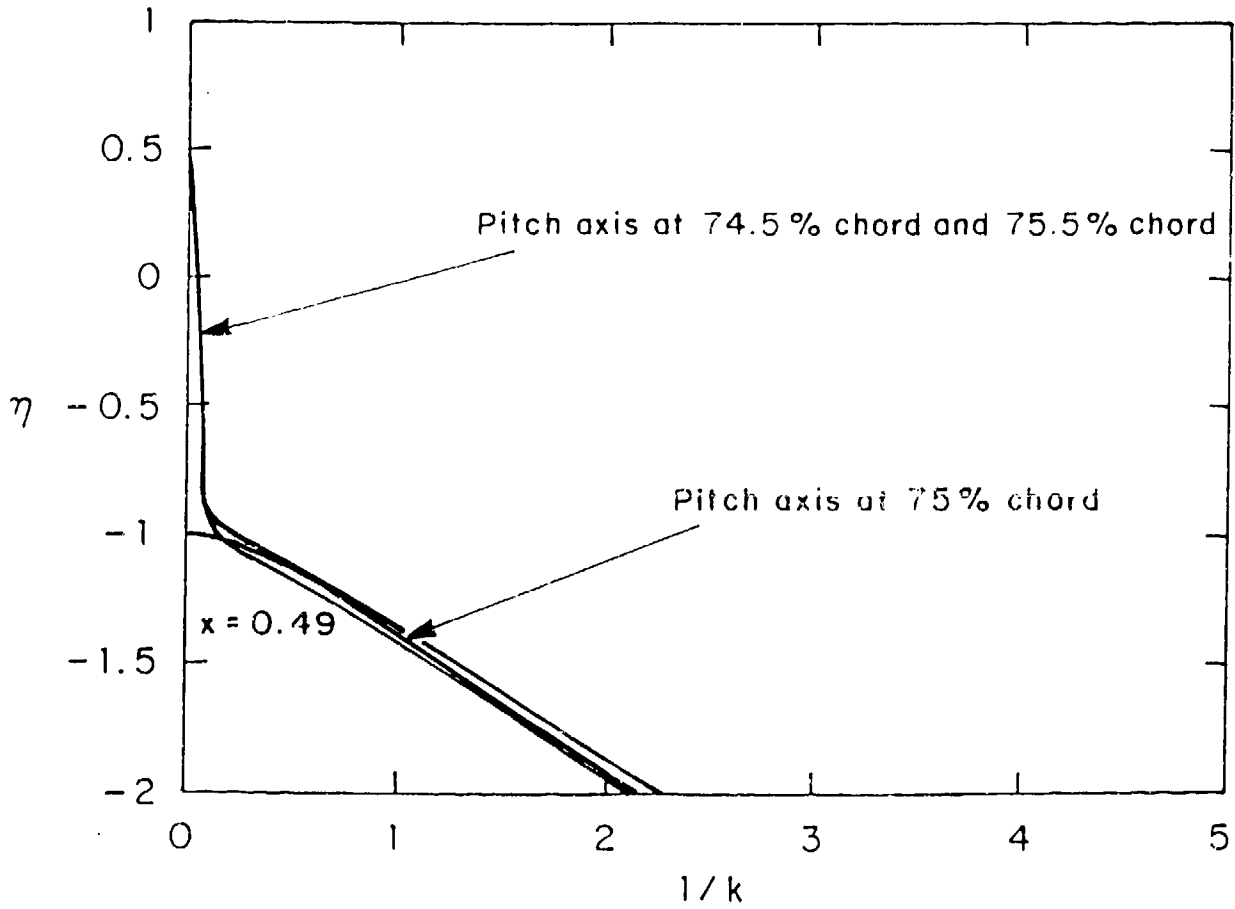


Figure (5.4) Propulsive Efficiency η versus $1/k$ for an airfoil pitching about the three-quarter-chord point

C. SINGLE-DEGREE-OF-FREEDOM AIRFOIL FLUTTER

Consider an airfoil hinged at its leading edge but elastically restrained from rotating about this axis by a torsion spring with constant K_{α} (ft-lb/rad). The airfoil is placed in a low-speed airstream so that the unstrained position of the spring corresponds to zero angle of attack α , Figure (5.5). The equation of motion for this single-degree-of-freedom system is given by :

$$I_{\alpha} \ddot{\alpha} + K_{\alpha} \alpha = M_y \quad (5.8)$$

M_y is the aerodynamic moment due to $\alpha(t)$ and I_{α} is the moment of inertia about the leading edge. Assuming that $\alpha(t) = \alpha_0 e^{i\omega t}$, then equation (5.8) can be written as

$$\frac{I_{\alpha}}{\pi \rho b^4} \left[1 - \left(\frac{\omega_{\alpha}}{\omega} \right)^2 \right] + m_y = 0 \quad (5.9)$$

where ω_{α} is the natural frequency of torsional vibration and is given by :

$$\omega_{\alpha} = \sqrt{\frac{K_{\alpha}}{I_{\alpha}}} \quad (5.10)$$

and m_y is shorthand for the dimensionless aerodynamic coefficient and can be written as [41]:

$$m_y = \frac{M_y}{\pi \rho b^4 \omega^2 \alpha_0 e^{i\omega t}} = M_{\alpha} - \left(L_{\alpha} + \frac{1}{2} \right) \left(\frac{1}{2} + a \right) + L_h \left(\frac{1}{2} + a \right)^2 \quad (5.11)$$

where "a" is the elastic axis position and at the leading edge $a = -1$. m_v is a complex number and it is a function only of reduced frequency, $k = \omega b/U$.

Equation (5.9) can be split into real and imaginary parts.

$$\text{Re} \{ m_v \} = \text{Re} \left(\frac{I_\alpha}{\pi \rho b^4} \left[\left(\frac{\omega_\alpha}{\omega} \right)^2 - 1 \right] \right) \dots \dots \dots (5.12 a)$$

$$\text{Im} \{ m_v \} = 0 \dots \dots \dots (5.12 b)$$

Flutter occurs at that value of the reduced frequency where the imaginary (out-of-phase) part of the aerodynamic moment becomes zero, provided that the corresponding real (in-phase) part yields a non-imaginary flutter frequency.

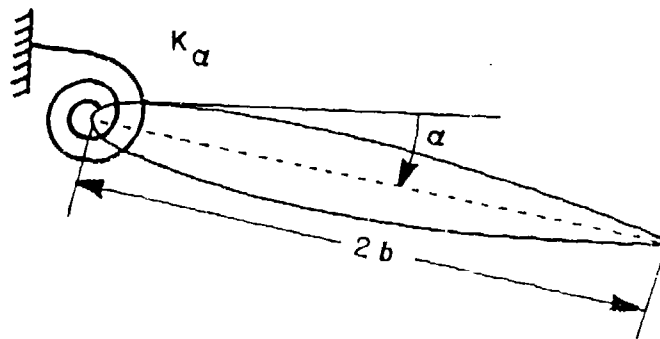


Figure (5.5) An airfoil restrained to rotate about its leading edge in two-dimensional flow.

Figure 5.6 shows the variation of the real and imaginary (damping) parts of the pitching moment for an airfoil pitching about the leading edge. It is seen that the pitch damping goes through zero at a reduced frequency of 0.038. This value agrees with the previously found value using propulsive efficiency (energy extraction) considerations.

Figure 5.7 displays the comparison between the pitch damping coefficients (note that the pitch damping coefficient is defined by Theodorsen [3] as :

$$C_m = \frac{\alpha \pi k^2}{2} M_{\alpha} - \left(\frac{1}{2} + a \right) (L_{\alpha} + M_h) + \left(\frac{1}{2} - a \right) L_h \dots \dots \dots (5.13)$$

The difference in Cm shown in Figure 4.8 is due to a difference between the M_{α} , L_{α} , M_h and L_h terms in Equation 5.13 as determined by panel code (Riestler [43]) and Theodorsen's theory [3]. The imaginary part in Figure 5.7 is obtained by Equation 5.11 computed by the panel code and Theodorsen's analysis. It is seen that the two computations are in reasonable agreement, recognizing the difference in geometry (NACA 0007 versus flat plate).

Systematic variation of the pitch axis location shows that zero pitch damping is possible for axis locations upstream of the quarter -chord point. No flutter is possible, on the other hand, for axis locations at or downstream of the quarter chord point, Figure 5.8. Loewy [4] has shown that wake interference greatly increases the possibility of flutter. The unsteady panel code provides an opportunity to investigate and to extend this well-known finding. This is a problem which should be studied in more detail.

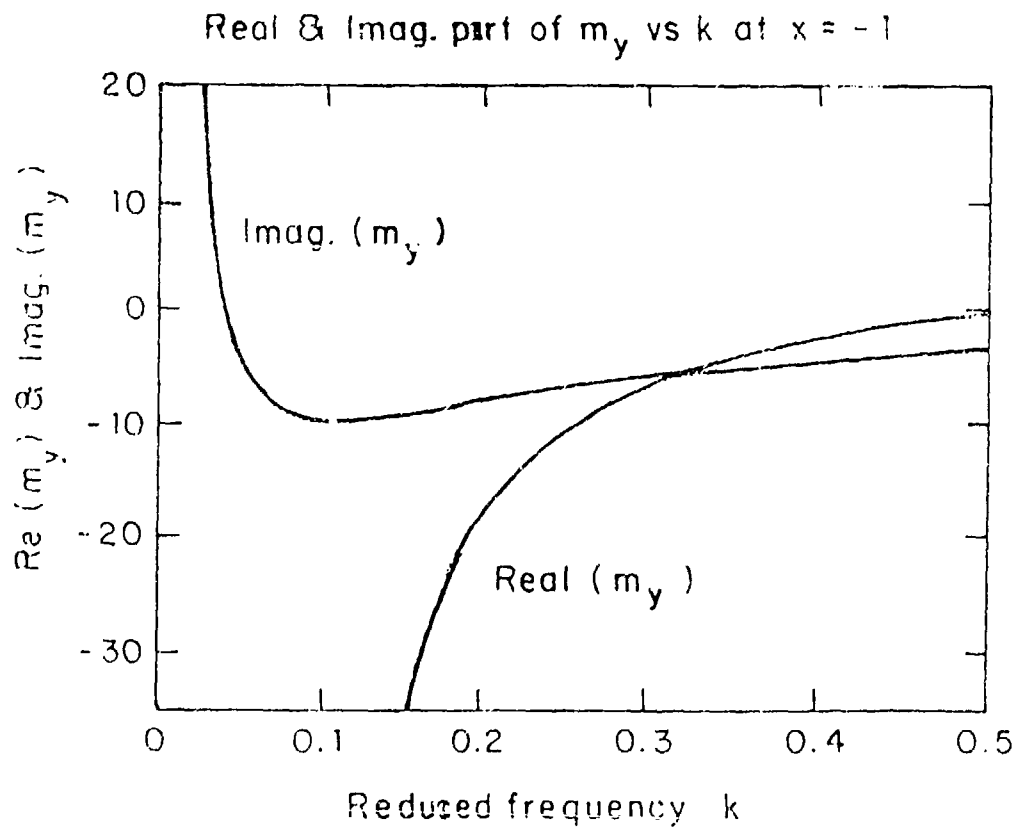


Figure (5.6) Variation with reduced frequency k of the real and imaginary parts of the non-dimensional aerodynamic moment m_y due to pitching of an airfoil about its leading edge in an incompressible flow.

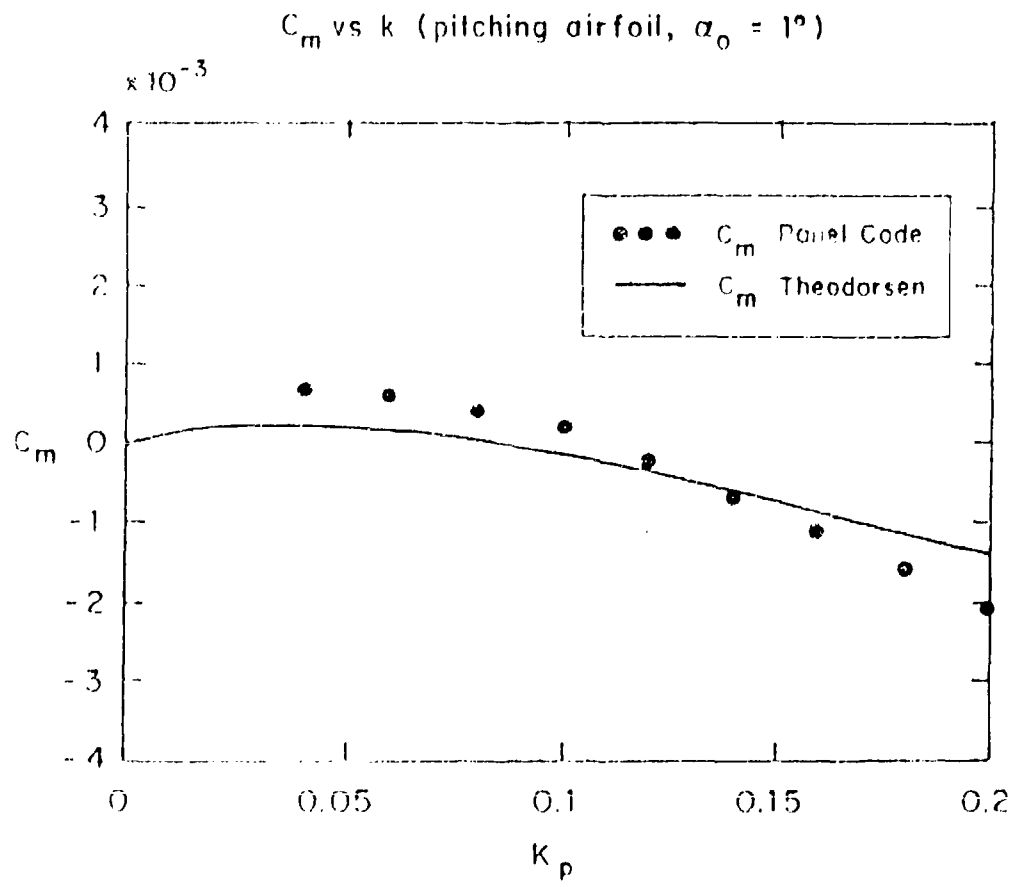


Figure (5.7) Comparison of C_m (Imag.) vs K_p for NACA0007 Oscillating in pitch about the leading edge for $\alpha_0 = 1^\circ$ and $N=200$ panels.

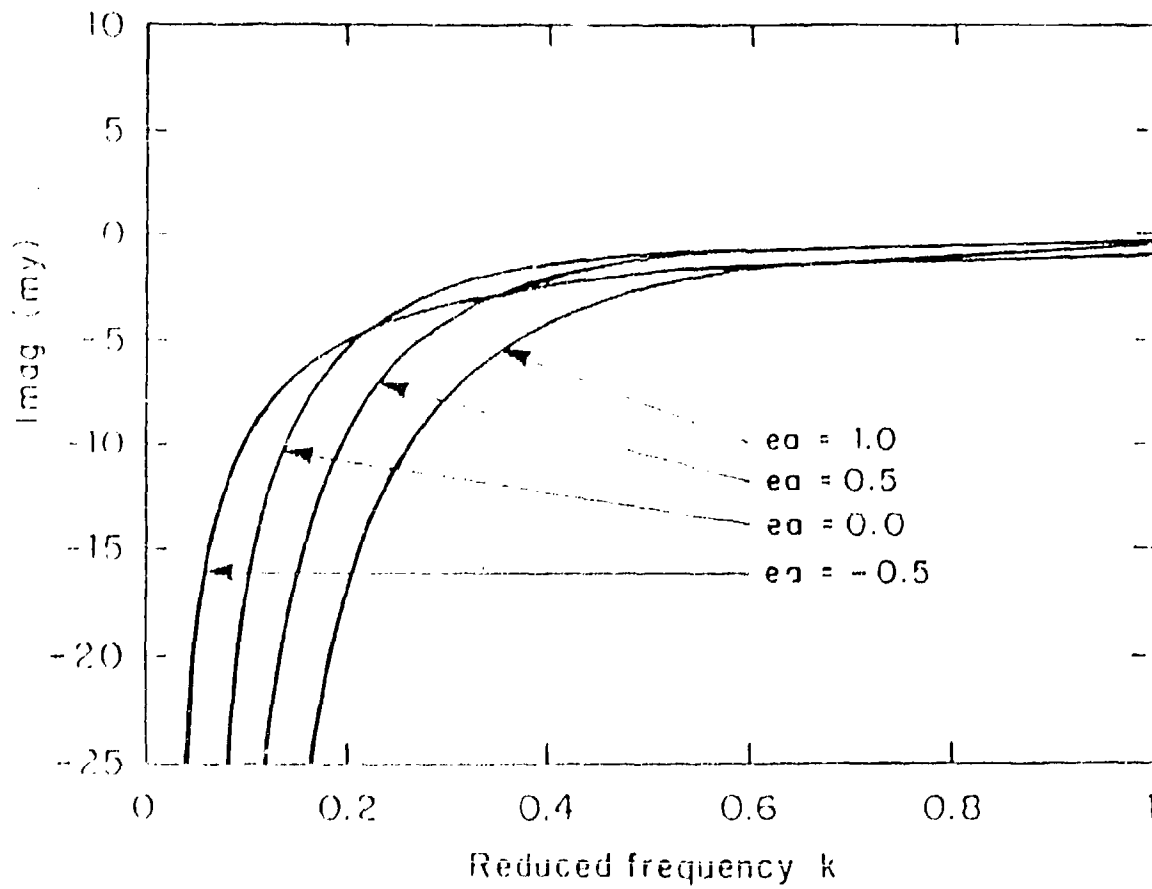


Figure (5.8) Imag. (my) vs k (for an airfoil pitching at ea = -0.5, 0.0, 0.5, and 1.0)

VI. RESULTS AND CONCLUSIONS

A DISCUSSION OF RESULTS

This research was undertaken to study the effect of unsteady aerodynamics on reductions of main rotor shaft torque and engine power measured when the HHC system was applied to the OH-6A rotor. In Chapter III we study propulsive force resulting from pure plunge oscillation of an airfoil in inviscid, incompressible flow. The results of flat plate theory, Theodorsen [3] and Garrick [5], are used to validate panel code results. Comparison with Garrick showed good agreement in pure plunge, especially, for lower values of reduced frequency and amplitudes of oscillation.

Figures 3.5 to 3, show the average drag coefficient versus plunging amplitude for three values of reduced frequency, $k = 0.1, 1, \text{ and } 2$ respectively. It is seen from Figure 3.5, (reduced frequency, k is 0.1) that agreement between the panel code and Garrick [5] is very good for a range of non-dimensional plunging amplitude up to 15 to 20 % of the blade chord. On the other hand, for higher values of k , the two results are in good agreement for a range of plunging amplitude up to approximately 10%. Single airfoil code, was used to compute the time history of the drag (thrust) coefficient of the NACA 0015 airfoil (the blade section of the OH-6A).

Figure 3.12 and Table 3.3 show the average drag coefficient versus reduced frequency for an NACA 0015 airfoil which executes plunging oscillation with 1" plunging amplitude. The OH-6A data presented in Table 3.1, Wood [42], and Figures 3.8 to Figure 3.11 from Ref. [27], were used to estimate the propulsive force per blade obtained due to plunging oscillation for 1 P frequency case. In these figures, the difference between the deflections when the HHC is "on" and "off" represents the plunging amplitude. The controller phase is also significant. Phase angle of 90° or 120° are those where helicopter vibrations were most severe, whereas at phase angle of 300° or 330° , the helicopter vibrations were significantly reduced.

We look for the greatest power benefit to occur at the phase angle of lowest vibration, that is 300° or 330° . Table 3.2 shows the amount of propulsive force and torque generated at each blade segment. The results of this table showed that the contribution of 1P (first harmonic) were 3 horsepower. Wood et al [27], applied the Garrick equation and considered the effect of blade plunge response in relation to the second to twelfth harmonic loads. He found for 2 P harmonic only (HHC "on", 330° phase at 60 knots), the power gained was about 11.3 horse power. For more detail, the reader is encouraged to study Table 2 of Ref. [27]¹.

¹ Wood E. R., Higman, J. and Ramesh Kolar. "Higher Harmonic Control Promises Improved Dynamic Interface Operations" AGARD Proceedings of the 78th Flight Mechanics Panel, May 1991, Seville, Spain

Chapter IV, considers the influence of the rotor wake interaction and examines whereas such interaction might cause favorable effects. First, the case of an isolated airfoil (single airfoil oscillating in plunge) with absence of wake was considered (or the wake located at great distance from rotor). This is the "Katzmayr effect" case where the resulting drag force is a propulsive force. It was the primary case considered by Garrick [5].

The advantage of the Panel Code is that it provides us with time histories of unsteady lift, drag, and the wake trajectory by which we can better understand and analyze the problem. In each case, the wake pattern was plotted in order to be sure that the wake produced by the second airfoil would not interfere with the reference airfoil. Also the lift and drag (or the propulsive force) were plotted versus non-dimensional time, T^* ($T^* = t.U/c$).

The closed form solutions are based upon a very thin flat plate airfoil undergoing very small motions when we model it in the unsteady panel code. For the calculations an NACA0007 airfoil was selected. The airfoil sets at zero mean angle of attack and the reduced frequency, k , is $= 0.0617$.

For the OH-6A, the value of reduced frequency, k at 70 % radial station, was calculated and found to be .1234 for the 32 Hz exciting frequency. The reference length used by the panel code is the blade chord or $2b$, so the 0.1234 reduced frequency corresponds to 0.0617 per the panel code definition. Non-dimensional wake spacing, for single airfoil analysis, was $h = 200$ (mathematically equivalent to infinite spacing, or we say that the interaction between the two airfoil is very small).

The amplitude of plunge oscillation was $h_0 = 0.14$ (by the panel code = .07, for the same reason). The panel code results are compared to other references in order to know the code limits. The comparison of the code results to that obtained by Ref. [44], is shown in Figure (4.2). This figure shows the relative lift coefficient of an airfoil (a wing of relatively long span) as it approaches the ground for different values of angles of attack. The figure, showed that the results estimated by the panel code and the results obtained by Ref. [44], are very close. For $h/c = 0.5$ the results obtained by the panel code are suspected.

Another comparison is shown in Figure(4.4). This figure and Table 4.1 show the correction factor, B , versus the chord-gap ratio in a biplane configuration. The correction factor, as defined by Ref. [45], is the reduction of the lift coefficient of an unstaggered biplane compared with that of monoplane at the same angle of incidence. On Figure (4.3) and Figure(4.5), the local speed ratio and pressure coefficient vs X/C are plotted and showed very good agreement with Wegley [46] and Bagley (1959), respectively.

The panel code is suspect whenever the wake generated by an airfoil impinges on another airfoil. The numerical panel code method also encounters difficulty with discontinuities. For these reasons it is important to carefully check the time history plots after each computer run.

In Figure (4.8), the time history of the lift coefficient, C_l , variation is plotted. Shown in Figure (4.9) is the drag coefficient, C_d , versus the non-dimensional time T^* . We observe from Figure (4.8) that the lift varies as the frequency of oscillation, with a mean lift value of zero as we expect. Amplitude of oscillatory lift was found to be ± 0.0510 . Figure (4.9) clearly shows the "Katzmayr effect". We noted that the calculated drag varies at twice the plunge oscillation frequency of the airfoil. Also, observe that the airfoil is generating a propulsive force as indicated by the mean value of drag coefficient, which is seen to have a negative value.

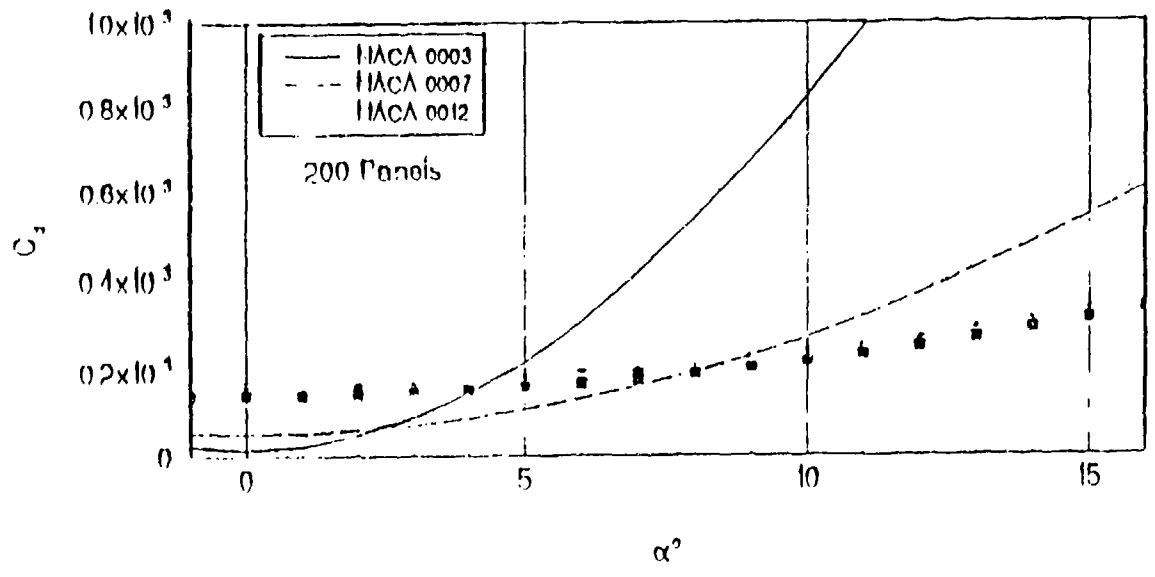
Looking to the computer printout at, at the non-dimensional time $T^* = 0.0$, steady state, the drag generated by the first airfoil was found to be $C_{dss} = .000131$ for NACA0007, which is the airfoil type that was used for most of our analyses at zero angle of attack, and a total number of panels $N = 100$ (i.e. 50 panels at the upper surface and 50 panels at the lower surface). For NACA0009, (this airfoil was used to compare the code results with that of Bosch's for a pitching case), the steady state drag C_{dss} was found to be .000196 at $N = 100$ and .000113 at number of panels $N = 150$.

It is known that, for an airfoil at zero angle of attack, in an inviscid incompressible flow field, steady state drag is zero, so in our calculations that steady state drag was subtracted from the drag generated at each time step. Shown in Figure (6.1) is the steady state drag coefficient vs angle of attack [37]. Figure (6.1a) shows the variation of steady state drag coefficient vs angle of attack for three different airfoils; NACA0003, NACA0007, and NACA0012 at total number of panel of 200.

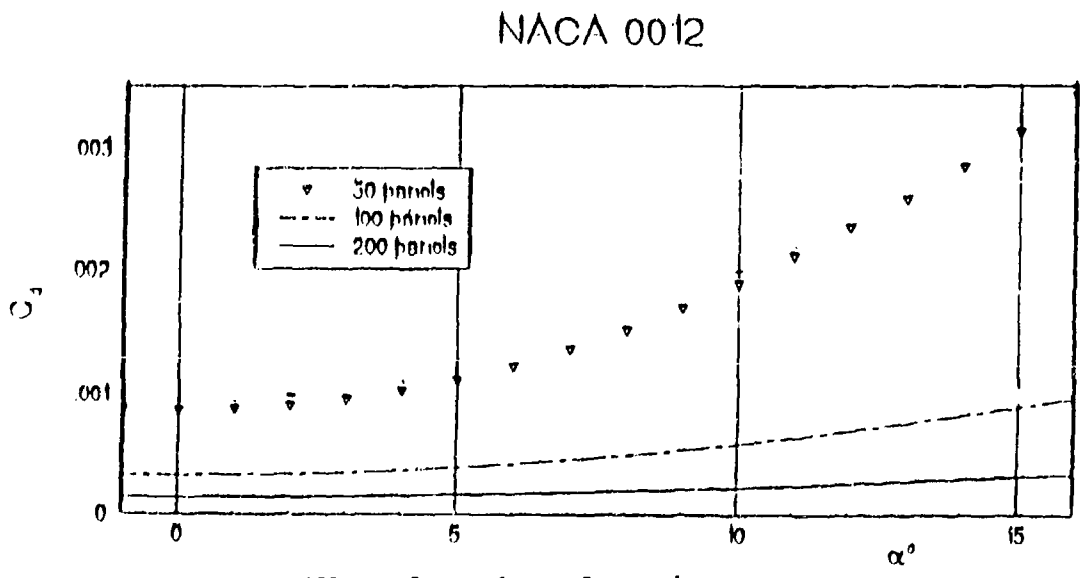
In this graph, it is shown that, for the thin airfoil NACA0003 at zero angle of attack, the drag coefficient is very small but as the angle of attack increases, the drag coefficient highly increases more than in the cases of NACA0007 and NACA0012. Figure (6.1b) shows the effect of increasing the total number of panels N on the drag coefficient of the airfoil NACA0012. As the total number of panels increases, the steady state drag coefficient accumulated error decreases.

Figures (4.10) through Figure (4.21), show the same case as above, that of an airfoil oscillating in plunge, but with the introduction of a wake layer in the near proximity of the reference airfoil (non-dimensional wake spacing, $h = 2$) for wake phasing, $m = 0, 0.20833, 0.25,$ and $m = 0.5$. These correspond to phase angles of $0^\circ, 75^\circ, 90^\circ$ and 180° , respectively.

We see that the phase angles relate to the phase relationship between the reference airfoil and the wake layer of shed vorticity. These phase angles were obtained in the panel code by establishing the proper time phase between the initiation of the wake vorticity and the oscillation of the reference airfoil. This time phase is in turn a function of the frequency of oscillation which is directly related reduced frequency, k . For the results presented here, for $k = 0.617$, this corresponds to 50.92 time units for $m=0.0$ (0° phase); 61.53 time units for $m = 0.2083$ (75° phase); and 76.38 time units for $m = 0.50$ (180° phase), etc.



a. Effect of airfoil type



b. Effect of number of panels

Figure (6.1) Drag coefficient vs angle of attack

If the reduced frequency, k , changes, this corresponds to a change in frequency (at given chord length and free stream velocity). For $k = 0.1234$, this correspond 50.92 time units for $m = 0.0$, 56.23 time units for $m = 0.2083$, and 63.65 time units for $m = 0.5$, etc.

Figure (4.10) shows the wake position for $m = 0.0$, the case where the wake shed from the second airfoil at $h = 2$ is in phase with wake shed from the reference airfoil itself. In Figure (4.21), the time history of lift variation is shown.

This is indicated by the solid line for Cl_1 . The dashed line, Cl_2 , indicates the variation of lift on a second airfoil located at the point of initiation of the wake layer at $h = 2$. Our discussion will focus airfoil₁, indicated by the solid line in the figures mentioned above. For an airfoil oscillating about zero angle of attack, the mean lift is zero. We found that, while the mean lift is zero, the amplitude of lift oscillation is smaller in the presence of the wake at zero phasing. From these figures, we conclude that the effect of wake vorticity at zero phasing is to reduce the "Katz nayr effect".

Comparison of oscillatory lift values of the 75° wake phasing case, with the case of no wake or single airfoil, shows that they are identical, since the values at 75 degrees phase are the same as that for infinite wake. Table 6.1 proves this result.

The time history of drag is seen to vary as twice the plunge oscillation frequency of the airfoil. We also observe that the airfoil is generating propulsive force as indicated by the mean value of drag, which is seen to have a negative value. Results of 75 degree wake phasing case, confirm that there is a phase angle, m , at which the effect of the wake vorticity on the reference airfoil gives the same results as when the wake is removed. It has been shown at a phase angle of zero degrees that the shed wake vorticity increases the drag on the oscillating reference airfoil, i.e. diminishes the "Katzmayr effect".

Conversely we found that at a phase angle of about 180 degrees, there is a significant decrease in drag at the reference airfoil due to the wake vorticity. This implies an intermediate phase angle at which the drag is identical to the "Katzmayr effect". It turns out that such a phase angle exists. In fact, at this phase angle the lift, drag and pitching moment are found to be identical to the case of no wake, and match the "no wake" values identically.

Table (6.1) show the aerodynamic coefficients $C_l(1)$, $C_l(2)$, $C_m(1)$, $C_m(2)$, $C_d(1)$, and $C_d(2)$ vs. Non-dimensional time. This table is a part of one of the output files. It shows these aerodynamic coefficient vs time from the nondimensional time unit 113.3 until 159.1. The phase angle at which this occurs is 75 degree or $m = 0.20833$, for the case considered here.

Table (6.1) Aerodynamic coefficients vs Non-dimensional time (from time step 113 to 159) for the case of wake phasing, $\alpha = 75$ degree, wake spacing $h = 2$, reduced frequency $k = 0.0617$ and plunging amplitude $\bar{h} = 0.14$)

TIME	CL(1)	CL(2)	CM(1)	CM(2)	CD(1)	CD(2)
113.290932	0.006952	0.014965	-0.001387	-0.003432	-0.000011	-0.000039
114.563866	-0.001073	0.001130	0.000665	-0.001427	0.000000	-0.000011
115.836800	-0.009081	-0.000881	0.002701	0.000614	-0.000009	0.000000
117.109734	-0.016877	-0.008871	0.004674	0.002639	-0.000036	-0.000008
118.382668	-0.024266	-0.016644	0.006534	0.004599	-0.000079	-0.000035
119.655602	-0.031067	-0.024005	0.008236	0.006446	-0.000133	-0.000078
120.928535	-0.037111	-0.030777	0.009738	0.008134	-0.000194	-0.000132
122.201469	-0.042247	-0.036791	0.011001	0.009621	-0.000255	-0.000193
123.474403	-0.046347	-0.041898	0.011994	0.010872	-0.000310	-0.000254
124.747337	-0.049307	-0.045974	0.012693	0.011855	-0.000355	-0.000309
126.020271	-0.051051	-0.048918	0.013077	0.012576	-0.000384	-0.000353
127.293205	-0.051534	-0.050659	0.013140	0.012929	-0.000394	-0.000382
128.566132	-0.050746	-0.051152	0.012878	0.012994	-0.000386	-0.000393
129.839066	-0.048701	-0.050385	0.012296	0.012738	-0.000358	-0.000384
131.112000	-0.045454	-0.048379	0.011412	0.012169	-0.000315	-0.000358
132.384933	-0.041083	-0.045182	0.010245	0.011301	-0.000260	-0.000315
133.657867	-0.035698	-0.040872	0.008825	0.010155	-0.000199	-0.000261
134.930801	-0.029433	-0.035556	0.007188	0.008758	-0.000138	-0.000200
136.203735	-0.022446	-0.029364	0.005375	0.007146	-0.000082	-0.000139
137.476669	-0.014910	-0.022450	0.003431	0.005358	-0.000038	-0.000084
138.749603	-0.007014	-0.014982	0.001404	0.003437	-0.000009	-0.000040
140.022537	0.001046	-0.007147	-0.000655	0.001432	0.000001	-0.000011
141.295471	0.009072	0.000865	-0.002696	-0.000608	-0.000007	0.000000
142.568405	0.016865	0.008855	-0.004668	-0.002634	-0.000035	0.000008
143.841339	0.024230	0.016627	-0.006521	-0.004593	-0.000078	-0.000035
145.114273	0.030990	0.023991	-0.008212	-0.006441	-0.000133	-0.000078
146.387207	0.036981	0.030761	-0.009700	-0.008128	-0.000194	-0.000132
147.660141	0.042057	0.036775	-0.010948	-0.009616	-0.000255	-0.000193
148.933075	0.046093	0.041883	-0.011926	-0.010867	-0.000310	-0.000254
150.206009	0.048996	0.045960	-0.012610	-0.011850	-0.000354	-0.000309
151.478943	0.050693	0.048903	-0.012985	-0.012541	-0.000382	-0.000353
152.751877	0.051145	0.050643	-0.013039	-0.012923	-0.000392	-0.000382
154.024811	0.050343	0.051136	-0.012775	-0.012988	-0.000384	-0.000393
155.297745	0.048306	0.050371	-0.012196	-0.012733	-0.000357	-0.000384
156.570679	0.045084	0.048364	-0.011319	-0.012164	-0.000314	-0.000357
157.843613	0.040757	0.045167	-0.010163	-0.011296	-0.000260	-0.000317
159.116547	0.035427	0.040858	-0.008757	-0.010150	-0.000199	-0.000260

The proper phasing is achieved by positioning the reference airfoil 76.38 time units to the right of the second airfoil, the airfoil that generates the wake. We found in the case of the plunging airfoil that the wake at zero degree phase increases the drag force, while the wake at 75 degree phase gives us close results to "no wake at all" case. So, we expect that the wake at 180 degree to increase the propulsive force. Shown in Figure (4.22), is the variation of the average propulsive force coefficient versus wake phasing, m . The circles in the graph represent panel code results for the parameters mentioned above.

Superimposed on the plot of the figure are the analytical closed form results of the Loewy theory as modified for one wake, as shown in Figure (4.22) from Wood et al [38]. Note the good agreement between the two sets of results. It is likely that the agreement can be further improved by increasing the number of panel from 100, used for these calculations, to 200 or 200 more.

As was done previously for an airfoil oscillating in plunge, we will now consider the case of an airfoil oscillating in pitch with particular emphasis on drag or propulsive force. We will first look at the case without presence of layers of adjacent wake, then look at the wake effect including the important consideration of phasing. We will begin by considering the numerical results and comparing these results with Garrick, Bosch, for "no wake" case, and then compare with Loewy's theory when the wakes are included.

Considered is the case of an NACA0007 airfoil set at zero degree angle of attack. The airfoil is oscillating with an amplitude 1 degree. The reduced frequency is taken at $k = 0.0617$ and the non-dimensional wake spacing was $h = 200$, which is numerically equivalent to having the wake at infinity. The time history of the lift variation, C_l , and the time history of drag variation, C_d , reveal the following. We observe that the lift varies as the frequency of oscillation, with a lift mean value of zero as we expect.

In contrast to the lift time history, the drag time history indicates that the calculated drag varies at twice the frequency of the pitch oscillation. The amplitude is given by $C_d = 0.000192$. The mean drag value is found to be $C_d = 0.00009$ and the mean lift is of course 0.0 at zero angle of attack.

For an airfoil oscillating in pitch with the wake layer near the reference airfoil at non-dimensional wake spacing, $h = 2$. The case of zero degree phase, where the wake below the airfoil at $h = 2$ is in phase the wake shed from the reference airfoil itself. Review of the results indicates a reduction in the amplitude of lift variation for the $m = 0.0$ case when compared to the case with no wake at all (wake at infinity). We see that the lift amplitude decreases. We also see an increase in mean steady drag accompanies the reduction in lift amplitude, for the case of zero wake spacing ($m = 0$). Proper phasing is achieved at $m = 0.5$. At this value, we found that the lift enhancement in this case of pure pitch, is similar to what we found in the plunge case.

B CONCLUSIONS

The most important conclusions that can be drawn from this research are:

1. For drag, in both cases of pure plunge and pure pitch, wake phasing can increase or decrease the steady component of drag acting on the airfoil. The increase in the steady component of propulsive force due to wake phasing in the case of pure plunge was sufficient to significantly enhance the "Katzmayr" effect value of propulsive force.
2. For an airfoil oscillating in plunge or pitch, for optimum reduction in drag and enhancement in vibratory lift, the phase angle of the wake vorticity in the single wake case with respect to motion of the reference airfoil should be about 180° .
3. For an airfoil oscillating in plunge or pitch, the largest value of steady drag and smallest value of oscillatory lift occurs when the phase angle of the wake vorticity with respect to motion of the reference airfoil is about 0° .
4. For lift, in both plunge and pitch in the single wake case, wake phasing can increase or reduce the oscillatory lift acting on the airfoil. Where in the absence of wake vorticity, the effect of oscillations decreases the lift (lift deficiency). With the wake present we also observe lift enhancement (lift efficiency).
5. There exists a phase angle, 75° for the case, (reduced $k = .0617$, wake spacing, $h = 2$), where the effect of wake vorticity on the reference airfoil is identical to the case of the wake at infinity (represented in the code by wake $h = 200$), or no wake vorticity at all.

Applying these findings to the OH-6A case, we can add the following conclusions :

6. Measured reductions in power are feasible when the "Katzmayr" effect and thesis-reported wake enhancements are included.

7. Measured higher harmonic control results show least benefit at 100 knots due to the wake being transported greatest distance from rotor at this speed.

8. Poor repeatability of measured open loop performance data is to be expected due to shifts in wake position¹.

9. For helicopters, it is standard rotor blade design to locate the center of gravity, aerodynamic center, and elastic axis at the quarter chord point to avoid flutter. This was illustrated in the analysis. Results of this thesis showed that flutter is impossible for this condition without wake interference. However, Loewy's results introduce the possibility of wake induced flutter. Future investigations, therefore, will have to explore this possibility in more detail.

¹ E. R. Wood, Max F. Platzer, Ahmed A. Jouahnia, Mark A. Couch
" On the Unsteady Aerodynamics of Higher Harmonic Control. "
Paper No. C-17, Nineteenth European Rotorcraft Forum, Cernobbio
(Como) Italy, September 1993.

C RECOMMENDATIONS

1. A new flight test program, directed at studying helicopter performance, is needed. The NASA-Army OH-6A program was dedicated to vibration testing.
2. Continued full scale HHC tests in the NASA Ames 40' x 80' wind tunnel is encouraged. In addition, it is suggested that tests be initiated in small university wind tunnels to verify the findings of this thesis.
3. Controlled whirl tower testing is also recommended, since this allows careful measurement and control of performance parameters.
4. A wind tunnel program is needed to explore similar cases and to verify the present research findings.
5. The panel method is a significant analysis tool that can be applied to study and solve similar problems. It provides an excellent method for studying single or two-degree-of-freedom flutter problems.

REFERENCES

1. Wood, E. R., Powers, R. W., Cline, J. H., and Hammond, C. E. "On Developing and Flight Testing a Higher Harmonic Control System." *Journal of A.H.S* January, 1985.
2. Wood, E. R., and Powers, R. W. "Practical Design Considerations for a Flightworthy Higher Harmonic Control System." 36 th. Annual Forum, A.H.S. Washington, D. C., May, 1980.
3. Theodorsen, T., "General Theory of Aerodynamic Instability and the Mechanism of Flutter", NACA T.R. 496, 1935.
4. Loewy, R. G., "A Two -Dimensional Approximation to the Unsteady Aerodynamics of Rotary Wings", *Journal of Aeronautical sciences*, vol. 24, No. 2, Feb. 1957.
5. Garrick, I. E., "Propulsion of Flapping and Oscillating Airfoil." NACA T. R. 567, 1936.
6. Platzer, M. F., Neace, K. S., and Pang, C. K., "Aerodynamic Analysis of Flapping Wing Propulsion", AIAA paper No. 93-0484, 31st Aerospace Sciences meeting, Reno, NV, January 11-14, 1993.
7. Katzmayr, R., "Effect of Periodic Changes of Angles of Attack on Behavior of Airfoils", NACA T.M. No. 147, Oct. 1922.
8. Richardson, "The Physical Aspects of Fish Locomotion ", *Journal of Experimental Biology*, Vol. III, No. 1, pp. 63-74, 1936.

9. Johnson, W. , "Helicopter Theory" Princeton University Press, New Jersey,1980.
10. Knoller, R. "Die Gesetze des Luftwiderstandes" Flug-und Motortechnik (Vienna) vol. 3, No. 21, pp. 1-7,1909.
11. Betz, A., "Ein Beitrag zur Erklarung des Segelfluges." Z. f. Flugtechnik und Motorluftschiffahrt, vol. 3, pp. 269-272. 1912.
12. Birnbaum, W., "Das Ebene Problem des schlagenden Fluegels. " z. angew. Mathematik und Mechanik, vol. 3, pp. 290-297. 1923.
13. von-Karman, T. and Burgers, J. M., "Aerodynamic Theory." vol. 2, pp. 280-310, Spriger, Berlin 1935.
14. Schmidt, W., "Der Wellpropeller, ein neuer Antrieb fuer Wasser-, Land-, und Luftfahrzeuge." Z. Flugwiss. vol. 13 , pp. 472-479 1965.
15. Bosch , H. , "Interfering Airfoils in Two-dimensional Unsteady Incompressible Flow." AGARD cp-227, Faber No. 7, September 1977.
16. Kussner, H. G., " Comprehensive Report on Unsteady Airfoil Lift " (in German), Luftfahrtfforschung, Vol. 13, No. 12, Dec. 1936.
17. Wagner, Herbert "Ueber die Entstehung des dynamischen Auftriebes von Tragfluegeln ." Z. f. A. M. M., Band 5, Heft 1, Feb. 1925, S. 17-35.
18. Glauert, H., " The Force and Moment on an Oscillating Airfoil." R. & M. No. 1212, British A. R. C., 1929.
19. Durcan, W. J. , "Introductory Survey." AGARD Manual on Aeroelasticity, Vol. I, Page 28.

20. McKinney, W. and Delaurier, J., "The Wingmill: An Oscillating Wing Mill." *Journal of Energy* , Vol. 5, No. 2. March-April 1981, pp. 109-115.
21. Hess, J. L. and Smith, A. M. O., " Calculation of Potential Flow about Arbitrary Bodies. " *Progress in Aeronautical Sciences*, vol. 8 ,pp. 1-138, Pergamon Press, Oxford, 1966.
22. Basu, B. C. and Hancock, G. J. , " The Unsteady Motion of a Two-Dimensional Airfoil in an Incompressible, Inviscid Flow." *J. of Fluid Mechanics*, vol. 87, pp. 159-168, 1978.
23. Kim, M. J. and Mook, D. T. , "Application of Continuous Vorticity Panels to General Unsteady Incompressible Two-Dimensional Lifting Flows." *Journal of Aircraft*, vol. 23, no. 6, pp. 464-471, 1986.
24. Teng, N. H. , " The Development of a Computer Code for the Numerical Solution for Unsteady, Inviscid, and Incompressible Flow over an Airfoil." *Master's Thesis* , Naval Postgraduate School, Monterey, CA, June 1987.
25. Pang, C. K., "A Computer Code for Unsteady Incompressible Flow Past Two Airfoils." *Aeronautical Engineer's Thesis*, Naval Postgraduate School, Monterey, CA, September 1988.
26. Neace, K. S. , " A Computational and Experimental Investigation of the Propulsive and Lifting Characteristics of Oscillating Airfoils and Airfoil Combinations in Incompressible Flow." *Aeronautical Engineer's Thesis*, Naval Postgraduate School, Monterey, CA, September 1992.

27. Wood, E. R., Higman, J. and Ramesh Kolar. "Higher Harmonic Control Promises Improved Dynamic Interface Operations" AGARD Proceedings of the 78th Flight Mechanics Panel, May 1991, Seville, Spain.
28. Scanlan, R. H. and Rosenbaum, R. "Introduction to the Study of Aircraft Vibration and Flutter." The MacMillan Company, New York, 1962.
29. Shipman, K. W., and Wood, E. R. "A Two-Dimensional Theory for Rotor Blade Flutter in Forward Flight." Journal of Aircraft, Vol. No. 8, Number 12, pp. 1008-1015, December 1971.
30. Schwarz, L., "Berechnung der Druckverteilung einer Harmonisch sich Verformenden Tragfläche in Ebener Stromung." Luftfahrtforschung, Band 17, No. 11 und 12, 1940.
31. Sohngen, H., "Die Lösungen der Integraleichung und deren Anwendung in der Tragflugeltheorie." Mathematische Zeitschrift, Band 45, 1939, pp. 245-264.
32. Donovan A. F. and Lawrence H. R. "Aerodynamic Components of Aircraft at High Speeds." Princeton, New Jersey, Princeton University Press, 1957.
33. Smilg, B. and Wasserman, L. S. "Application of Three-Dimensional Flutter Theory to Aircraft Structures (with correction for the effects of control surface aerodynamic balance and geared tabs." AAF TR 4798, Material Division, Dayton, Ohio, July 19, 1942.
34. Platzer, M. F. Class Lecture Notes, Naval Postgraduate School, Monterey, CA, Sep. 1991. pp. 1-20.

35. Karman, Th. von. and Sears, W. R. "Airfoil Theory for Non-Uniform Motion." *Journal of Aeronautical Sciences* 5, 1936. pp. 379-390.
36. Wood, E. R. "An Introduction to Helicopter Engineering", Lectures Published by California Institute of Technology, Fall 1984.
37. Johnston, Thomas A. "Computational Investigation of the Compressible Dynamic Stall Characteristics of the Sikorsky SSC-A09 Airfoil." Master's Thesis, Naval Postgraduate School, Monterey CA, September 1993.
38. Wood, E. R., Platzer, Max F. Abourahma, A., and Couch M. A. ." On the Computation of Helicopter Wake Induced Unsteady Aerodynamics due to Higher Harmonic Control." Paper No. 2-2, Fifth Workshop on Dynamic and Aeroelastic Stability Modeling of Rotorcraft Systems, Rensselaer Polytechnic Institute, Troy, New York, 18-20 October 1993.
39. Wood, E. R., Platzer, Max F., Abourahma, A., Couch, M. A., " On the Unsteady Aerodynamics of Higher Harmonic Control. " Paper No. C 17, Nineteenth European Rotorcraft Forum, Cernobbio (Como), Italy, September 1993.
40. Couch, M. A. " A Finite Wake Theory for Two-Dimensional Rotary Wing Unsteady Aerodynamics" Master's Thesis, Naval Post graduate School, Monterey, CA, September, 1993.
41. Bisplinghoff, R. L., Ashley, H., Halfman, R. L., " Aeroelasticity" Addison-Wesley Publishing Company, Inc., 1955.

42. E. R. Wood "Class Notes" Sep. 1991.
43. Riestler, P. J. "Computational and Experimental Investigation of Incompressible Oscillatory Airfoil Flow and Flutter Problem" Master's Thesis, Naval Postgraduate School, Monterey, CA, June, 1993.
44. D. Kuechemann, FRS " The Aerodynamic Design of Aircraft." Pergamon Press, Oxford.
45. H. Glauert, M. A. " The Elements of Airfoil and Airscrew Theory " Cambridge University Press, 1926.
46. Bagley, J. A. ' The Pressure Distribution on Two-Dimensional Wings Near the Ground " R & M No. 3238 February, 1960. (previously issued as R. A.E. Report Aerc. No. 2625 - A.R.C. 22,060.
47. Loewy, R. G. and Tseng, S. P., " Smart Structures Stabilized Unstable Control Surface" , presented at the 34th Structures, Dynamic, and Materials (SDM) Conference, La Jolla, CA, April 19-22, 1993.
48. Loewy, R. G. and Tseng, S. P., " Exploiting Instabilities for Control Purposes Using Smart Structures" . presented at the Symposium honoring Dr. Holt Ashly, Stanford, CA, September 23, 1993.
49. Loewy, R. G. and Tseng, S. P., ' Amplifying Pitching Response Using Dynamic Instabilities ", presented at Fifth International Workshop on Dynamic and Aeroelastic Stability Modeling of Rotorcraft Systems, Rensselaer Polytechnic Institute, October 18-20, 1993.

50. Barrett, R.. " Aeroservoelastic DAP Missile Fin Development" presented at the 3rd International Conference on Adaptive Structures, San Diego, CA, November 9-11, 1992.
51. Wood, E. R." Higher Harmonic Control for The Jet Smooth Ride" Vertiflite May/June 1983.
52. Hammond, C. E., "Wind Tunnel Results Showing Rotor Vibratory Loads Reduction Using Higher Harmonic Blade Pitch." Journal of the American Helicopter Society, Vol. 28, No. 1, pp. 10-15, Jan. 1983.
53. Giesing, J. P., " Unsteady Two-Dimensional Potential Flow for Two Bodies with Lift " Technical Paper No. DAC-33552, Douglas Aircraft Division, Long Beach, CA, March 1967.

INITIAL DISTRIBUTION LIST

1. Superintendent 2
Attn : Library, code 1424
Naval Postgraduate School; Monterey, California 93943-5000
2. Chairman, Code AA/Co 1
Attn : Library, code 1424
Naval Postgraduate School; Monterey, California 93943-5000
3. Dr. E. Roberts Wood 3
Dept. of Aeronautics and Astronautics, Code AA/Wd
Naval Postgraduate School; Monterey, California 93943-5000
4. Dr. Max. F. Platzer. 3
Dept. of Aeronautics and Astronautics, Code AA/PI
Naval Postgraduate School; Monterey, California 93943-5000.
5. Dr. Garth Hobson. 1
Dept. of Aeronautics and Astronautics, Code AA/Ho
Naval Postgraduate School; Monterey, California 93943-5000.
6. Dr. Donald Dannielsen. 1
Dept. of Mathematics, Code MA/Dd
Naval Postgraduate School, Monterey, California 93943-5000.
7. Dr. James Sanders. 1
Dept of Physics, Code PH/Sd
Naval Postgraduate School, Monterey, California 93943-5000.

7. **Armament Authority-Training Department (Egypt) 2**
c/o American Embassy (Cairo,Egypt)
Office of Military Cooperation, Box 29 (TNG)
FPO, NY 09527-0051.
8. **Dr. Dev Banerjee 1**
Director, Research and Technology
McDonnell Douglas Helicopter Company
Bldg. 530/B325
5000 E. McDowell Road
Mesa, Az 85215.
9. **Dr. Robert G. Loewy, Director 1**
School of Aerospace Engineering
Georgia Institute of Technology
Atlanta, GA 30332.
10. **Mr. Robert V. Doggett, Jr. 1**
Asst. Chief Structural Dynamics Division
NASA Langley Research Center
Hampton, VA 23665.
11. **Dr. John Shaw, Deputy Director, Research & Technology 1**
Boeing Defense and Space Group
Helicopter Division
Box 16858
Philadelphia, PA 19142.

12. **Dr. C. Eugene Hammond** 1
Director, Mechanical Engineering
Martin Marietta Aerospace
Orlando, FL 32817.
13. **Dr. Raymond G. Carlson** 1
Chief Advanced Research Development
Sikorsky Aircraft Division. UTC
6900 Main Street
Stratford, CT 06601.
14. **Professor David A. Peters** 1
Department of Mechanical Engineering
Campus Box 1185
Washington University
St. Louis, MO 63130.
15. **Professor Peretz P. Friedmann** 1
Dept. of Mechanical, Aeronautical
and Nuclear Engineering
46-147N ENG IV
University of California
Los Angeles, CA 90024.